PNNL-11148
UC-404

BEATRIX-II, Phase II: Data Summary Report

O. D. Slagle
G. W. Hollenberg

Other Key Contributors:

R. J. Puigh[a]
D. E. Baker[a]
D. A. King[a]
D. R. Precechtel[a]
G. T. Taylor[a]
R. W. Truitt[a]

T. Kondo[b]
T. Kurasawa[b]
K. Noda[b]
N. M. Masaki[b]
T. Takahashi[b]
T. Tanifuji[b]
H. Watanabe[b]

I. J. Hastings[c]
J. M. Miller[c]
R. A. Verrall[c]

S. E. Berk[d]

D. L. Baldwin
N. J. Wildung

May 1996

Work supported by
The U. S. Department of Energy
under Contract DE-AC06-76RLO 1830

Pacific Northwest National Laboratory
Richland, Washington 99352

(a) Westinghouse Hanford Company
Richland, Washington
(b) Japanese Atomic Energy Research Institute
Tokai-mura, Ibaraki-ken, Japan
(c) AECL Research
Chalk River, Ontario, Canada
(d) U. S. Department of Energy
Washington, D.C.

DISTRIBUTION OF THIS DOCUMENT IS UNLIMITED

DISCLAIMER

Abstract

The BEATRIX-II experimental program was an International Energy Agency sponsored collaborative effort between Japan, Canada, and the United States to evaluate the performance of ceramic solid breeder materials in a fast-neutron environment at high burnup levels. This report addresses the Phase II activities, which included two *in situ* tritium-recovery canisters: temperature-change and temperature-gradient. The temperature-change canister contained a Li_2O ring specimen that had a nearly uniform temperature profile and was capable of temperature changes between 530 and 640°C. The temperature-gradient canister contained a Li_2ZrO_3 pebble bed operating under a thermal gradient of 440 to 1100°C. Postirradiation examination was carried out to characterize the Phase II *in situ* specimens and a series of nonvented capsules designed to address the compatibility of beryllium with lithium-ceramic solid-breeder materials.

The results of the BEATRIX-II, Phase II, irradiation experiment provided an extensive data base on the *in situ* tritium-release characteristics of Li_2O and Li_2ZrO_3 for lithium burnups near 5%. The composition of the sweep gas was found to be a critical parameter in the recovery of tritium from both Li_2O and Li_2ZrO_3. In general, increasing the amount of hydrogen in the sweep gas resulted in a transient tritium recovery peak indicative of a decrease in tritium inventory in the specimen. The ability of the Phase II temperature-change canister to vary temperature between 530 and 630°C indicated that increasing temperature resulted in transient tritium-recovery peaks whose magnitude and duration were indicative of a relatively small tritium inventory in the Phase II Li_2O ring specimen at these temperatures. Throughout the Phase II irradiation, the centerline temperature of the Li_2ZrO_3 specimen was nearly constant, inferring that the pebble bed remained physically the same throughout the irradiation.

Tritium inventories measured during postirradiation examination confirmed that Li_2O and Li_2ZrO_3 exhibited very low tritium retention during the Phase II irradiation. The tritium inventories in Li_2ZrO_3 after Phase II tended to be larger than those found for Li_2ZrO_3 in other *in situ* experiments, but the larger values may reflect the larger generation rates in BEATRIX-II.

A series of 20 capsules was irradiated to determine the compatibility of lithium ceramics and beryllium under conditions similar to a fusion blanket. The lithium ceramics (Li_2O, Li_2ZrO_3, $LiAlO_2$, and Li_4SiO_4) in contact with beryllium resulted in no observable chemical interaction for lithium burnups up to 4% and irradiation times up to 500 effective full-power days.

The results of the Phase I and Phase II *in situ* tritium recovery and postirradiation examination provide insight on the physical stability and tritium-release behavior of Li_2O and Li_2ZrO_3. Based on these results, it is concluded that Li_2O and Li_2ZrO_3 should remain leading candidates for use in a solid-breeder fusion-blanket application.

Executive Summary

The BEATRIX-II (Breeder Exchange Matrix) experimental program was an International Energy Agency sponsored collaborative effort between Japan, Canada, and the United States. The experimental activities were carried out under ANNEX-III to the IEA Implementing Agreement on a Programmme of Research and Development in Fusion Materials. The purpose of the program is to evaluate the performance of ceramic solid-breeder materials in a fast-neutron environment at high burnup levels. The irradiations were carried out in the Fast Flux Test Facility which is operated by Westinghouse Hanford Company at the Hanford Site near Richland, Washington. The Pacific Northwest Laboratory together with the Japan Atomic Energy Research Institute and Atomic Energy of Canada Limited Research acted jointly to conduct the experiments.

The BEATRIX-II program was divided into two phases. This report addresses the Phase II activities that were based on irradiations carried out between May 27, 1991, and March 19, 1992, for a total exposure of 200 effective full power days (EFPD). The final lithium burnups for the vented canisters were between 4.5 and 6%. Postirradiation examination was carried out to characterize the Phase II vented canisters and the Phase I and II non-vented capsules.

In Phase II, the irradiation test assemblies included two *in situ* tritium-recovery canisters: temperature-change and temperature-gradient. These *in situ* canisters were installed on a materials open test assembly, which permitted not only thermocouple instrumentation, but also temperature control via changes in the gas composition of a gas gap. The temperature-change canister contained a Li_2O ring specimen that had a nearly uniform temperature profile and was capable of temperature changes between 530 and 640°C. The temperature-gradient canister contained a Li_2ZrO_3 pebble bed operating under a thermal gradient of 440 to 1100°C. The data obtained from the temperature-gradient canister were prototypic of a worst-case thermal environment in a fusion blanket. Nonvented capsules designed to address the compatibility of beryllium with lithium-ceramic solid breeder materials that had been previously irradiated in Phase I received additional irradiation in Phase II.

The BEATRIX-II apparatus provided an excellent test bed for developing methods to monitor tritium and handle it safely during an *in situ* tritium-recovery experiment. The tritium handling system for Phase I and II divided the outlet streams from each of the two *in situ* tritium-recovery-specimen canisters into two separate analysis streams. Each analysis gas stream provided continuous real-time monitoring of the flow rate, total moisture, tritium concentration, and proportion of reduced versus oxidized tritium in the sweep gas from the individual canisters. Throughout the irradiation, the ionization chambers provided a sensitive record of the tritium recovery with good response times and a slowly increasing background. The *in situ* calibration of the ionization chambers indicated that the ionization-chamber response was dependent on the sweep-gas composition, and specific correction factors were established throughout the course of the experiment. Ceramic electrolysis cells (CEC) were used to reduce the tritiated water (HTO) in one of the analysis streams to HT for real-time determination of the total tritium. Overall, the efficiency of the CECs approached 99% except for two occasions when the operation of a cell was briefly interrupted. Tritium getter beds were designed to remove the tritium from the sweep gas before release to the environment, and these units performed better than specified in the original design requirements.

The results of the BEATRIX-II, Phase II irradiation experiment provided an extensive data base on the *in situ* tritium-release characteristics of Li_2O and Li_2ZrO_3 for lithium burnups in the range of 4.5 to 6%. Helium sweep gas with additions of 0%, 0.01%, 0.1%, and 1.0% hydrogen were used to study the effect of sweep-gas composition on the tritium recovery. The composition of the

sweep gas was found to be a critical parameter in the recovery of tritium from Li_2O and Li_2ZrO_3. In general, decreasing the amount of hydrogen in the sweep gas decreased the measured tritium recovery rate. This decrease in recovery rate translates to higher tritium inventories for sweep gases with lower hydrogen concentrations.

The ability of the Phase II temperature-change canister to vary temperature between 530 and 640°C provided data that added confirmation to conclusions reached previously based on the Phase I data and resulted in additional insight on the irradiation behavior of Li_2O. The primary qualitative conclusions reached from the temperature-change results on Li_2O were

- *Tritium Inventories* - Increasing the temperature resulted in transient tritium-recovery peaks whose magnitude and duration were indicative of a relatively small tritium inventory in the Phase II Li_2O ring specimen at these temperatures.

- *Sweep-Gas Composition* - As in Phase I, for a given temperature change, the Phase II transient tritium recovery peaks were successively larger for lower hydrogen concentrations. This behavior suggested that for Li_2O, larger changes in tritium inventories occurred for temperature transients carried out in sweep gases with lower hydrogen concentrations. These observations are consistent with the behavior observed for changing sweep-gas composition, i.e., decreasing hydrogen concentration in the sweep gas leads to higher tritium inventories in Li_2O.

- *Lithium Burnup/Exposure* - During Phase II, the temperature recovery peaks primarily consisted of HT, and no apparent change in recovery behavior occurred as seen in Phase I. At the start of Phase I, the tritium-recovery peaks for temperature increases were found to consist of an initial HT peak and a second larger peak of HTO. At the end of Phase I, the form of the tritium in the recovery peaks changed so that HT was the predominant species. Because Phase II did not exhibit the double peaks, this change in tritium-recovery behavior during Phase I probably resulted from changes such as lower surface moisture in the tritium-handling system rather than from a change in Li_2O-specimen-release characteristics due to lithium burnup/exposure.

The temperature-gradient canister contained a Li_2ZrO_3 pebble bed that was irradiated under a large thermal gradient typical of fusion-blanket designs. The results of this irradiation provided verification of the viability of a Li_2ZrO_3 pebble bed as a candidate for a fusion solid blanket. Similar to the behavior of the Phase I Li_2O temperature-gradient canister, changing sweep-gas composition in the Phase II temperature-gradient canister led to higher tritium inventories in Li_2ZrO_3 for lower hydrogen concentration in the sweep gas. Throughout the 200 EFPD of irradiation, the centerline temperature of the specimen remained nearly constant when operated at full power, decreasing as the local neutron flux decreased with fuel burnup. This observation inferred that the pebble bed remained physically the same throughout the irradiation. Postirradiation examination indicated that limited sintering occurred between the pebbles, but this sintering resulted in no observable shrinkage of the bed.

Tritium inventories measured during postirradiation examination confirmed that Li_2O exhibited very low tritium retention during the irradiation to 4.6% burnup. The Phase II experiment was shut down over a period of 10 hours in contrast to the 2-minute shutdown for Phase I. It was hypothesized that the Phase II inventory could be higher due to a buildup in the tritium while the specimen was operated at the lower temperatures during shutdown. However, for the Li_2O in the Phase II temperature-change canisters, the measured tritium inventories (0.19 to 0.25 wppm) were lower than the Phase I inventories (0.2 to 0.7 wppm). A prediction of the tritium recovered versus the tritium generated during shutdown was not precise enough to determine whether the tritium inventory changed during shutdown.

Postirradiation tritium-inventory measurements on the Li_2ZrO_3 pebble bed confirmed that the tritium inventory was very low after the 5.1% lithium burnup. For purposes of comparing the postirradiation tritium inventories, the Phase II Li_2ZrO_3 pebble-bed specimen was divided into three radial zones. The average tritium inventories in the three zones decreased from the lower temperature circumference to the higher temperature centerline: 0.32 wppm at 395 to 770°C, 0.15 wppm at 770 to 945°C, and 0.032 wppm at 945 to 1025°C. A comparison of the tritium recovered during the final shutdown versus the predicted tritium generated indicated that no significant change in the inventory occurred during shutdown. The tritium inventories in Li_2ZrO_3 after Phase II tended to be larger than those found for Li_2ZrO_3 in other *in situ* experiments, but the larger values may reflect the larger generation rates in BEATRIX-II.

A series of 20 capsules was irradiated to determine the compatibility of lithium ceramics and beryllium under conditions similar to a fusion blanket. The lithium ceramics (Li_2O, Li_2ZrO_3, $LiAlO_2$, and Li_4SiO_4) in contact with beryllium resulted in no observable chemical interaction for lithium burnups up to 4% and irradiation times up to 500 EFPD.

The results of the Phase I and Phase II *in situ* tritium recovery provide insight on the effects of temperature and sweep-gas composition on the tritium-release behavior of Li_2O and Li_2ZrO_3. Postirradiation examination of the specimens indicated that the material underwent extensive microstructural changes, but remained physically intact while efficiently releasing the generated tritium to maintain a low tritium inventory. Based on these results, it is concluded that Li_2O and Li_2ZrO_3 should remain leading candidates for use in a solid-breeder fusion-blanket application.

Contents

Figures

Tables

1.0 Introduction

The BEATRIX-II (Breeder Exchange Matrix) program is an International Energy Agency (IEA) sponsored collaborative effort between Japan, Canada, and the United States conducted under ANNEX-III to the IEA Implementing Agreement on a Programmme of Research and Development on Radiation Damage in Fusion Materials. The purpose of the program was to evaluate the performance of ceramic solid-breeder materials in a fast-neutron environment at high burnup levels. The irradiation of selected solid breeder materials was carried out in the Fast Flux Test Facility (FFTF) operated by Westinghouse Hanford Company (WHC) at the Hanford Site near Richland, Washington. The Pacific Northwest National Laboratory (PNNL)[a] together with the Japan Atomic Energy Research Institute (JAERI) and Atomic Energy of Canada, Limited (AECL) Research acted as experimenter.

1.1 Objective

The objective of the BEATRIX-II program was to design, fabricate, and conduct an irradiation experiment to evaluate the *in situ* recovery of tritium from solid-breeder materials during neutron irradiation. To accomplish this, the performance of selected candidate solid-breeder materials was continuously monitored with respect to temperature stability and tritium release, and after irradiation, the materials were examined to characterize the effect of the irradiation.

1.2 Scope

The BEATRIX-II program consisted of two Phases: 1) Phase I irradiation activities were carried out in Cycle 11 of FFTF between January 4, 1990, and March 20, 1991, for a total irradiation exposure of 300 effective full-power days (EFPD), and 2) Phase II irradiations were carried out between May 27, 1991, and March 19, 1992, for a total irradiation exposure of 203 EFPD.

The lithium burnups for both Phase I and Phase II were in the range of 4.5 to 6%. Postirradiation examination of Phase I and II followed the irradiation periods.

1.2.1 Phase I Scope

The scope of the Phase I experiment included the irradiation of two Li_2O *in situ* tritium recovery canisters: temperature-change and temperature-gradient. The temperature-change canister contained a Li_2O ring specimen that had a nearly uniform temperature and was capable of temperature changes between 550 and 640°C. The temperature-gradient canister contained a solid column of Li_2O operating with a radial temperature difference of 440 to 1000°C. The data obtained from the temperature-change canister are more useful for understanding the intrinsic behavior of the ceramic, and those from the temperature-gradient canister are more directly applicable to the performance of Li_2O in a fusion-blanket environment. Nonvented capsules were included to determine the mechanisms of radiation damage in single crystals and the compatibility of beryllium with solid-breeder materials.

1.2.2 Phase II Scope

The scope of the Phase II experiment also included the irradiation of two *in situ* tritium-recovery canisters: a temperature-change canister containing a Li_2O ring specimen and a

(a) Pacific Northwest National Laboratory (previous name was Pacific Northwest Laboratory) is operated for the U. S. Department of Energy (DOE) by Battelle under Contract DE-AC06-76RL0 1830.

temperature-gradient canister containing a solid Li_2ZrO_3 pebble-bed specimen composed of 1-mm pebbles. To achieve the desired burnup in Phase II, the ^6Li enrichment was higher than Phase I for both specimens, and the canister containing the Li_2ZrO_3 pebble-bed specimen was located in a higher fluence position. Nonvented capsules included selected beryllium-lithium ceramic compatibility specimens from Phase I.

1.3 Responsibilities

The BEATRIX-II program involved contributors from a wide range of organizations. The organization of the program is diagrammed in Figure 1.1. The IEA Executive Committee had the overall responsibility for approving and signing the ANNEX-III. The BEATRIX-II Working Group was a technical steering committee responsible for the preparation and supervision of budgets, schedules, and scientific activities. Each of the participating countries is represented in the working group. The original working group members were H. Watanabe (JAERI), I. J. Hastings (AECL), and S. E. Berk (DOE). During the operation of the experiment, the JAERI and AECL representatives changed and are currently K. Noda and R. A. Verrall, respectively. The operating agent for the experiment is DOE, who is responsible for executing the program. The DOE person originally responsible for this interaction was T. C. Reuther (retired); he was replaced by R. E. Price. The BEATRIX-II Task Manager, G. W. Hollenberg (PNNL), coordinated the operation of the experiment following the guidance of the working group and the operating agent.

The operation of the experiment was carried out by WHC with oversight by the BEATRIX-II Experimenters. The operations at the reactor site were conducted by D. E. Baker, D. A. King, and the reactor operations personnel of FFTF under the cognizance of R. J. Puigh. Major contributors to the design and fabrication of the experiment at WHC were D. E. Baker, M. M. Paxton, R. W. Truitt, R. E. Bauer, R. C. Knight, and R. D. Redekop. J. Miller (AECL) played a major role in developing and fabricating the ionization chambers (hereafter referred to as ion chambers) and the tritium-removal system. T. Takahashi (JAERI) and J. D. Sullivan (AECL) fabricated the lithium ceramic specimens for the Phase II *in situ* tritium-recovery canisters.

Technical planning and data analysis were carried out by the BEATRIX-II Experimenters: O. D. Slagle (PNNL), T. Kurasawa (JAERI), and R. A. Verrall (AECL). The BEATRIX-II experimenters for the postirradiation examination were O. D. Slagle (PNNL), T. Takahashi, K. Noda , T. Tanafugi, and N. M. Masaki (JAERI), and R. A. Verrall (AECL).

1.4 Report Scope

This report specifically addresses the BEATRIX-II, Phase II experiment and not Phase I. It includes a description of

- the specimens/canisters
- the operation of the experiment in the FFTF
- the *in situ* tritium-recovery results
- the Phase II postirradiation examination, which included
  - the Phase II *in situ* canisters
  - the lithium ceramic-beryllium compatibility capsules irradiated in Phase I and II
  - the Phase I single-crystal capsules (completing the examination).

Details of the Phase I specimen matrix and experiment operation are given in the Phase I Data Summary Report (Slagle and Hollenberg 1994),

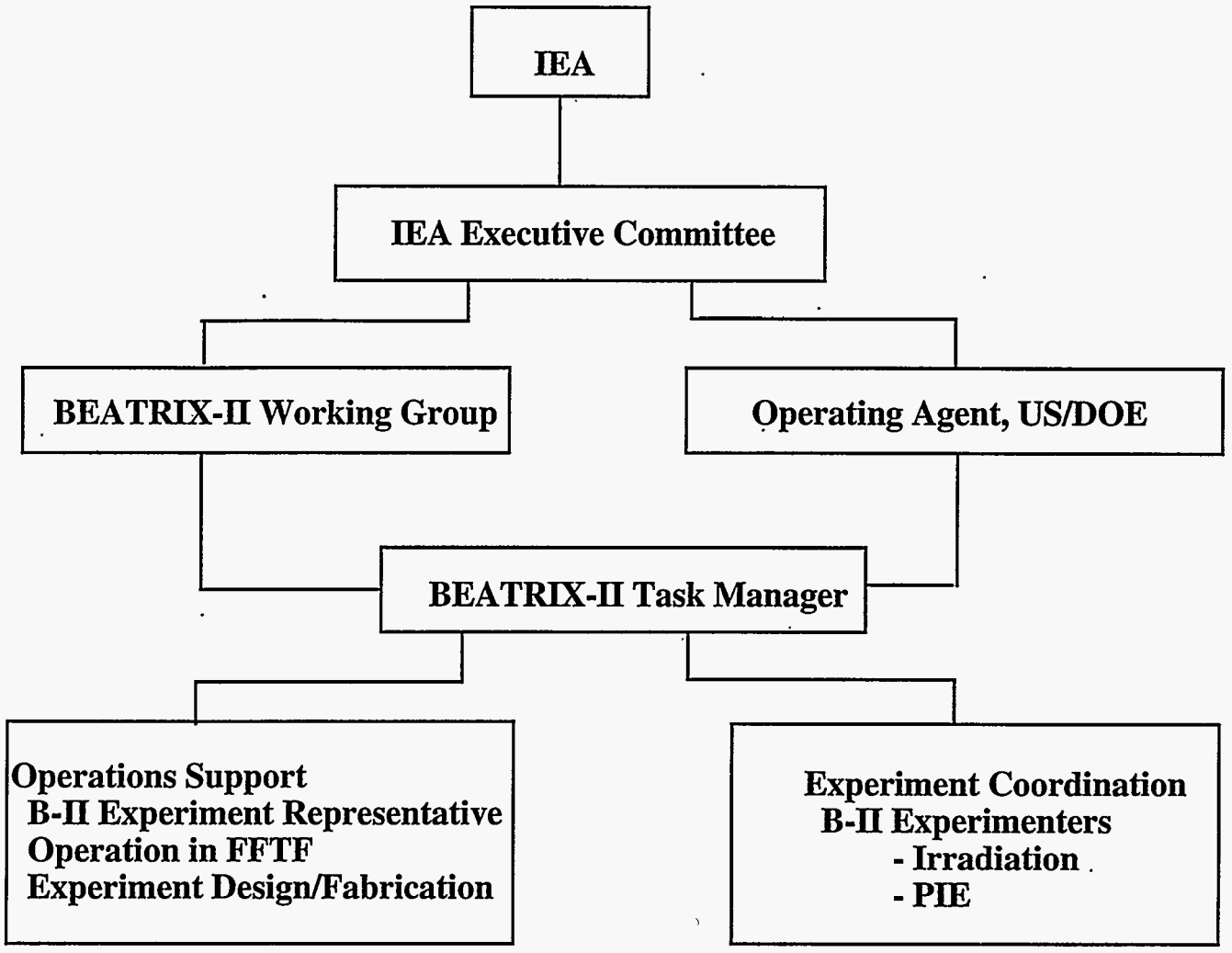

Figure 1.1. Organizational Structure of BEATRIX-II

2.0 Specimen/Canister Matrix

Phase II of the BEATRIX-II *in situ* tritium-recovery experiment contained a Li_2O ring specimen and a Li_2ZrO_3 solid specimen, the latter in the form of 1-mm pebbles. The Phase I Li_2O ring specimen had been prepared in the United States, but the ring specimen for Phase II was prepared in Japan. Improved fabrication techniques were used to give a higher density, larger grain size material that would allow fabrication of a ring specimen with a thinner wall. The alternative ternary breeder material most suitable for additional characterization was determined to be Li_2ZrO_3. In previous vented (Briec et al. 1988) and nonvented (Hollenberg and Baldwin 1985; Slagle et al. 1991) tests, L_2ZrO_3 had been found to be dimensionally and chemically stable during irradiations and to have relatively short tritium-residence times. The material used was 1- to 1.5-mm-diameter Li_2ZrO_3 pebbles prepared by AECL Research.

2.1 Temperature-Change Canister

The Phase II temperature-change canister was nearly identical to the Phase I temperature-change canister. The primary emphasis in establishing the Phase II design was to achieve a higher lithium burnup and to lower the minimum specimen temperature. These requirements together with other improvements identified during the operation of Phase I presented challenges to the designers.

2.1.1 Thermal Design

The design requirements for the Phase II temperature-change specimen extended those for Phase I and included considerations such as the sensitivity of tritium measurements, minimizing the loss of tritium to the reactor, and the temperature of the specimen. A major change in the requirements was an increase in the end-of-life lithium burnup. This increase in burnup rate was partially achieved by increasing the ^6Li enrichment from 61 to 95 at %.

The design objectives of Phase II were to achieve temperatures in the range from 450 to 650°C. The pre-test thermal analysis for the Phase I design had predicted temperatures in the range from 468 to 645°C. The temperatures, however, were in the range from 510 to 680°C. These higher temperatures were attributed to the existence of larger-than-expected gaps between the capsule and the specimen wall and a lower specimen density (Slagle and Hollenberg 1994). Achieving lower temperatures for the ring specimen was given a high priority in Phase II.

Figure 2.1 is a schematic diagram of a cross section of the temperature-change canister for Phase II. The tritium sweep gas entered at the bottom end of the canister, flowed along the inner diameter of the specimen, and exited out of the upper plenum. A perforated inner stainless steel sleeve ensured that if the specimen should fracture during testing, the cylindrical geometry would be maintained. This sleeve also positioned the two inner thermocouples. In Phase I, this inner sleeve was fabricated from a nickel screen, but a stainless steel tube was chosen for Phase II to reduce the types of metal surfaces interacting with the sweep gas. This simplification reduces the number of surface reactions that must be taken into account in the data interpretation. The temperature in the specimen is controlled by varying the conductance of the thermal gap of the canister by adjusting the composition of the argon-helium gas in the gap. A computer-controlled gas-blending system allows temperature control continuously throughout the 300-day irradiation.

A major goal of Phase II was to achieve temperatures as low as possible for the ring specimen. The following design changes were made to the Phase I design to achieve the lower temperatures:

1. The wall thickness of the ring specimen was decreased from 0.15 cm in Phase I to 0.10 cm in Phase II, and the specimen density was increased from 80% theoretical density (TD) for Phase I to 85% for Phase II. The heating rate in the Phase II specimen was kept constant by keeping the total amount of ^6Li approximately constant. A reduction in wall thickness resulted in a smaller volume of Li_2O and compensated for the increase in ^6Li enrichment. The higher density increased the thermal conductivity. Both of these changes should reduce the temperature drop across the specimen.

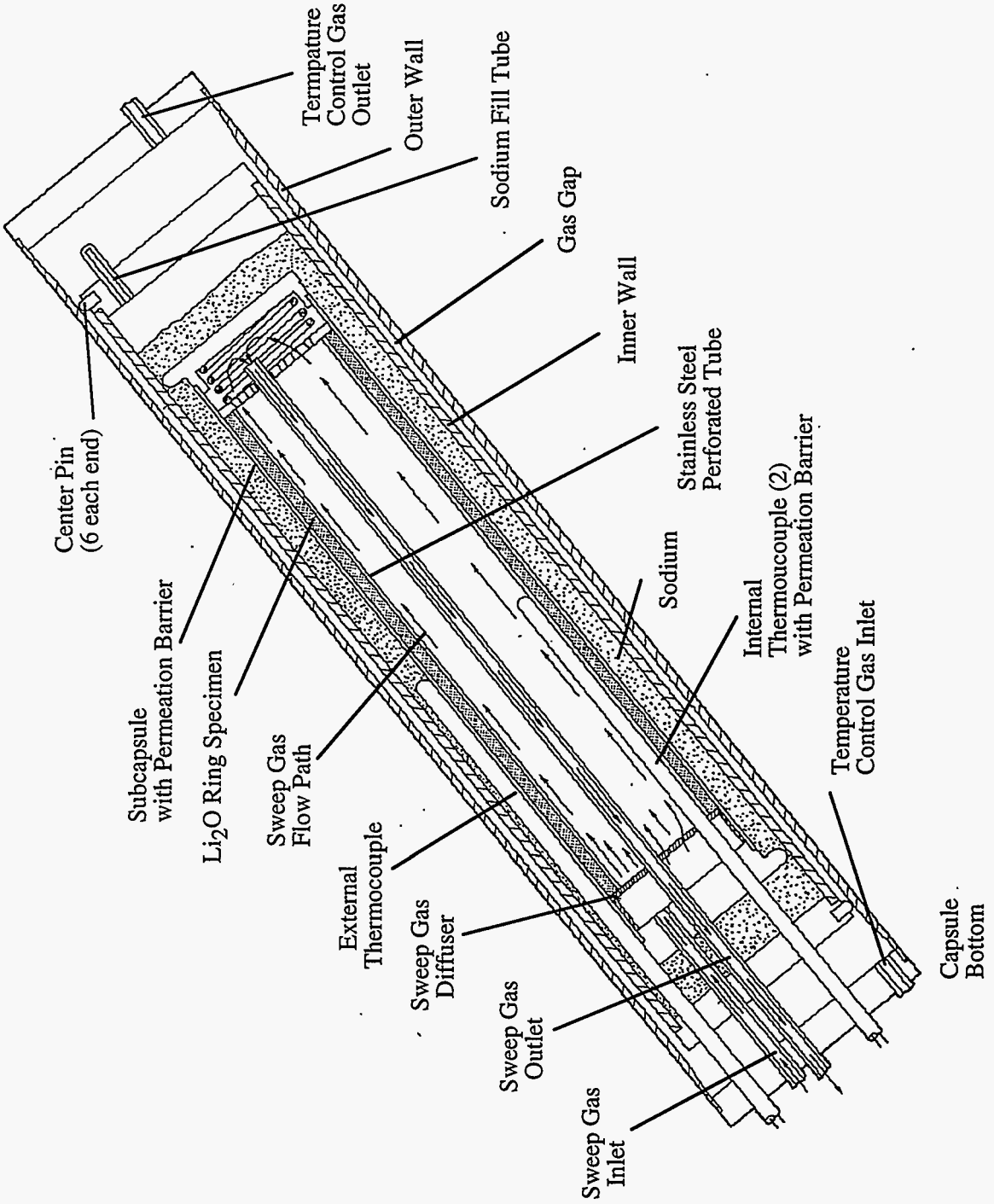

Figure 2.1. Schematic Diagram of the Temperature-Change Canister for Phase II

2. The specimen-capsule gap was minimized by placing a closer tolerance on the specimen outer diameter. The previous tolerance of 0.013 cm was reduced to 0.005 cm. The inner diameter of the capsule was machined 0.010 cm larger than the largest specimen diameter. This radial gap (0.005 cm) is predicted to ensure closure at 500°C. Final machining on the capsule was done to fit the as-fabricated specimen. This design change required that the tritium-barrier coating not be applied to the inner diameter of the canister.

3. The inner nickel liner used previously as a compatibility barrier between the specimen and the capsule was removed. This eliminated the possibility that the nickel liner would separate from the capsule and form a thermal gap. The expected interaction of the specimen and the 316 stainless steel subcapsule wall was estimated to be 2 to 10 μm of general surface corrosion and possibly 25 μm of intergranular attack (Porter et al. 1984).

2.1.2 Specimen Fabrication/Loading

A description of the final Phase II ring specimen is given in Table 2.1. The Phase II ring specimen was a single section of tube, 8.85 cm long in contrast to the Phase I specimen, which consisted of two sections. The final density was 87.3% TD with a grain size of 22 μm. The variation in diameter along the specimen was 0.003 cm, which is within the specified range of 0.005 cm. The wall thickness was 0.10 cm, as specified.

Table 2.1. Description of BEATRIX-II, Phase II Ring Specimen

	Phase II Ring Specimen
^{6}Li Enrichment	95 at %
Outer Diameter	1.850 to 1.853 cm
Inner Diameter	1.651 to 1.653 cm
Straightness	0.003 cm
Wall Thickness	0.100 cm
Length	8.850 cm
Weight	8.103 g
Density	87.3% TD
Grain Size	22 μm

The Li_2O used to fabricate the ring specimen was prepared by decomposing 95 at % ^{6}Li enriched Li_2CO_3 to a Li_2O powder. The powder preparations and sintering procedures were similar to those used for preparing the temperature-gradient specimen in Phase I (Slagle et al. 1990; Takahashi and Watanabe 1989). The Li_2CO_3 powder was decomposed to the oxide by heating to 700°C in a vacuum of 6×10^{-2} Pa in the initial stage and to 5×10^{-5} Pa in the final stage. The ring specimen was fabricated by sintering a cylindrical-shaped compact from which the final specimen was machined. The compact was formed by isostatic pressing at 200 MPa and sintering at 1170°C for 8 hours. The as-sintered compact was a 2.1-cm-diameter cylinder with a 1.15-cm inner annulus and a length of 9.43 cm.. A "rock lathe" was used to machine the final thin-walled specimen in an atmosphere of dry air. Because of the inherently fragile nature of the thin-ring specimen, a second specimen of the same dimensions was also prepared to serve as a backup.

Figure 2.2 shows the capsule with the specimen in place, the "backup" specimen, and the inner perforated sleeve before final loading. The specimen slid easily into the capsule, which had an inner diameter of 1.863 cm or a 0.010-cm diametral gap. The inner sleeve was a perforated stainless steel tube. Stainless steel was used to minimize the types of metal surfaces interacting with the purge

gas. A perforated tube was chosen over the screen used in Phase I because the tube was a more rigid structure and allowed a more definite positioning of the thermocouples than the screen.

Figure 2.3 is an x-ray radiograph of the capsule after loading. This radiograph shows clearly the configuration of the different components. The positioning of the inner thermocouples in the slots provided by the inner sleeve can be seen. The assembly shown in Figure 2.3 was thermally bonded with sodium inside the gas-gaped thermally controlled canister. The sodium also serves to minimize axial temperature gradients. The thermocouple in the center of the radiograph is the outer thermocouple, which measures the temperature in the sodium used as a thermal contact.

2.1.3 Predicted Performance

The thermal and neutronic performance of the ring specimen was calculated on the basis of the expected neutron flux in the materials open test assembly (MOTA) Cycle 12, and the heat generation in the Li_2O ring specimen (110 W/g). Using this heat generation rate, the specimen temperatures were calculated for two different control gases in the canister temperature-control gap. The results are summarized in Table 2.2. The minimum temperatures were calculated for 100% He, and the temperature range across the specimen was determined to be 485 to 503°C. These temperatures were substantially less than the temperatures achieved in Phase I, which were 500 to 540°C across the specimen. The upper temperature in the Phase I test matrix was 650°C, and this temperature was found to be achievable with a 1:7 ratio of He:Ar temperature-control gas. The total tritium generation for 203 EFPD was predicted to be 850 Ci. This corresponds to a 5.3% burnup in the total lithium.

2.2 Temperature-Gradient Canister

The Li_2ZrO_3 specimen in the Phase II temperature-gradient canister was a pebble bed composed of 1-mm particles. This "solid" specimen with its inherent temperature gradient is similar to the Li_2O specimen used in Phase I and provides a comparison for evaluating the relative merits of the two materials. The diameters of the Li_2ZrO_3 pebbles were specified to be in the range from 1 to 1.5 mm with a ^6Li enrichment of 85 at % and were provided by AECL Research.

Table 2.2. Predicted Thermal and Neutronic Performance of BEATRIX-II Li_2O Ring Specimen in FFTF/MOTA Cycle 12

Thermal Heat Generation	110 W/gm
Specimen-Capsule Diametral Gap	0.005 cm
Specimen Minimum Temperature (100% He)	
Outer Diameter	485°C
Inner Diameter	503°C
Specimen Maximum Temperature (1:7, He:Ar)	
Outer Diameter	632°C
Inner Diameter	654°C

During the initial stages of planning, a temperature-change canister using a ring-type specimen was considered. However, the low thermal conductivity of a lithium zirconate pebble bed resulted in a calculated thermal difference across the ring that was on the order of 100°C for a ring with a wall thickness equal to a pebble diameter. Such a large temperature difference limits the usefulness of a temperature-change canister, and a temperature-gradient canister was chosen. The low thermal conductivity of the pebble bed also placed restraints on the maximum diameter of the "solid" specimen in the temperature-gradient canister.

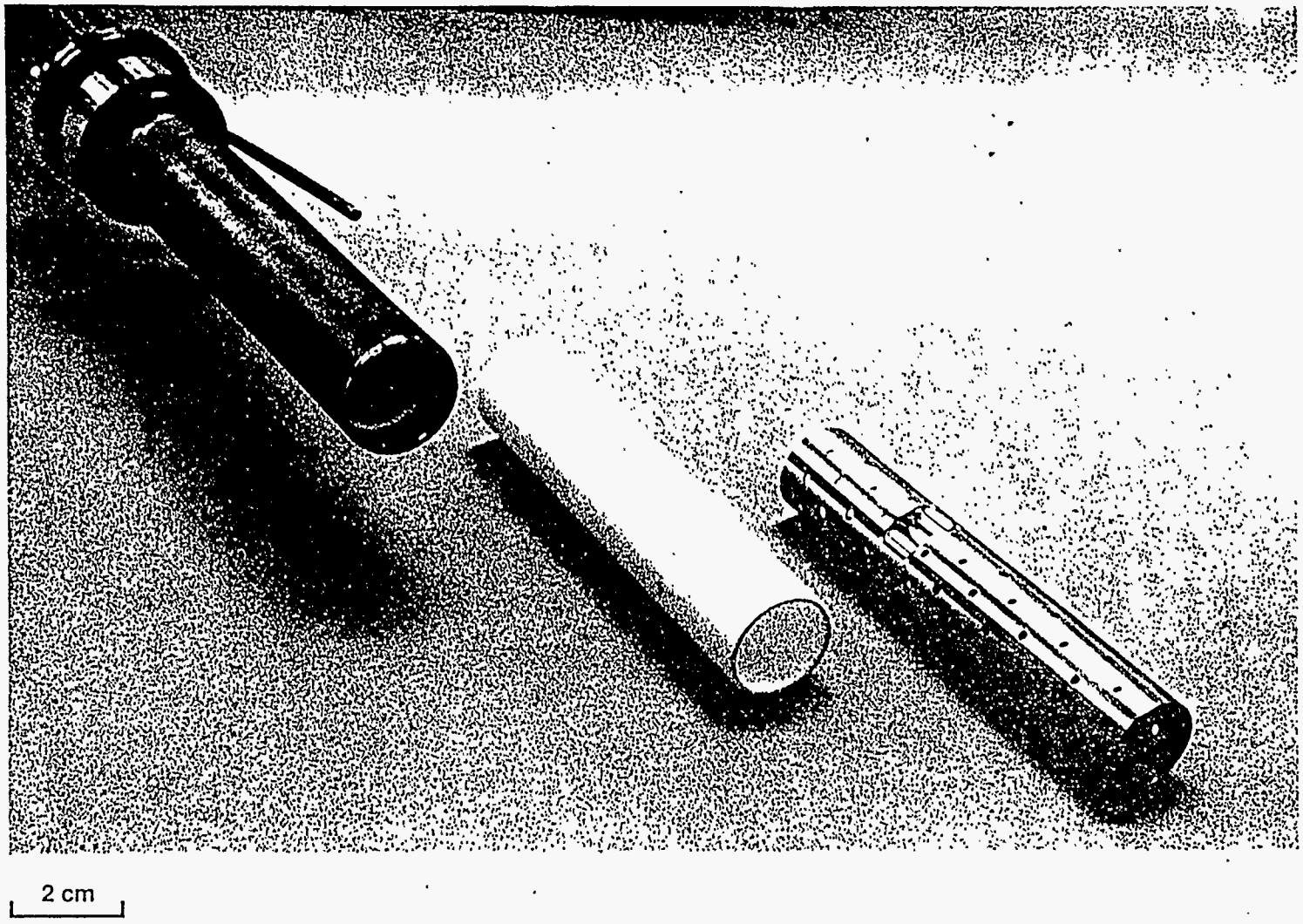

Figure 2.2 Phase II Temperature-Change Capsule with the Loaded Specimen, the "Backup" Specimen, and the Inner Perforated Tube before Final Assembly

2.2.1 Design Requirements

The desired centerline temperature in the pebble bed was in the range from 1000 to 1200°C. These limits were chosen based on the desire to obtain data at temperatures as high as possible without changing the microstructure of the lithium zirconate. Confirming the reliability of the solid breeder material over a broad range of temperatures minimizes the design restrictions imposed in the future when actual blanket designs are being considered. Achieving these temperatures was dependent on the neutron environment and the diameter of the pebble bed or capsule.

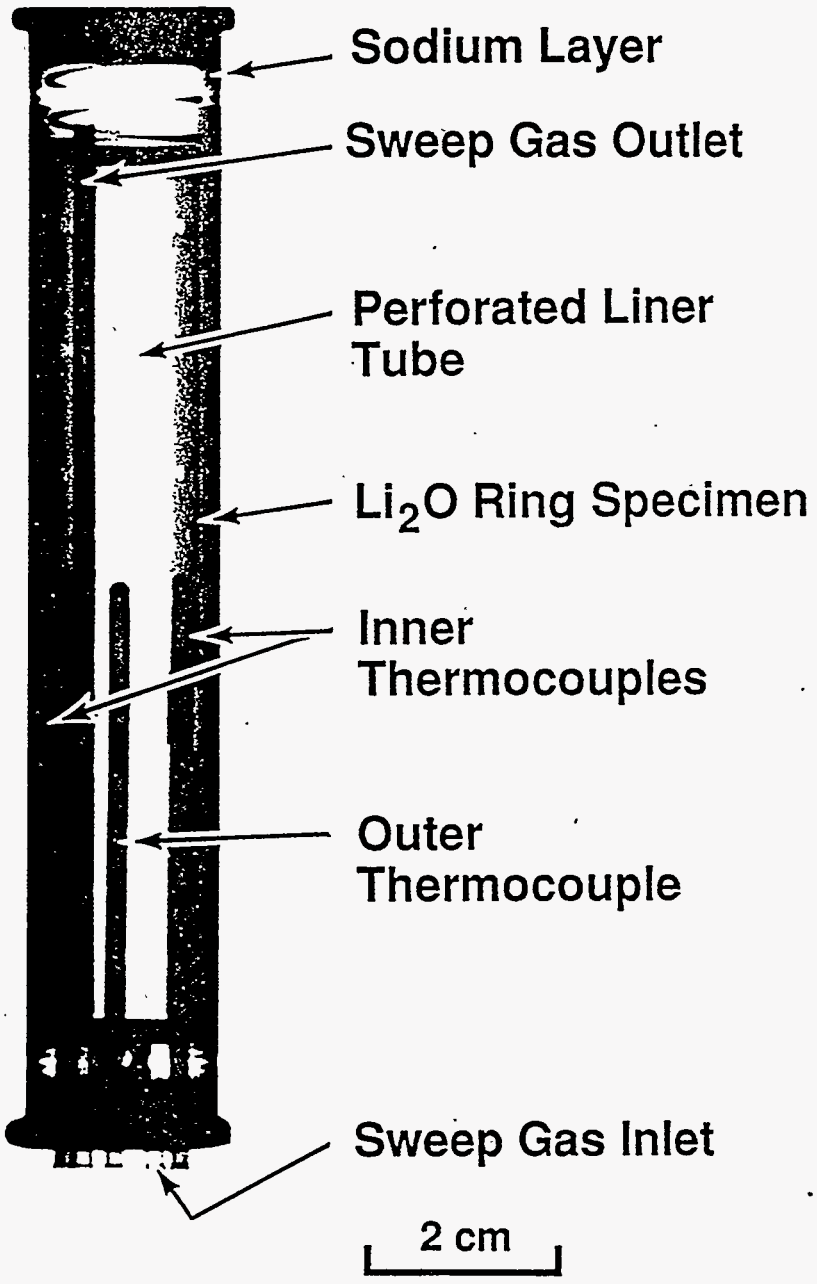

Figure 2.3. X-Ray Radiograph of the Temperature-Change Canister As-Fabricated

A total tritium generation of 650 Ci for the 203 EFPD cycle was desired to achieve tritium concentration levels compatible with the flow rates and ion chambers currently being used in the tritium measurement system. Because of the lower lithium density in Li_2ZrO_3 relative to Li_2O, the temperature-gradient canister was placed in a higher flux position, nearer the center of the reactor core than the temperature-change canister, to increase the tritium production rate.

2.2.2 Canister Design

The design of the temperature-gradient canister is shown schematically in Figure 2.4. The Li_2ZrO_3 pebble bed was contained in a stainless steel capsule between porous nickel screens at either end. The porous nickel screens allow the passage of sweep gas into and out of the bed. A high temperature spring was used to hold the pebble bed in place, especially during handling operations before loading the MOTA into the reactor. The spring was designed to withstand the 600°C outgassing of the canister before irradiation. A center tube was used for inserting the thermocouple into the centerline of the specimen after the pebble bed had been loaded to the required density by vibrating.

A type K thermocouple was chosen for one of the thermocouples with an alternative, higher temperature thermocouple for the other end of the canister. Type K thermocouples have performed well up to fluences equivalent to 300 EFPD in FFTF, but have a limited lifetime as temperatures approach and exceed 1200°C. A Nb-1% Zr/Mo thermocouple was under development at WHC and appeared to offer good stability in a neutron field plus reliability at the higher temperatures. Irradiation testing of this thermocouple has been described by Knight and Greenslade (1991). As the alternative thermocouple for the solid specimen canister, the operation of Phase II provided additional confirmation of the suitability of this thermocouple for high-temperature applications in a high-fluence neutron environment.

2.2.3 Calculated Performance

From the predicted heat generation and the thermal conductivity of the pebble bed, a pebble bed diameter was determined that would result in the desired centerline temperatures. The specimen parameters and the resulting operational predictions are given in Table 2.3. The thermal conductivity of the individual Li_2ZrO_3 pebbles (k_{sphere}) was taken from the data for 80% TD polycrystalline Li_2ZrO_3 obtained by Hollenberg and Baker (1982) and Kennedy et al. (1986). The data were interpolated to the anticipated experimental conditions using the expression of Billone et al. (1993).

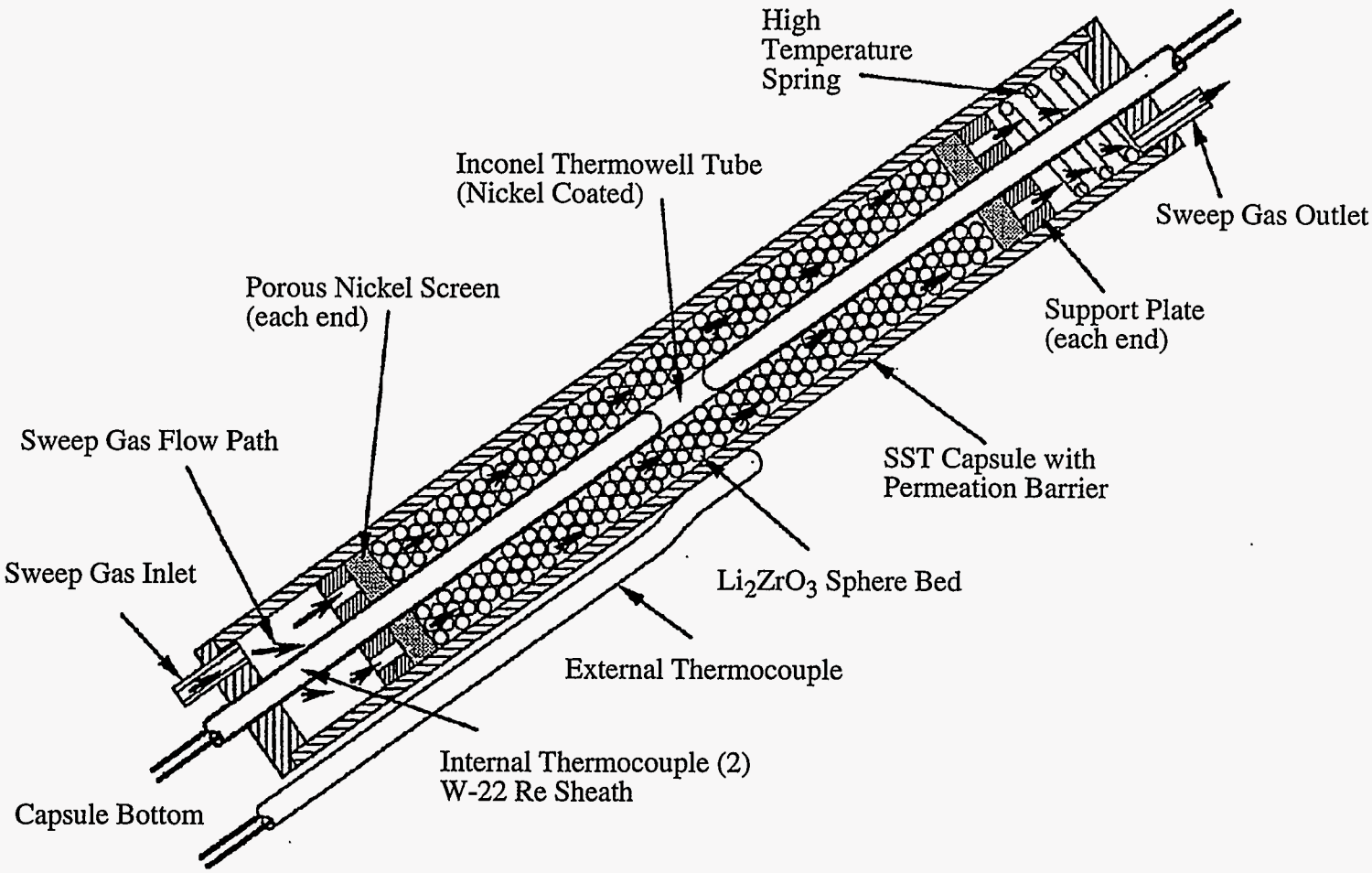

Figure 2.4. Schematic Diagram of the Temperature-Gradient Canister for BEATRIX-II, Phase II

Table 2.3. Predicted Thermal and Neutronic Performance of the BEATRIX-II Li_2ZrO_3 Pebble-Bed Temperature-Gradient Canister

Thermal Heat Generation	27.3 W/gm
Properties of the Pebble Bed	
Pebble Diameter	1 to 1.5 mm
^6Li Enrichment	85 at %
Pebble Matrix Density	80% TD
Pebble Packing Density	60% TD
Outer Diameter	1.32 cm
Inner Diameter	0.23 cm
Specimen Length	10.34 cm
Specimen Centerline Temperature	1095 ± 65°C
Tritium Generation (203 EFPD)	560 Ci
Total Lithium Burnup	6.0 Atom %

$$k_{sphere} = (1-p)^{5/3}\left(\frac{3.643}{(1 + 0.001549\,T)} + 7.579 \times 10^{-10}\,T^3\right) \qquad (2.1)$$

where p is the fractional porosity of the pebbles, in this case 20%, and T is temperature. The thermal conductivity of the predominantly helium sweep gas was calculated from the following expression from Gandhi and Saxena (1968):

$$k_g = 3.36 \times 10^{-3}\,T^{0.688} \qquad (2.2)$$

Packing tests were performed using a plexiglas model of the capsule, employing both steel and zirconia spheres. It was found that both sphere types packed to a packing fraction of 60% in this geometry.

The thermal conductivities of the packed bed were calculated using the model proposed by Hall and Martin (1981). The results of these calculations indicated that for a canister inner diameter of 33.5 mm, a centerline temperature of 1095 ± 65°C would be expected. The uncertainties include both thermal conductivity and neutronic heating.

The calculated tritium generation for the temperature-gradient canister during the 300 EFPD cycle was 828 Ci. This tritium production was less than one-fourth the tritium generated in the Phase I Li_2O solid specimen. The factors tending to increase the tritium production, such as higher neutron flux and ^6Li enrichment, were not sufficient to offset the smaller volume and lower lithium density in the Li_2ZrO_3 pebble bed. However, the tritium generation rate was only slightly less than that of the temperature-change capsule, and it was adequate to allow characterization of the tritium recovery from the temperature-gradient canister during the Phase II irradiation.

2.2.4 Specimen Fabrication/Loading

The Li_2ZrO_3 pebbles are shown in Figure 2.5(a) as received from AECL Research before loading. The diameters of the slightly nonspherical Li_2ZrO_3 pebbles fell approximately in the range of 1 to 1.5 mm with a nominal diameter of 1.2 mm. Figure 2.5(b) shows the top of the pebble bed as loaded into the temperature-gradient canister. This view gives an indication of the pebble diameters

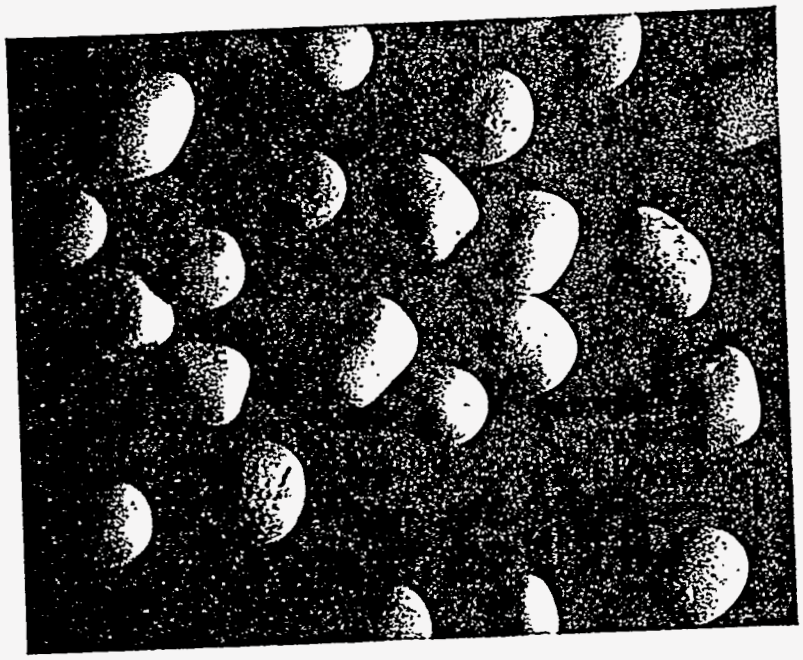

(a)

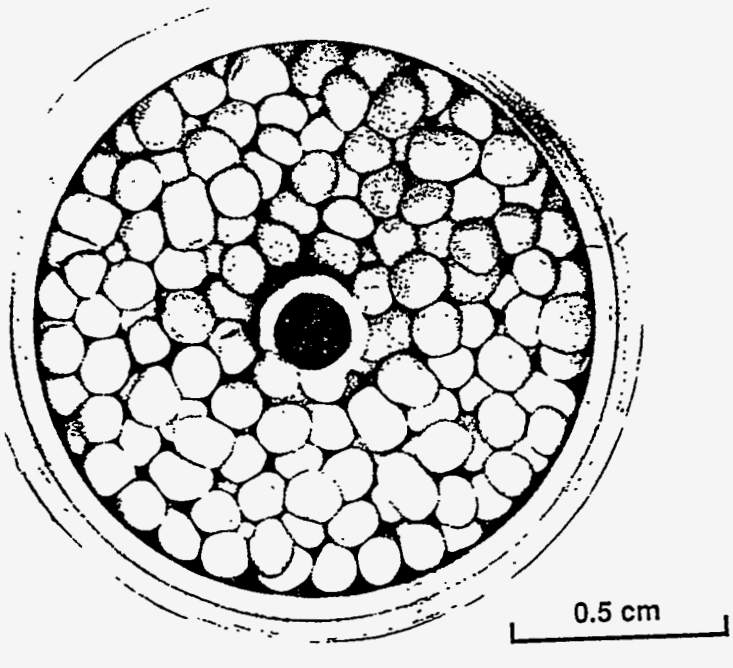

(b)

Figure 2.5. . Li_2ZrO_3 Pebbles (a) As-Fabricated by AECL and (b) As-Loaded in the Temperature-Gradient Canister

relative to the capsule dimensions. The center tube is the thermal well into which the upper thermocouple was inserted to complete the assembly.

The pebble porosity was characterized by a mercury porosimeter analysis. The density of the individual pebbles was 80 to 82% TD, indicating a total porosity of 18 to 20%. Approximately 4.5% of the porosity was closed. Open porosity was found to be in the range of 0.03 to 2.0 μm. Two scanning electron microscope (SEM) microstructures (see Figure 2.6) of a fracture surface in an individual Li_2ZrO_3 pebble indicates that the grain size was approximately 10 μm with an intergranular porosity consistent with the 2-μm upper limit determined from the porosimetry results.

The capsule was loaded by vibrating 29.47 g of pebbles into a volume of 13.75 cm^3. The resultant density was 2.143 g/cm^3 indicating a packing density of 63%. The density of the individual pebbles was 82% TD (TD = 4.112 g/cm^3). The higher density of Li_2ZrO_3 in the capsule compared to the design density was predicted to not significantly change the resulting temperature distribution. The increase in heat generation from the higher ^6Li loading was offset by the anticipated increase in thermal conductivity. The centerline temperatures observed during the irradiation testing served as a check on the effect of this increased packing density and on the assumptions made in the design calculations.

Figure 2.7 is an x-ray radiograph of the final assembled canister. The pebble-bed nature of the specimen and the size of the pebbles relative to the total pebble-bed dimension can be seen. Because of the small size and brittle nature of the W-Re thermocouple sheath, the alignment of the thermocouples relative to the end caps was a very critical operation to ensure that the thermocouple sheathes remained intact during assembly.

For the temperature-gradient canister, the diameter of the specimen was constrained by the comparatively low thermal conductivity of the Li_2ZrO_3 pebble bed together with the maximum temperature limit. These constraints resulted in the volume of the temperature-gradient specimen being nearly half that of the Li_2O specimen in Phase I. This smaller volume, together with the lower lithium density in a Li_2ZrO_3 pebble bed results in a predicted tritium generation rate that was only 25% of the rate for the Phase I temperature-gradient canister. However, the predicted tritium generation rate was more than adequate to allow characterization of the tritium recovery during the Phase II irradiations.

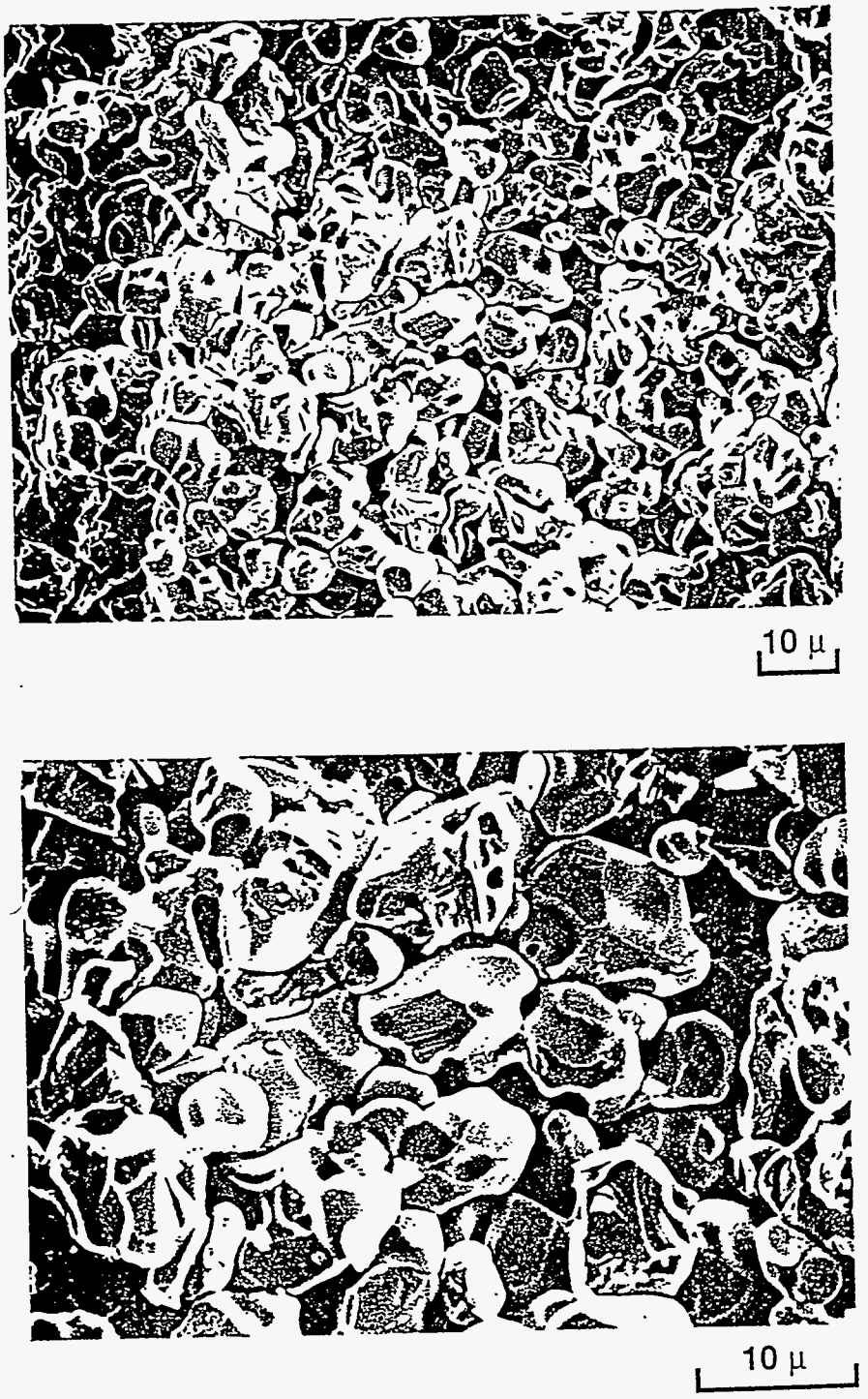

Figure 2.6. SEM Microstructure of a Fracture Surface for the Li_2ZrO_3 Pebbles As-Fabricated by AECL

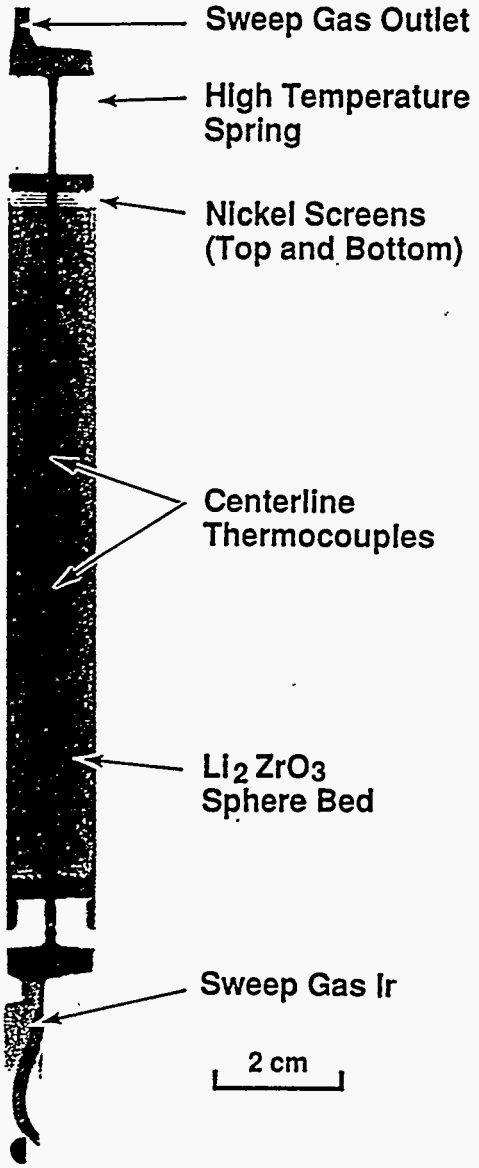

Figure 2.7. X-Ray Radiograph of the Temperature-Gradient Canister As-Fabricated

3.0 Tritium Handling System

The tritium handling system for the BEATRIX-II, Phase II irradiation experiment was the same system used for the Phase I experiment, and the reader is referred to the Phase I Data Summary report for a detailed description (Slagle and Hollenberg 1994). The system was designed to provide on-line measurements of tritium in the sweep gas recovered from either of the two *in situ* vented canisters. Two separate gas-analysis systems were devoted to monitoring the exit sweep gas flow streams from each of the two *in situ* vented canisters. Figure 3.1 is a diagram of the sweep-gas streams from one of the canisters. Each system provided continuous monitoring of the flow rate, total moisture, total tritium concentration, and oxidized tritium concentration. The gas streams from both canisters were combined before reaching the tritium removal system that removed the tritium from the sweep gas before it was released into the environment.

The sweep-gas inlet system provided for the selection of a reference or an alternate sweep gas for each canister. The reference gas for the experiment was helium with 0.1% H_2; the alternative gas was helium with either 0, 0.01, or 1% H_2. After passing through the *in situ* vented canister in the MOTA vehicle, the sweep gas was routed to the tritium glovebox where it entered the respective tritium measurement system (Figure 3.1). The sweep gas from each canister was monitored for moisture and then split into two branches. The reference flow rate was 50 mL/min through either branch for a total flow through the canister of 100 mL/min. One branch flowed through a ceramic electrolysis cell (CEC) that decomposed water vapor, ensuring that all the tritium was in the form of HT rather than HTO. In the other branch, the water vapor was removed using a molecular sieve so that only tritium in the form of HT or T_2 continued in the flow stream. The ion chamber in the CEC gas stream monitored the total tritium concentration recovered from the canister. The ion chamber following the molecular sieve measured the concentration of tritium that was in the reduced or elemental form. The difference in the response of the ion chambers in these two branches indicated the amount of tritium removed by the molecular sieve, i.e., the HTO.

The tritium-removal system was based on tritium getters that were designed to reduce the tritium level in the sweep gas by a factor greater than 4000. This reduction was necessary to achieve tritium levels acceptable for release into the environment. Provisions were made for purging selected regions of the gas handling system with an optional "injection gas"—for example, purging the ion chambers before calibration to accurately determine the background at that time. When sweep gases of helium and 0.01% H_2 were used, an injection gas of 0.1% H_2 was added to the sweep gas before the tritium getter beds to increase the hydrogen concentration. This higher concentration of hydrogen provided "isotopic swamping" and ensured that the tritium getter beds would operate effectively. The glovebox containing the tritium-handling system was located within the FFTF reactor containment on the operating deck.

3.1 Ion Chambers

Ion chambers were used to continuously monitor the tritium concentrations in the sweep gas recovered from the *in situ* canisters. During Phase II, the sweep-gas composition varied from helium to helium with hydrogen concentrations up to 1%. Two ion chambers were in the measurement systems for both temperature-change and temperature-gradient canisters. Although ion chambers were also located at the inlet to the tritium removal system and after the first getter bed, this report will only discuss those four chambers used to record the tritium levels recovered in the four individual streams. During the experiment, several corrections were mathematically applied to the apparent ion-chamber reading, T_{IC}, to obtain the corrected tritium concentration in the sweep gas.

In Phase I, the *in situ* calibrations indicated that the ion chamber response was enhanced when small amounts of hydrogen were added to the helium sweep gas. Because the original calibration curves were done for a helium sweep gas, a discrepancy was found when these calibration curves were used for tritium recovery using the reference sweep gas (0.1% H_2). This discrepancy was not fully resolved during the operation of Phase I, and the following tests were carried out during Phase II to resolve the discrepancy: 1) *in situ* ion chamber calibrations were conducted in both 0.1% H_2 and helium; 2) during the temperature-gradient canister Test Series A2, a helium sweep gas was maintained while injecting specific levels of hydrogen into the sweep gas before entering the ion chamber, and 3) a laboratory experiment was conducted to study the effect of hydrogen additions on

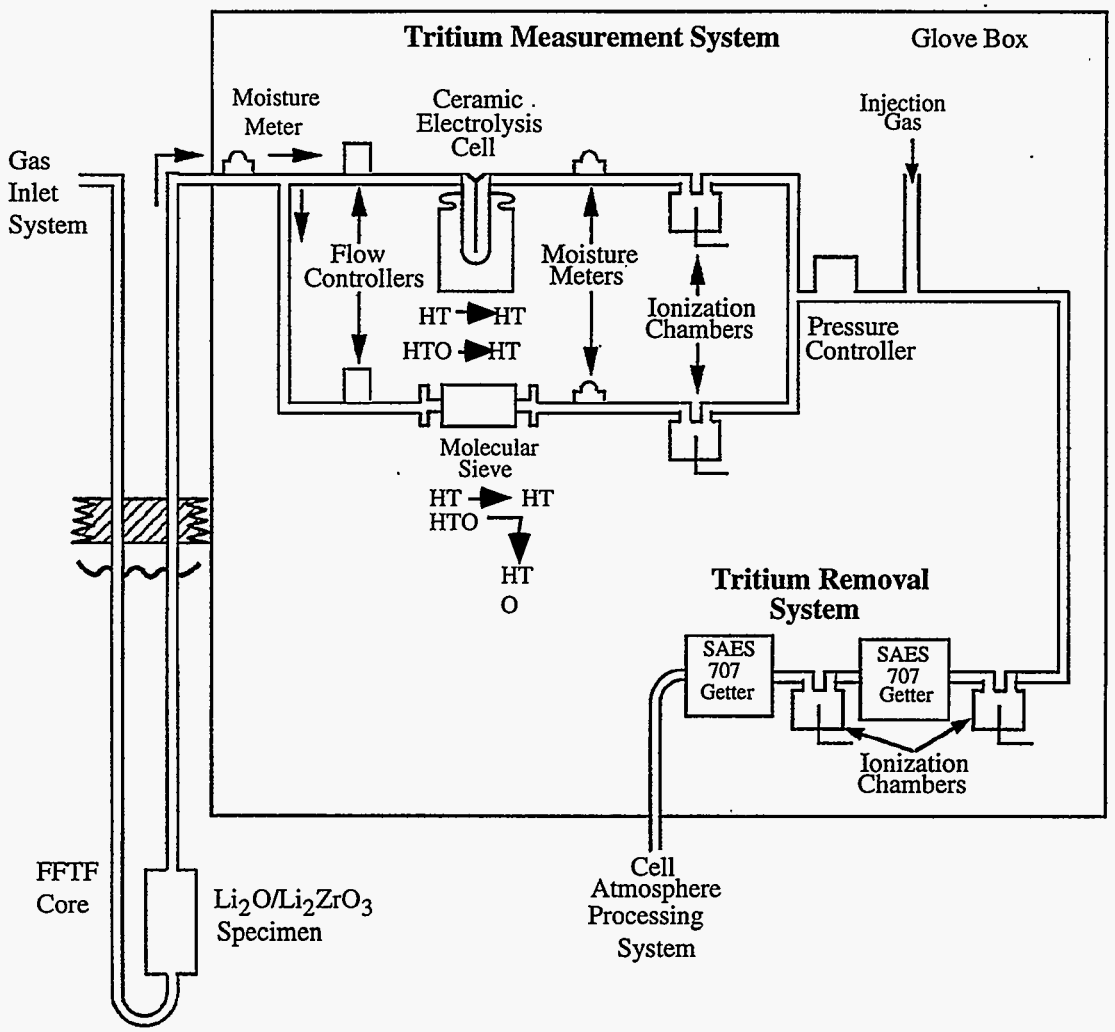

Figure 3.1. Diagram of the Sweep-Gas Stream from One of the *In Situ* Canisters

the response of an ion chamber (Rodrigo and Yin 1993). The results of these tests were used to define a "hydrogen enhancement factor" (F), which was a function of hydrogen additions to the helium sweep gas. This enhancement factor for a given sweep gas composition was defined by

$$F_x = \frac{(\text{ion-chamber response in helium - x\% } H_2)}{(\text{ion-chamber response in helium})} \quad (3.1)$$

The ion-chamber response includes the response from the tritium concentration (T) in the sweep gas plus the ion chamber background (BG). Equation 3.1 becomes

$$F_x = \frac{(T_x + BG_x)}{(T_{He} + BG_{He})} \quad (3.2)$$

3.1.1 *In Situ* Calibration

In situ calibration of the ion chambers during Phase II was carried out both in 0.1% H_2, as was done in Phase I, and also in helium. The procedures were the same as in Phase I (Slagle and Hollenberg 1994) except that in the case of helium, both the specimen sweep gas and the injection gas used to purge the ion chamber were helium. Table 3.1 is a compilation of the results.

Table 3.1. Results for *In Situ* Calibration in 0.1% H_2 and Helium for the Ion Chamber on the CEC Flow Stream from the Phase II Temperature-Change Canister

	0.1% H_2	He
Phase II-A		
Scintillation Analysis (Ci/m^3)	20.00	19.40
Ion-Chamber Reading (Ci/m^3)	36.30	24.20
Ratio (Ion Chamber/Scintillation)	1.82	1.24
Phase II-B		
Scintillation Analysis (Ci/m^3)	29.80	—
Ion-Chamber Reading (Ci/m^3)	36.40	—
Ratio (Ion Chamber/Scintillation)	1.22	—
Phase II-C		
Scintillation Analysis (Ci/m^3)	27.50	19.00
Ion-Chamber Reading (Ci/m^3)	35.90	23.70
Ratio (Ion Chamber/Scintillation)	1.31	1.25
Phase II-D		
Scintillation Analysis (Ci/m^3)	28.70	22.30
Ion-Chamber Reading (Ci/m^3)	34.26	21.71
Ratio (Ion Chamber/Scintillation)	1.19	0.97

The *in situ* calibration results in Table 3.1 lists the 1) tritium concentrations determined from a scintillation analysis of a liquid solution prepared by oxidizing a sample of the sweep gas taken during the calibration and bubbling through water and 2) tritium concentration as read from the ion chamber (uncorrected for hydrogen additions). The ratio of the ion-chamber reading to the scintillation analysis is an indicator of the enhancement in the ion-chamber reading that resulted from adding hydrogen to the sweep gas. From the initial calibration data, it was expected that for 0.1% H_2, the ratio would be 1.3, and for helium the ratio would be 1. For 0.1% H_2, three of the four results were close to 1.3, but the 1.82 value of Phase II-A was much too large. For helium only the Phase II-

D result of 0.97 was close to 1 with the other two values being closer to 1.3 than 1. The results indicate difficulties associated with *in situ* calibration. The 1.82 ratio for Phase I-A may be an experimental error. The larger ratio values for helium were attributed to difficulties associated with the slow response of the system to pure helium with no hydrogen additions.

3.1.2 Sweep Gas Composition Effect on Ion chamber Response (*In Situ* Data)

During Phase I, substantial evidence was obtained that ion-chamber response was affected by sweep-gas composition. Test Series A2 on the temperature-gradient canister was carried out to quantify the enhancement of ion-chamber response by additions of hydrogen. The test was described previously by Slagle et al. (1992) and in the Phase I Data report because they were used to explain the correction procedures used in Phase I. The results of the test will be summarized in this report. The sweep gas through the temperature-gradient canister during the test was helium, and it was assumed that the tritium concentration in the sweep gas coming from the canister remained constant. An injection gas of 1% H_2 was added to the helium sweep gas after the specimen canister, but ahead of the ion chamber, to give successively higher levels of hydrogen in the sweep gas through the ion chamber. The response of the ion chamber was observed at various levels of hydrogen concentration from 0.05 to 0.5% H_2 and a return to helium. From the ion chamber response, hydrogen enhancement factors (F_x) were calculated and are listed in Table 3.2 for 100% power.

A test series similar to Test Series A2 was carried out during the time when the reactor was shut down between Phase II-A and II-B. Since the tritium concentration was zero, the ion-chamber response reflected changes in the ion-chamber background. Variations in the ion-chamber background with changes in hydrogen concentration were used to calculate hydrogen enhancement factors that are listed in Table 3.2 for 0% power. The close agreement of the enhancement factors for 100% and 0% power suggest that the enhancement factors apply both to the response of the ion chamber to tritium in the sweep gas and to the background.

3.1.3 Sweep Gas Composition Effect on Ion-Chamber Response (Laboratory Experiment)

Rodrigo and Yin (1993) at AECL Research conducted a series of experiments to investigate the effect of various impurities on ion-chamber response. They found that adding hydrogen to a helium sweep gas increases the response of an ion chamber, and for hydrogen concentrations of 0.01%, 0.1%, and 1.0%, the enhancement was determined to be 1.10, 1.31, and 1.43, respectively. Rodrigo and Yin's experimental results supplied a fundamental understanding of the effects observed in the BEATRIX-II system and provided justification for using hydrogen-enhancement factors to correct the ion-chamber response in different sweep gases.

Because of the measurements during the BEATRIX-II experiment and the results of Rodrigo and Yin, a decision was made to use hydrogen enhancement factors to correct the BEATRIX-II *in situ* tritium-recovery data for operation in sweep gases containing hydrogen additions. These correction factors apply to the ion-chamber response both for the tritium in the sweep gas and the effect of the ion-chamber background. For 0.1% H_2, a value of 1.3 was chosen as a compromise between Rodrigo and Yin's result, the Phase I results (Slagle and Hollenberg 1994), the results in Table 3.2, and the ion-chamber calibrations in Table 3.1. For 0.01% H_2, their value of 1.1 was considered to be more accurate than the 1.04 factor obtained in Phase I (Slagle and Hollenberg 1994), and the factor of 1.1 was adopted for 0.01% H_2. For 1.0% H_2, a value of 1.43, from the data of Rodrigo and Yin, was rounded to 1.4.

Table 3.2. Hydrogen Enhancement Factors Determined from Test Series A2 for the Temperature-Gradient Canister

Hydrogen Additions (%)	Enhancement Factors 100% Power	0% Power
0	1.00	1.00
0.05	1.27	1.20
0.10	1.29	1.30
0.20	1.34	1.37
0.50	1.42	1.44
0	0.97	1.00

3.1.4 Enhancement-Factor-Correction Relationship

The effect of sweep-gas composition on the response of the ion chamber was taken into account using the same expression used in Phase I. Equation 3.2 can be rearranged to give

$$T_{He} = \frac{(T_x + BG_x)}{F_x} - BG_{He} \tag{3.3}$$

To be consistent with the Phase I Data Summary Report, the total tritium concentration indicated by the ion chamber in a sweep gas of x% H_2 is denoted as T_{IC}. That is

$$T_{IC} = T_x + BG_x \tag{3.4}$$

Equation 3.3 then becomes

$$T_{He} = \frac{T_{IC}}{F_x} - BG_{He} \tag{3.5}$$

Because the ion chamber was calibrated in a helium sweep gas, the tritium concentration in a helium sweep gas (T_{He}) is the corrected tritium concentration in the sweep gas. Equation 3.5 is identical to Equation 3.5 in the Phase I Data Summary Report (Slagle and Hollenberg 1994).

3.1.5 Ion-Chamber Background Correction

At the start of the Phase II *in situ* testing, significant ion-chamber background levels remained from the Phase I testing. During the 300 EFPD operation of Phase I, the ion-chamber backgrounds (BG_x) reached levels as high as 45% of the total response of the ion chamber. A method was developed for correcting the Phase I ion-chamber response for changes in background. All of the BEATRIX-II, Phase II tritium recovery data were corrected for sweep-gas composition and ion-chamber background using the same technique described in the Phase I Data Summary Report (Slagle and Hollenberg 1994). The Phase II correction was done in combination with the data compilation discussed in Section 5 and Appendix B.

In the background correction process, a set of procedures to derive an equivalent ion-chamber background in helium (BG_{He}) was developed (Equation 3.5). During times when the tritium concentration through the ion chambers (T_{He}) was known to be zero, the background (BG_{He}) was set equal to the ion chamber reading corrected for the sweep gas enhancement (T_{IC}/F_x). At other times in the experiment when the background was not zero, but could be expected to change, an

alternative method was used. During these times, the background was established by comparing the concentration of recovered tritium (T_{He}) under reference conditions (0.1% H_2 sweep gas, 100 mL/min flow rate, and the temperature-change specimen at 640°C) to the tritium concentration in the sweep gas that would be recovered due to the expected generation of tritium in the specimen.

Deriving the ion-chamber backgrounds then becomes a problem of calculating the expected generation for the specimen. We define the generation concentration (G) to be the tritium concentration in the recovered sweep gas due to the generation rate in the specimen (at a reference flow rate of 100 mL/min). During ion-chamber calibration, BG_{He} was determined by purging the ion chamber, and the tritium concentration in the sweep gas is assumed to equal the generation concentration. The tritium recovery concentration at calibration (for a flow rate of 100 mL/min) was set equal to the generation concentration at the time of the calibration, G_C. At times of ion chamber calibration,

$$G = G_C = T_{He} \tag{3.6}$$

The generation concentration for other times in the irradiation cycle was calculated from the generation concentration at calibration, G_C, by the following relationship:

$$G = N \bullet BU \bullet G_C \tag{3.7}$$

where N is a correction for the relative neutron flux as determined from the response of a self-powered neutron detector (SPND) located in the region of the canister, and BU is a factor that accounts for the burnup of lithium. Equation 3.7 is the same as Equation 3.6 in the Phase I Summary Data Report. The notation for the generation concentration (G_{Ex}) in the Phase I report was changed to G in this report. The change was made to clarify the description of how the correction was made.

Because the self-powered neutron detector in Phase II was not operative, temperature variations in the temperature-gradient specimen were used to account for variations in flux level. For small changes in power generation, heat generation in the solid specimen is proportional to the temperature difference across the solid specimen (ΔT_s). The heat generation in the solid specimen was proportional to the relative flux level (ϕ) and lithium enrichment (E). This gives a relationship:

$$\Delta T_s \propto \phi \bullet E \tag{3.8}$$

Rearranging we have:

$$\phi \propto \frac{\Delta T_s}{E} \tag{3.9}$$

The relative flux ϕ was used to establish the ion-chamber background as described above.

3.2 Moisture Meters

The sweep gas from each *in situ* canister was first monitored for moisture content when it reached the tritium-handling system (see Figure 3.1). The accuracy of the moisture meters at installation, before Phase I, was $\pm$ 1 ppm with a resolution limit of 0.01 ppm. At the start of the Phase II irradiation, both moisture meters registered significant levels of moisture consistent with off-gassing during heatup to the operating temperature. After an initial peak of 2300 ppm, the indicated moisture from the meter on the Phase II temperature-gradient-canister sweep gas went to zero. Following parameter changes where moisture peaks were observed in Phase I, such as increasing hydrogen concentration in the sweep gas, very small peaks were observed. These peaks were

typically 0.01 to 0.03 ppm where 0.01 ppm is the detection limit. The moisture levels recorded for the Phase II temperature-change canister were similar to the Phase I temperature-change canister operation, and after an initial 5500-ppm peak, peaks after transient changes were on the order of several ppm.

The low moisture levels for the Phase II temperature-gradient canister are of concern if they indicate that the moisture meter for the Phase II temperature-gradient canister was not operating correctly. Although the moisture meters can be expected to decalibrate over time, the meter on the Phase II temperature-gradient-canister flow stream appeared to operate correctly during the startup. Hence, it is likely that the low moisture levels are indicative of low moisture levels in the sweep gas from this canister.

3.3 Ceramic Electrolysis Cell

The function of the ceramic electrolysis cells was to decompose the water in the sweep gas to HT, H_2, and T_2 using a solid ceramic electrolyte of yttria-stabilized zirconia. The solid electrolyte operated at a temperature of 600°C with a nominal voltage bias of 1.6 volts to remove oxygen out of the sweep gas stream.

During Phase II, the operation of the CEC on the temperature-change-canister flow stream was interrupted after 11 days of operation. On June 7, 1991, a loss of current indicated that the CEC had failed. The power to the cell was immediately turned off. After a delay of approximately one-half hour, power was restored. The cell resumed operation, and no further problems concerning the operation of the cell were experienced during Phase II.

4.0 Experiment Operation

The operation of the BEATRIX-II experiment in the FFTF was conducted primarily by WHC. The operational activities included the initial setup, operation in the FFTF, removal of the canisters from the MOTA vehicle, and delivery of the canisters to PNNL in the 324 Building hot cells. PNNL interfaced with WHC, the BEATRIX-II experimenters, and the BEATRIX-II Working Group to coordinate the experiment and, in particular, to define the experimental requirements and test matrices. In addition, PNNL developed test plans, monitored the experimental operation, compiled/analyzed the data, executed the postirradiation examination, and distributed the data to the BEATRIX-II participants and the BEATRIX-II Modelers and Code Developers (see Section 7).

4.1 Installation in FFTF

Installation of the out-of-reactor BEATRIX-II apparatus in the FFTF was carried out before Phase I. The Phase II design was established at the Final Design Review in September 1990, and fabrication of the canisters was initiated at that time. The finished canisters were installed on the MOTA-2B vehicle in March 1991. The vehicle was inserted into the reactor in May 1991, and reactor startup occurred on May 25, 1991.

4.2 Experimental Test Plan

The operation of the experiment was defined by a test plan that was established before the start of each reactor operation cycle. The test plan was prepared by the BEATRIX-II experimenters with additional input solicited during BEATRIX-II working group and experimenters' meetings. The test plan established at the start of each reactor cycle was continuously modified, based on the results of the experiments. The test plan specified temperature, sweep-gas compositions, flow rate, ion-chamber purges/calibrations, and startup/ shutdown procedures. The design of the inlet gas system limited the system to only one alternative sweep gas (helium, 0.01% H_2, or 1.0% H_2) at a time. To limit the tritium concentration in the sweep gas arriving at the tritium recovery system, situations were avoided in which large tritium recovery peaks could be expected to occur simultaneously from both specimens.

The BEATRIX-II experimental test plan was based on a rapid change of selected system parameters, i.e., temperature, sweep-gas flow rate, and sweep-gas composition) with subsequent monitoring of the resultant transients in tritium recovery. These changes were completed in logical sets that were designed to efficiently use the available irradiation time (203 EFPD) and yet provide systematic data for analysis. A detailed record of the experiment was compiled in the experimenter's log, which was a chronological record of the parameter changes that were made during the operation of the experiment. The experimenter's log for Phase II is included in Appendix A. Individual parameter changes in this report are referenced using the parameter change numbers (PCN) in Appendix A. Descriptive overviews of the test plans for the Phase II temperature-change and temperature-gradient specimen are given in Tables 4.1 and 4.2. These tables describe changes in operating parameters away from parameters for operation in the reference condition. The reference sweep-gas conditions are a helium sweep gas with a 0.1% addition of hydrogen and a flow rate of 100 mL/min. The reference temperature for the temperature-change specimen is an inner temperature of 640°C. The relationship of Tables 4.1 and 4.2 to the experimenter's log in Appendix A is indicated by including the PCN from Appendix A in brackets, [], in Tables 4.1 and 4.2.

Table 4.1. Test Plan Overview for BEATRIX-II, Phase II, Temperature-Change Canister. (Sweep gas composition changes are from the reference sweep of 0.1% H_2. Numbers in Brackets [] refer to PCN in Appendix B.)

Phase II-A May 27, 1991, to July 20, 1991 (52.8 EFPD)

- A1. Temperature Transients in 0.01% H_2 [11-13] 640-590-530-640°C
- A2. Ion-Chamber Calibration in Helium and 0.01% H_2 [14-21]
- A3. Temperature Transients in 0.01% H_2 [22-28] 640-590-530-640°C
- A4. Temperature Transients in 0.01% H_2 [31-33] 640-590-530-640°C
- A5. Temperature Transients in Helium [36-39] 640-590-530-640°C
- A6. Temperature Transients in 0.01% H_2 [43-45] 640-590-530-640°C

Phase II-B July 30, 1991, to September 21, 1991 (48.6 EFPD)

- B1. Burnup Effect [57-61]. Reference Sweep-Gas Conditions 640-590-530-640-530-640°C
- B2. Sweep-Gas Composition Effect at 640°C
  1) 2 days Helium, 2 days 0.01% H_2 [62-65]
  2) 4 days Helium, 2 days 0.01% H_2 [66-68]
  3) 8 days Helium, 2 days 0.01% H_2 [70-74]
- B3. Ion-Chamber Calibration in 0.01% H_2 [76-79]
- B4. Shutdown in He

Phase II-C November 21, 1991, to January 14, 1992 (50.3 EFPD)

- C1. Startup in Helium
- C2. Ion Chamber Calibration in Helium and 0.01% H_2 [106-111]
- C3. Sweep Gas Composition Effect at 530°C
  1) 2 days Helium, 2 days 0.01% H_2 [113-115]
  2) 4 days Helium, 2 days 0.01% H_2 [117-119]
  3) 2 days 0.01% H_2, 4 days Helium, [120-123]
- C4. Burnup Effect [128-132]. Reference Sweep Gas Conditions 640-590-530-640-530-640°C

Phase II-D January 29, 1992, to March 19, 1992 (51.6 EFPD)

- D1. Ion-Chamber Calibration in Helium and 0.01% H_2 [137-141]
- D2. Temperature Transients (640-590-530-640-530-640°C)
  1) 0.01% H_2 Sweep Gas [143-151]
  2) Helium Sweep Gas [154-159]
- D3. Burnup Effect [166-170]. Reference Sweep Gas Conditions 640-590-530-640-530-640°C

Table 4.2 Test Plan Overview for BEATRIX-II, Phase II, Temperature-Gradient Canister. (Sweep gas composition changes are from the reference sweep gas of 0.1% H_2. Numbers in Brackets [] refer to PCN in Appendix B.)

Phase II-A May 27, 1991, to July 20, 1991 (52.8 EFPD)

- A1. Sweep Gas Flow Test: 200 mL/min [18-21]
- A2. Effect of Sweep-Gas Composition on Ion-Chamber Behavior [22-28]
- A3. Sweep-Gas Composition Effects
  1) 2 days in 0.01% H_2 [34-35]
  2) 2 days in He [38-40]

Phase II-B July 30, 1991, to September 21, 1991 (48.6 EFPD)

- B1. Sweep-Gas Composition Effects
  1) 4 days in 0.01% H_2 [63-65]
  2) 4 days in Helium [66-67]
  3) 8 days in Helium [69-71]
- B2. Effect of Sweep-Gas Flow Rate on Ion-Chamber Behavior [73-77]
- B3. Ion-Chamber Purges [80-81]
- B4. Shutdown in He

Phase II-C November 21, 1991, to January 14, 1992 (50.3 EFPD)

- C1. Startup in Helium
- C2. Sweep-Gas Flow Test: 200 mL/min [108-111]
- C3. Sweep-Gas Composition Effect
  1) 2 days Helium, 2 days 0.01% H_2 [113-115]
  2) 4 days Helium, 2 days 0.01% H_2 [117-119]
  3) 2 days 0.01% H_2, 2 days Helium, [120-122]
- C4. Ion-Chamber Purges [129-130]

Phase II-D January 29, 1992, to March 19, 1992 (51.6 EFPD)

- D1. Sweep-Gas Flow Test: 200 mL/min [139-141]
- D2. Ion-Chamber Purges [145-149]
- D3. Sweep-Gas Flow Test: 50 mL/min [152]
- D4. Sweep-Gas Composition Change: 1% H_2 [162-163]

Parameter-change sequences are denoted by using the number sequences from the Tables 4.1 and 4.2. For instance, Test Series B2.3 of the temperature-change canister refers to the Phase II-B Test Series described as

B2. - Sweep-Gas-Composition Effect at 535°C
B2.3. - 8 days helium, 2 days 0.01% H_2.

This test is described in the Phase II experimenter's log by PCN 70 to PCN 74. The test plans for each of the four cycles are also illustrated graphically in Appendix B where plots of tritium recovery data and temperature include labels indicating sweep-gas composition for each of the two canisters.

4.2.1 Temperature-Change Canister

The initial test series in Phase II-A was a series of temperature transients in the reference sweep gas, 0.1% H_2. The temperature sequence was in the order of 640-590-530-640°C. This series established the shape of the recovery peaks after a temperature-change characteristic of the start of the experiment. Test Series A2 was the calibration of the ion chamber on the CEC flow stream in both helium and 0.01% H_2. Calibration in both gases was done to establish the difference in response of the ion chamber in the two different gases. The results of these tests were used to derive the enhancement factors for each sweep gas that were then used to correct the data. Test Series A3 to A6 was a systematic series of temperature transients (640-590-530-640°C) carried out in the three different sweep gases: 0.01% H_2, 0.01% H_2, and helium. The test series in 0.1% H_2 was repeated at the end to determine if changes in specimen response had occurred during irradiation.

The first test series in Phase II-B was a temperature-transient series in the reference gas that was identical to the series used in Phase I to monitor the change in behavior with burnup. The temperature transients (640-590-530-640-530-640°C) were similar to that used in Phase II-A with the addition of a 640-530-640°C series at the end. Test Series B2 addressed the effect of sweep-gas composition changes for a specimen temperature of 640°C. The tests all began in 0.1% H_2 with a transition to helium. The time duration in helium varied, starting at 2 days and increasing to 4 days and then 8 days. After helium, the sweep gas was changed to 0.1% H_2 for 2 days before returning to 0.1% H_2 to end the test. Test Series B3 was a series of operations to calibrate the ion chamber on the CEC flow stream in a 0.1% H_2 sweep gas. Because of the limited time remaining in the cycle, the calibration was not able to be carried out in helium. Test Series B4 involved changing the sweep gas to helium two days before the end of Phase II-B so that the shutdown behavior in helium could be recorded.

The startup of Phase II-C was carried out in helium as a continuation of the shutdown of Phase II-B. Test Series C2 was the calibration of the ion chamber on the CEC flow stream in both helium and 0.1% H_2 identical to Test Series A2. Test series C3 addressed the effect of sweep-gas composition changes for a specimen temperature of 530°C. The first two tests began in 0.1% H_2 with a transition to helium. The time duration in helium was 2 days for Test C3.1 and 4 days for Test C3.2. After helium, the sweep gas was changed to 0.1% H_2 for 2 days before returning to 0.1% H_2 to end the test. Test C3.3 reversed the sequence of helium and 0.01% H_2, starting with 2 days in 0.01% H_2 and switching to 4 days in helium. Test Series C4 was a temperature transient series (640-590-530-640-530-640°C) in the reference gas to monitor the change in behavior with burnup.

Phase II-D started with the calibration of the ion chamber on the CEC flow stream in both helium and 0.1% H_2 as was done in Phase II-A and C. The temperature transient series (640-590-530-640-530-640°C) was carried out in 0.1% H_2 and helium in Test Series D2 with a return to 0.1% H_2 for Test Series D3. Final shutdown was in 0.1% H_2.

4.2.2 Temperature-Gradient Canister

In Phase II-A, the initial Test Series, A1, for the operation of the temperature-gradient canister in Phase I-A involved increasing the flow rate from 100 to 200 mL/min. The increase in flow rate through the temperature-gradient canister coincided with the calibration of the temperature-change canister in a helium sweep gas. This flow rate increase through the temperature-gradient canister was used to increase the hydrogen in the sweep gas to the tritium recovery system. Normally when helium sweep gas was used, additional 0.1% H_2 sweep gas was introduced into the tritium recovery system using a provision for introducing an injection gas. During the calibration in helium, the injection-gas system was used for purging the ion chamber with helium and therefore was not available to introduce 0.1% H_2 into the tritium recovery system. Test Series A2 was designed to introduce a sequence of sweep gases with varying levels of hydrogen into the ion chamber while

maintaining a known amount of tritium in the sweep gas. These data were used to determine the response of the ion chambers to tritium for different levels of hydrogen additions. Test Series A3 addressed the effect of changing sweep-gas composition on the tritium recovery behavior. Test Series A3.1 changed from 0.1% H_2 to 0.01% H_2 for 2 days before returning to 0.1% H_2 while the Test Series A3.2 changed from 0.1% H_2 to helium for 2 days before returning to 0.1% H_2.

In Phase II-B, the Test Series B1 extended the times for alternative sweep-gas additions. Test Series B1.1 changed from 0.1% H_2 to 0.01% H_2 for 4 days before returning to 0.1% H_2 while the Test Series B1.2 and B1.3 changed from 0.1% H_2 to helium for 4 and 8 days, respectively, before returning to 0.1% H_2. Test Series B2 addressed the question of flow-rate effects on ion-chamber operation by changing the relative distribution of the flow rate between the ion chambers on the CEC and molecular-sieve flow streams. In Test Series B3, the ion chambers on both the CEC and molecular-sieve flow streams were purged to reduce and establish backgrounds. Two days before shutdown, the sweep gas was changed to helium (Test Series B4) to determine the effect of helium sweep gas on the tritium recovery during a reactor shutdown.

The startup of Phase II-C was a continuation of the shutdown of Phase II-C in that it was carried out in a helium sweep gas. Test Series C2 was a flow test similar to Test Series A1 in which the flow rate was increased to the temperature-gradient canister to compensate for the helium purge/calibration of the temperature-change ion chamber. Test Series C3 addressed the effect of sweep gas composition changes with all tests beginning and ending in 0.1% H_2. Test Series C3.1 and C3.2 began with a change to helium with respective durations of 2 and 4 days. The helium sweep gas was then changed to 0.1% H_2 for 2 days before returning to 0.1% H_2 to end the test. Test Series C3.3 began with a change to 0.1% H_2 for 2 days and then a change to 0.1% H_2 for 2 days before returning to 0.1% H_2 to end the test. In Test Series C3, the ion chambers on both the CEC and molecular-sieve flow streams were purged to reduce and establish backgrounds.

At the start of Phase II-D, Test Series D1 was a flow test similar to Test Series A1 in which the flow rate was increased to the temperature-gradient canister to compensate for the helium purge/calibration of the temperature-change ion chamber. In Test Series D2, the ion chambers on both the CEC and molecular-sieve flow streams were purged to reduce and establish backgrounds. Test Series D3 involved a change in sweep-gas flow rate to 50 mL/min to aid in locating a leak in the tritium recovery system in the glovebox. Test Series D4 was a change in sweep-gas composition from 0.1% to 1% H_2 for 1 day and then a return to 0.1% H_2.

4.3 Data Acquisition/Compilation

The experiment was continuously monitored in the FFTF using the BEATRIX-II data acquisition system (DAS) that recorded the specified data channels and, in addition, provided operational information for assessing the performance of the test equipment. The DAS was in direct communication with the reactor control room, and an alarm signal was activated if selected signals exceeded specified limits. Figure 4.1 is a diagram of the flow path of the data. A total of 59 data channels were monitored by the DAS during the experiment. The continuously monitored data set was compiled on a data disc at the FFTF site. When the disc was full, or at shorter intervals if requested by the experiment coordinator (PNNL), the disc was removed from the DAS and processed. The complete set of 59 channels in time intervals as short as 10 seconds was converted to specified experimental units and retained as the complete operational database at WHC.

Twenty-six channels of data were designated as the prime data set on the basis that they were the data that were specifically needed to characterize the behavior of the solid-breeder specimens. The prime data set and the units in which they were supplied are given in Table 4.3. The prime data set was normally transferred from WHC to PNNL in time increments of 2 minutes, although shorter intervals were supplied when requested. At PNNL, the prime data set was used to generate the more

concise experimental database and a series of data plots. The experimental database was distributed to the BEATRIX-II experimenters. The data plots were used as the basis for evaluating the progress of the experiment and for formulating future test plans. The Phase II experimental database consisted of 45 individual LOTUS 123 data files, each about 5 to 8 days. The PNNL experimental database was used to generate the final corrected/compiled databases for the temperature-change and temperature-gradient databases.

Because of the complexity of the database, an overall compilation of the experimental database was carried out to create a manageable set of data that could be used by modelers and code developers needing access to the information. To facilitate this compilation, the experimental database was reduced by one third by increasing the time interval between data points from 2 minutes to 6 minutes. The original 26 prime data channels were reduced to 20 channels based on which channels were most important for understanding the tritium-release behavior of the solid breeder. The database was then divided into individual databases for the temperature-change and the temperature-gradient canisters. The resulting compiled spreadsheets for the individual canisters are

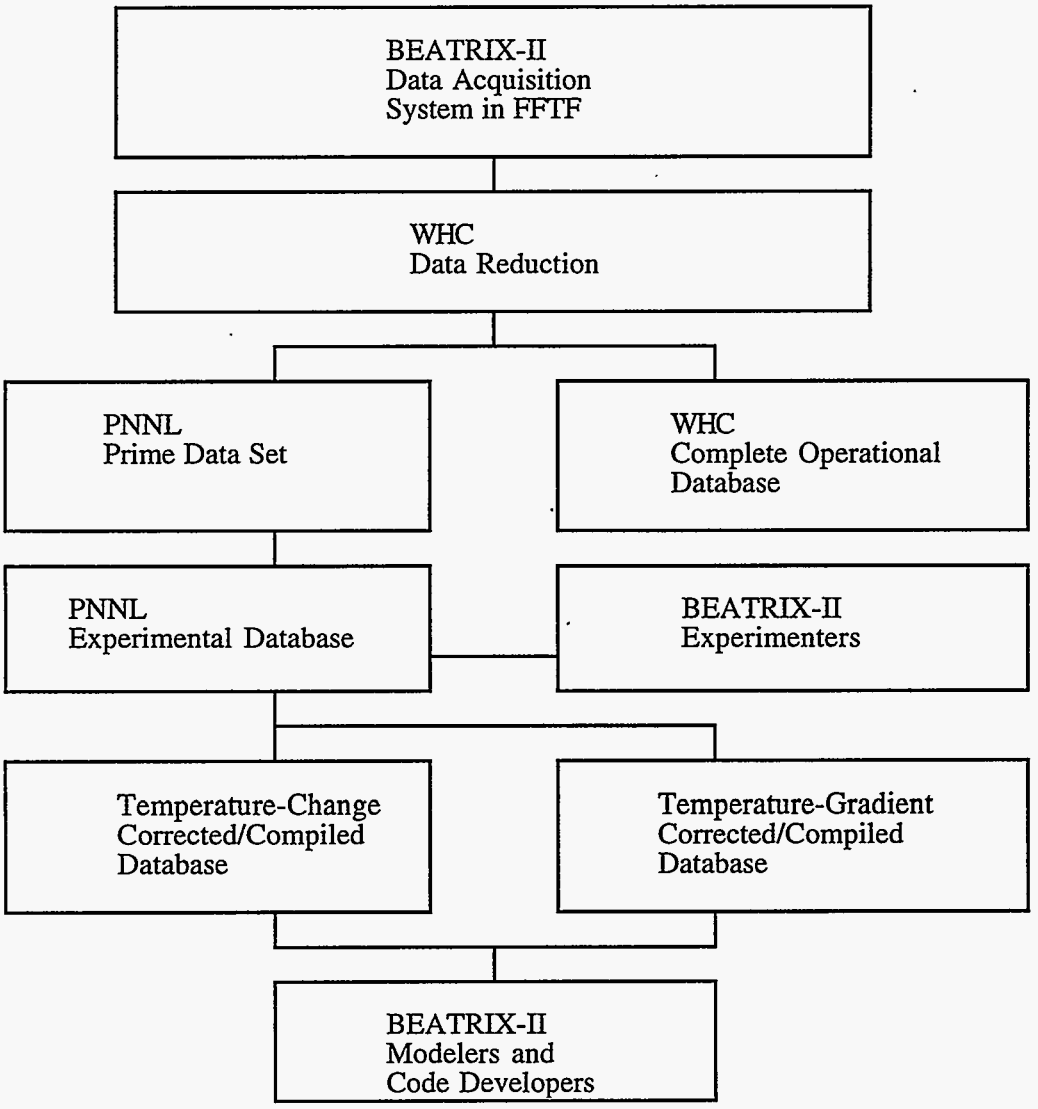

Figure 4.1. Flowpath for BEATRIX-II Data

Table 4.3. Prime Data Set for BEATRIX-II, Phase I

Channel	Units	Description
1	atm	Ring-specimen inlet gas pressure
2	atm	Solid-specimen inlet gas pressure
3	ppm	Reference-gas inlet moisture
4	ppm	Alternate-gas inlet moisture
5	ppm	Ring-specimen sweep-gas moisture
8	ppm	Solid-specimen sweep-gas moisture
11	atm	Ring-specimen sweep-gas pressure
12	atm	Solid-specimen sweep-gas pressure
17	cc/min (STP)	Ring-specimen injection sweep-gas flow
18	cc/min (STP)	Ring-specimen sweep-gas flow, CEC
19	cc/min (STP)	Ring-specimen sweep-gas flow, MS
20	cc/min (STP)	Solid-specimen injection sweep-gas flow
21	cc/min (STP)	Solid-specimen sweep-gas flow, CEC
22	cc/min (STP)	Solid-specimen sweep-gas flow, MS
35	Relative Intensity	Self-powered neutron detector
43	°C	Glovebox Temperature
44	°C	Solid-specimen outer temperature
45	°C	Solid-specimen center temperature - top
46	°C	Solid-specimen center temperature - bottom
47	°C	Ring-specimen outer temperature
48	°C	Ring-specimen inner temperature, CEC
49	°C	Ring-specimen inner temperature, MS
1001	Ci/m^3	Ring-specimen sweep-gas tritium, CEC
1002	Ci/m^3	Ring-specimen sweep -gas tritium, MS
1003	Ci/m^3	Solid-specimen sweep-gas tritium, CEC
1004	Ci/m^3	Solid-specimen sweep-gas tritium, MS

CEC and MS refer to the sweep-gas flow stream through the ceramic electrolysis cell and the molecular sieve.

described in Appendix B. The Phase I tritium-recovery data were then corrected for the effect of sweep-gas composition on ion-chamber response and for the buildup of ion-chamber background. These corrections were carried out as described in the Phase I Data Summary Report, Section 3.1.4.1 (Slagle and Hollenberg 1994) and in Section 3.1.3 of this report. The final spreadsheets are referred to as the Phase II Corrected/Compiled Database. In Appendix B, the results of the data correction/compilation are presented in two different types of data plots versus time. The first series of plots are the recovered-tritium concentration, the ion-chamber correction factor, and the ion-chamber background. The other series of plots is the ratio of recovered to generated tritium and the inner-specimen temperatures. These plots also include a description of the sweep-gas-composition changes. These two types of plots are included in Appendix B for each of the four irradiation cycles for each of the two *in situ* recovery canisters.

5.0 *In Situ* Results

The BEATRIX-II Phase II *in situ* tritium recovery experiment was carried out in Cycle 12 of the FFTF between May 1991 and March 1992. The *in situ* testing included the operation of the temperature-change and temperature-gradient canisters. Details of the test plan are given in Tables 4.1 and 4.2. This section describes the *in situ* results and discusses some of the implications.

5.1 Total Lithium Burnup

The tritium recovery rates in the corrected/compiled database (Section 4.3) were integrated to determine the total tritium recovered from each cycle of Phase I. The total recovered tritium from the integration is compared to the value of total tritium generated based on the predicted neutronics for each reactor cycle[a] in Table 5.1. In all cases, the predicted value is higher than the measured value. The difference between the overall totals of predicted versus measured tritium for both canisters is over 10%, but they agree within the expected uncertainties: ±10% for the prediction of the amount generated and ± 10% for the accuracy of the ion-chamber measurements. The total lithium burnup was calculated on the basis of the predicted/measured tritium.

Table 5.1. Predicted Amount of Tritium Generated Compared to Measured Amount Recovered

		Predicted (Ci)		Measured (Ci)	
Cycle	EFPD	Temperature Change	Temperature Gradient	Temperature Change	Temperature Gradient
Phase II-A	52.8	221.8	158.9	203.8	149.2
Phase II-B	48.6	204.1	146.3	192.6	134.0
Phase II-C	50.3	216.3	156.4	186.9	143.5
Phase II-D	51.6	216.7	160.5	185.4	149.2
Total	203.3	858.9	622.1	768.5	575.9
Lithium Burnup		5.3%	5.7%	4.6%	5.1%

5.2 Temperature-Change Specimen

The test plan for the irradiation of the Phase II temperature-change canister is detailed in Table 4.1. The primary parameter changes are temperature, sweep-gas composition, and sweep-gas flow rate. The reference condition was selected to be an inner specimen temperature of 640°C, a sweep gas of helium with 0.1% H_2, and a flow rate of 100 mL/min. An inner surface temperature of 640°C corresponds to a specimen outer surface temperature of 620°C. In the following discussion, the inner specimen temperature was used to designate the temperature of the temperature-change specimen.

5.2.1 Experiment Startup

During reactor startup, the temperature history of the temperature-change specimen suggested that unexpected changes occurred in the specimen/canister configuration. At reactor startup, the sweep gas through the temperature-change canister was 0.1% H_2 and the mixture of helium and argon in the thermal-conductance gas gap was 100% He. Figure 5.1 is a plot of the

(a) R. C. Knight. "Actual and Predicted BEATRIX Phase 2 Tritium Production Rates." Letter to O. D. Slagle, August 3, 1992. WHC-9255855. Westinghouse Hanford Company, Richland, Washington.

temperatures recorded from the two inner specimen thermocouples for the first 550 hours of Phase II-A. The two inner thermocouples were located 180° apart on opposite sides of the inner diameter. During the initial heatup, the two temperatures were identical. However, when the reactor reached full power (approximately 110 hours), the temperatures of the two thermocouples diverged by 15°C (548 and 533°C). When the gas in the thermal conductance gap was changed to 3% He-97% Ar, the temperatures increased, resulting in temperatures of 651 and 644°C for a difference of only 7°C. When the temperature was again reduced by returning to 100% He in the gas gap, the temperatures remained substantially different: 550 and 536°C. The sample temperature was then raised back up to 645°C and held for the duration of the 550-hour plot. Throughout this latter period, the difference in temperature between the thermocouples appeared to decrease with time. It is to be noted that the thermocouples were labeled as #1 and #2, and the one labeled #1 was always less than #2 during the operation shown in Figure 5.1. At the end of Phase II-A, the readings for a gap gas of 100% He were very close: 528°C (#1) and 533°C (#2). At the upper temperature, the order was reversed with #1 reading 647°C and #2 reading 645°C.

One possible explanation for the temperature behavior of the temperature-change canister during reactor startup is that sintering caused the specimen's diameter to decrease. This decrease in diameter introduced larger specimen-subcapsule gaps. This sintering appeared to have started sometime before the reactor reached full power at approximately 110 hours. A large peak in the sweep-gas moisture flowing out of the temperature-change canister at 110 hours suggests that the sintering could have occurred concurrently with the decomposition of residual LiOH. When the proposed sintering occurred, it is possible that the specimen did not remain centered in the capsule. If the gap on one side was larger than the other, a temperature difference would result. Because Li_2O has a higher thermal expansion than steel, increasing the temperature of the specimen reduces the total gap and this tighter fit of the specimen in the capsule could have effected a centering of the specimen in the capsule. The disappearance of the temperature difference by the end of Phase II-A may have resulted because the specimen swelled and reduced or possibly eliminated the gap.

The design calculations (Section 2) indicated that inner temperatures would be 503°C for 100% He and 654°C for 12% He-88% Ar. During operation the inner temperatures were 530°C for 100% He and 640°C for 3% He-97% Ar. It appears as if the lowest and highest temperatures were off by approximately 20°C, but in opposite directions. That is, the lowest temperature was high while the highest temperature was low. The design calculations were carried out assuming no thermal gap between the specimen and the capsule. The decrease associated with the maximum temperature could have been associated with the incomplete closure of the specimen-subcapsule gap and/or a lower power generation rate, as suggested by the lower measured tritium generation rate in Table 5.1. The higher temperatures at the minimum temperature could result from an increase of the specimen-capsule gaps during cool-down from the higher temperatures.

To interpret the data, two calculated values from the design will be used: 1) the temperatures of the inner thermocouples are 6°C higher than the inner surface of the ring, and 2) the temperature drop across the specimen is 20°C. The temperature drop across the specimen could be expected to increase as the specimen swells. Specimen swelling was observed during the postirradiation examination in Section 6.

5.2.2 Temperature-Change Effects

As was observed in Phase I, temperature transients in Phase II were followed by positive tritium recovery peaks for temperature increases and negative recovery peaks for temperature decreases. Figure 5.2 shows typical tritium recovery peaks for a temperature-change series of 640-530-640°C in the reference sweep gas of 0.1% H_2. These temperature changes were included in Test Series B1 of the test plan, were carried out at 61 EFPD, and were typical of the first 100 EFPD of operation.

The tritium recovery peaks in Figure 5.2 consisted of tritium primarily in the reduced form (HT) and are similar to the tritium recovery peaks found after temperature transients at the end of Phase I. Figure 5.3 shows a progression of recovery peaks for a 550-640°C temperature transient during Phase I compared with a 530-640°C transient at the start of Phase II (Test Series A1). At the start of Phase I, the recovery consisted of two peaks: an initial HT peak followed by an extended HTO peak. By the end of Phase I, (300 EFPD) the HT peak dominated the recovery. What caused this change was uncertain. Two proposed explanations were burnup effects in the specimen or a drying out of the system (Slagle and Hollenberg 1994). The occurrence of a predominantly HT peak at the start of Phase II suggested that the effect seen in Phase I was not due to burnup effects in the specimen. Therefore, the cause of the change in Phase I may be due to a drying out of the system that continued into Phase II.

Effect of Sweep-Gas Composition

During the first 50-day cycle of irradiation, the temperature-change sequence 640-590-530-640°C was carried out in different sweep-gas compositions. Figure 5.4 compares recovery curves for the temperature change from 530 to 640°C in the three different sweep gases: 1) 0.1% H_2 (Test Series A3), 2) 0.01% H_2 (Test Series A4), and 3) helium (Test Series A5). Decreasing the hydrogen in the sweep gas resulted in a larger tritium recovery. Integration over the peaks was used to determine the respective amount of tritium associated with the three peaks: 0.04, 0.23, and 0.76 Ci, respectively. This trend of increasing inventory with decreasing hydrogen concentration is consistent

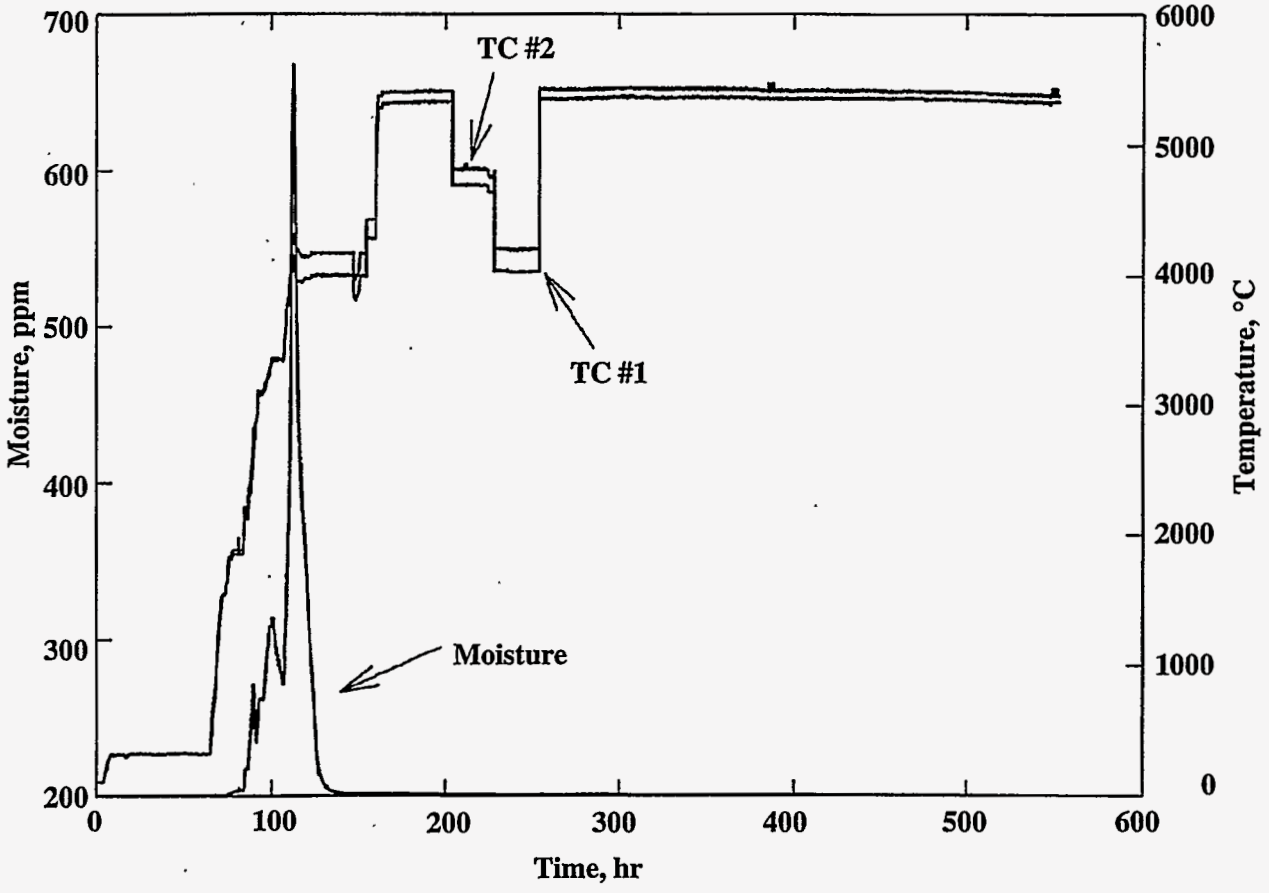

Figure 5.1. Inner Temperatures and Sweep-Gas Moisture for the First 550 Hours of Operation of the Temperature-Change Canister in Phase II-A

with the increasing tritium inventories in the Li_2O specimen found for decreasing hydrogen seen previously in Phase I (Slagle and Hollenberg 1994).

Effect of Burnup

Burnup does not appear to affect tritium release from Li_2O, but other historic factors do seem to influence the release rate. A series of temperature transients was carried out at different stages of the test (Test Series B1, C4, and D3) to characterize the effect of burnup. These series were carried out in 0.1% H_2 and consisted of temperature changes in the order of 640-590-530-640-530-640°C. The tritium recovery peaks from the last 530 to 640°C temperature change in this series are compared in Figure 5.5. Similar peaks from Test Series A1 and A6 are included as examples at the lower EFPDs. The first three peaks at 4, 51, and 61 EFPD are similar in shape, as was expected. The last two peaks at 151 and 200 EFPD are preceded by small negative peaks. The peak at 142 EFPD was not a part of a series of temperature transients, but was for an isolated 530 to 640°C temperature transient following an extended period of operation at 530°C in helium and 0.01% H_2. This transient (PCN # 124) recovery peak at 142 EFPD was preceded by a small negative peak followed by a large positive peak consisting primarily of HTO in contrast to the previous temperature transient peaks that were primarily HT. The subsequent peak in a temperature-transient series was carried out at 151 EFPD and was appreciably smaller than the peak at 142 EFPD. Although the 151 EFPD peak

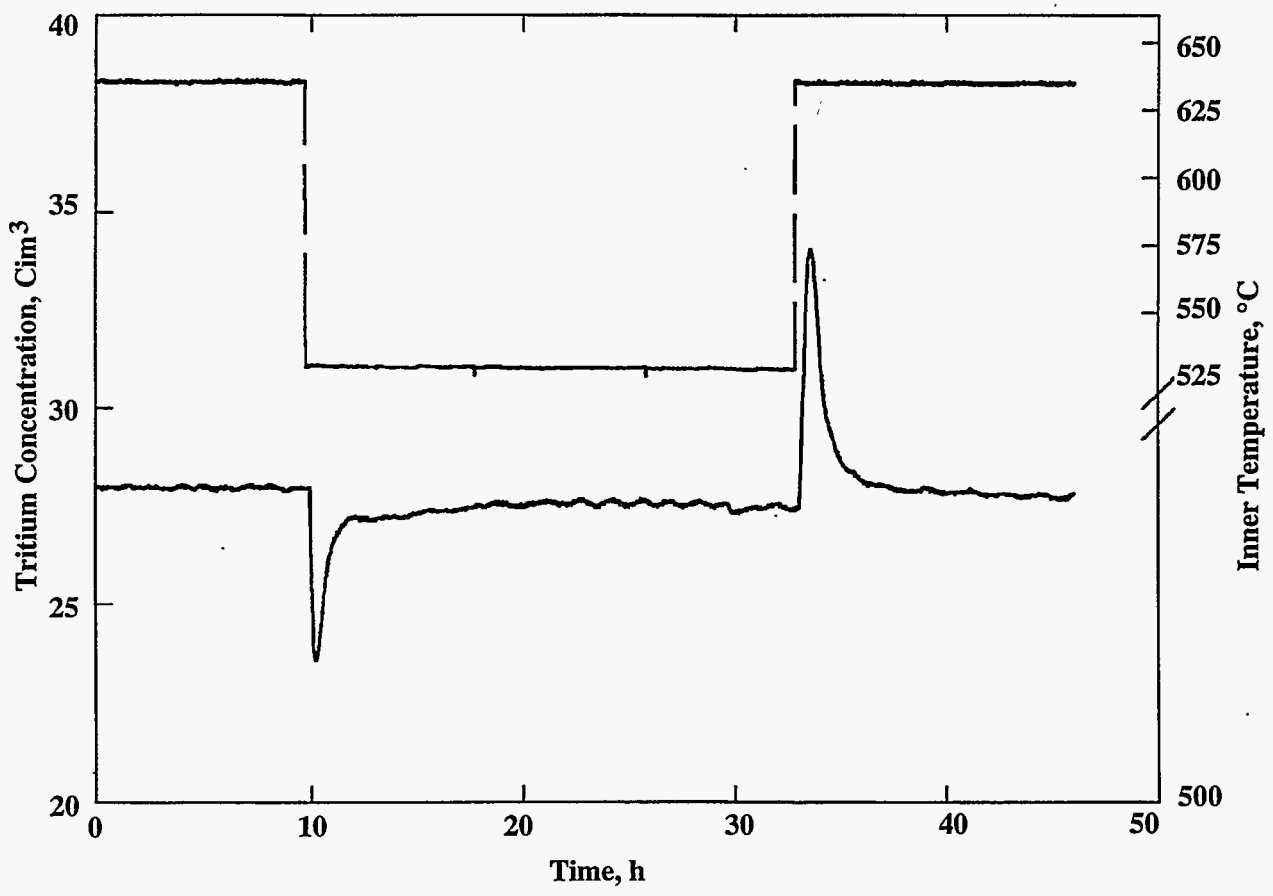

Figure 5.2. Tritium Recovery Peaks for a Temperature Change Series of 640-530-640°C in the Reference Sweep Gas of 0.1% H_2

consisted primarily of HT, it retained the initial negative peak feature. The peak at 200 EFPD continues to have the initial negative peak, suggesting that changes had been effected in the specimen during the low temperature operation in helium or 0.01% H_2 sweep gases and that these changes were not annealed out during the subsequent irradiation.

5.2.3 Sweep-Gas Composition

The effect of increasing hydrogen concentration in the helium sweep gas was to decrease the tritium inventory in the specimen. This decrease in inventory occurs by an increase in the tritium release rate reflected in a positive transient tritium recovery peak. Conversely, decreasing hydrogen concentration in the sweep gas resulted in a steep drop in recovery rates followed by a slowly increasing recovery rate. The behavior following a decrease in hydrogen concentration could be considered to be a broad negative peak that required a longer time to reach equilibrium than in the case of an increase in the hydrogen concentration. Temperature transients in a helium sweep gas typically required 2 days to establish equilibrium compared to less than a day for 0.1% H_2. Similarly, the faster recovery times observed for increasing hydrogen concentrations to final sweep gas of 0.1% H_2 (as compared to a change to helium) is probably due to a faster return to equilibrium in the higher hydrogen concentration rather than indicating that inventory decreases in the Li_2O occurred more rapidly than inventory increases.

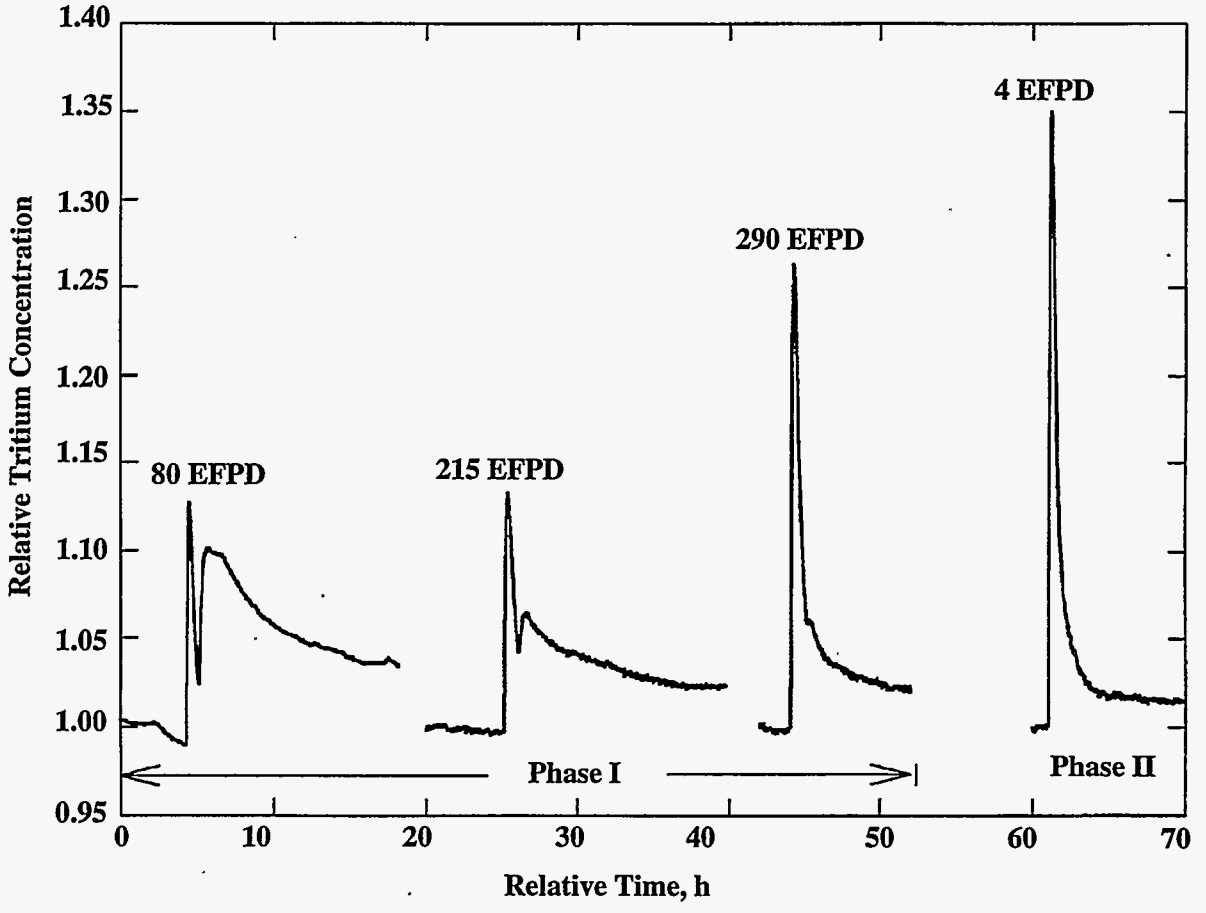

Figure 5.3. Progression of Tritium Recovery Peaks for a 550 to 640°C Temperature Transient in Phase I Versus a 530 to 640°C Temperature Transient in Phase II

Sequences of sweep-gas-composition changes described in the test plan (Table 4.1) started and ended with 0.1% H_2 sweep gas. Figure 5.6 compares the tritium recovery curves measured during the sequence of four days in helium followed by two days in 0.01% H_2 at temperatures of 640 and 530°C. These are Test Series B2.2 and C3.2, respectively. The tritium recovery for 640°C test series involved smaller peaks with faster returns to a steady-state recovery rate than for the series at 530°C. Note also that the 530°C recovery peak for the return to 0.1% H_2 had an initial peak followed by a smaller secondary peak. The second peak corresponded to a peak in sweep-gas moisture, and this suggests that the first peak was HT and the second peak HTO. This is analogous to the separation of the HT and HTO peaks observed in the Phase I temperature transient (Slagle and Hollenberg 1994). The larger recovery peaks at 530°C reflect a larger buildup in tritium inventory than occurred for the 650°C tests for the cases of helium or 0.01% H_2. The occurrence of an HTO peak at 530°C also suggested that an appreciable part of the inventory buildup was in the form dissolved of moisture. This importance of dissolved moisture in the inventory buildup at 530°C is also indicated by the large HTO peak found for the 530 to 640°C temperature transient at 142 EFPD noted above (Figure 5.5).

Phase I and Phase II behavior are compared in Figure 5.7, which is a plot of tritium recovery during a sweep-gas-composition sequence of 8 days in helium followed by 2 days in 0.01% H_2 at 640°C for Phase I and II (Test Series B2.1). The tritium-recovery behavior for Phase II exhibited sharper, smaller tritium-recovery peaks than Phase I.

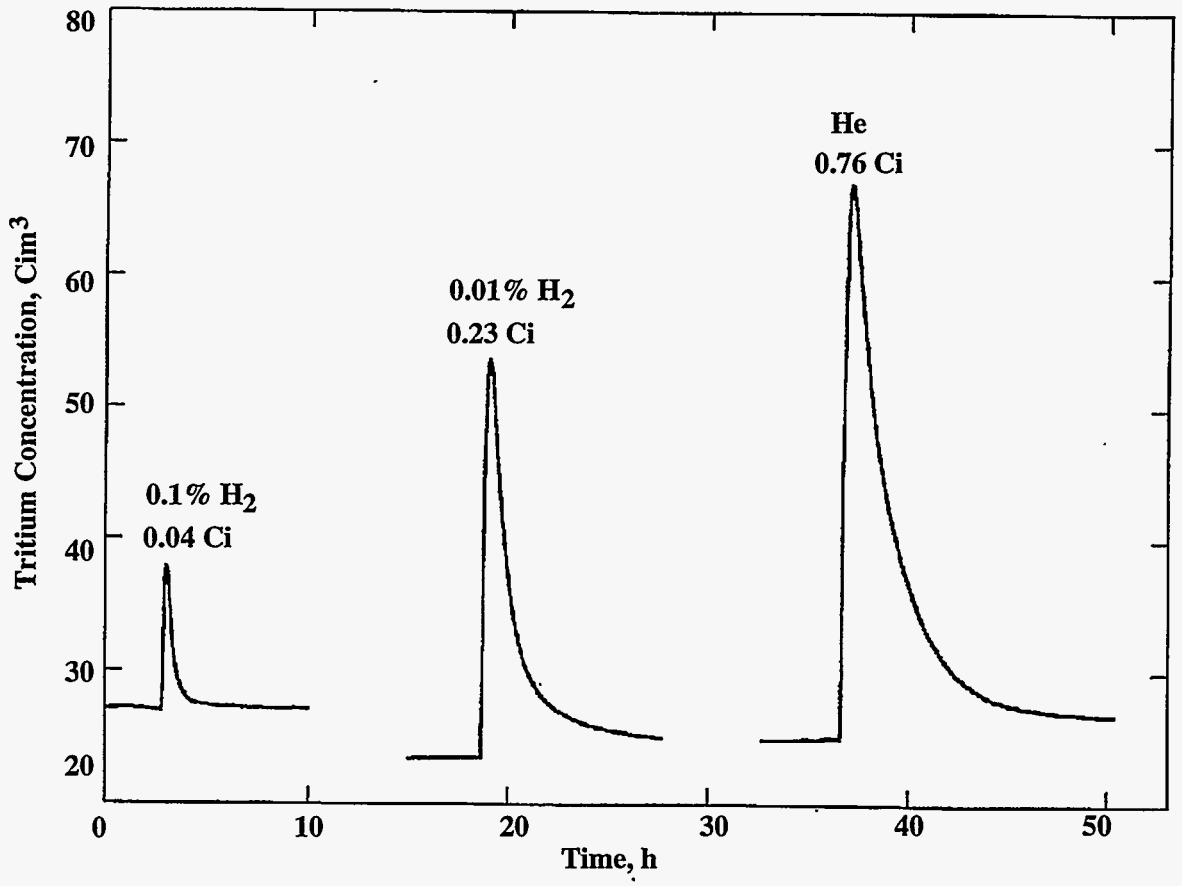

Figure 5.4. Tritium Recovery Curves for a Temperature Change from 530 to 640°C in the Three Different Sweep Gases: 0.1% H_2, 0.01% H_2, and Helium

5.2.4 Reactor Power Changes

Reactor power changes resulted in complex tritium recovery data that were influenced by associated tritium generation and thermal variations. However, power changes, particularly startup and shutdown, did provide an opportunity to study temperature changes in the specimen that are outside the range of normal operating conditions. Power changes resulted in changes in the neutron flux, resulting in associated changes in tritium and heat generation rates, and it is difficult to know which change was the dominant parameter change affecting the tritium-recovery behavior. In Phase I, reactor startup and shutdown behavior of both canisters containing Li_2O was strongly dependent on the composition of the sweep gas (Slagle and Hollenberg 1994). In a 0.1% H_2 sweep gas, decreasing the power (tritium generation rate/specimen temperature) resulted in a decrease in the tritium recovery rate as expected. However, in a helium sweep gas, the recovered tritium-concentration curve during decreasing power contained two positive recovery peaks. Such an observation suggests a decreasing tritium inventory in the Li_2O specimen with decreasing temperature. For the Phase I temperature-change canister, the major peak started at about 470°C and continued to the end of shutdown. A much smaller recovery peak occurred near the start of the shutdown at about 620°C.

Phase II reactor shutdowns and startups were typically carried out using a 0.1% H_2 sweep gas. At the end of Phase II-B (103 EFPD), the sweep gas was changed to helium before the shutdown (Test Series B4) and was then also used during the startup of the next cycle. The recovered tritium concentration curve and inner specimen temperature during the shutdown are shown in Figure 5.8. The deviation of tritium-recovery concentration from a decreasing curve occurs near the middle of the curve and at the bottom. These peaks or deviations are much smaller than the major recovery peak in Phase I that started at 470°C. In Phase II, the peaks started at 580 and 450°C versus 620 and 470°C in Phase I. No discernible anomalous behavior occurred during the startup of Phase II-B. Analysis of startups was more difficult than shutdowns because during shutdowns, the power increments were in smaller more uniform steps than those occurring in startups.

5.2.5 Discussion

The tritium-recovery behavior for the BEATRIX-II, Phase II Li_2O canister was similar to the behavior previously observed in Phase I. Transient recovery peaks indicated reduced inventories at higher temperatures or at higher hydrogen concentrations in the sweep gas. Two more detailed observations common to both Phase I and II invite further discussion. The first was the occurrence of small "negative" peaks preceding the positive recovery peaks that resulted from temperature changes from 530 to 640°C occurring after 142 EFPD in Phase II. The other observation was the reduction in inventory as the temperature was being decreased during shutdown in a helium sweep gas, i.e., "inverted" peaks.

Negative Recovery Peaks

The occurrence of small negative peaks preceding the larger positive peaks after temperature increases was observed in BEATRIX-II, Phase I, in the CRITIC-I experiment by Miller et al. (1988); Verrall, et al. (1989a); and Tanaka et al. (1994). In BEATRIX-II, Phase I, these negative peaks were only observed early in the experiment. In CRITIC-I, the behavior was observed before conditioning at 800 to 850°C, and it was proposed that conditioning of the specimen decomposed a surface layer of Li_2CO_3. Kopasz et al. (1990) have shown that the CRITIC-I behavior could be modeled using a desorption activation energy that varies with surface coverage. Tanaka et al. (1994) found a strong relationship between the occurrence of the negative peaks and water vapor in the recovered sweep gas. Alternatively, Asaoka et al. (1992) have shown a correlation of these negative peaks with the production of F^o centers.

In BEATRIX-II, Phase II, the occurrence of negative peaks appeared to have been brought on by the extended operation in helium and 0.01% H_2 at the lower temperature of 530°C. Upon returning to the reference state (0.1% H_2 at 640°C) after operation at the lower temperature in sweep gases with reduced hydrogen (<<0.1% H_2), the tritium recovery peaks had a large component of HTO. Analogous to the conditioning of the CRITIC-I specimen at 800 to 850°C, this recovery behavior suggests that a "reverse" conditioning of the specimen may have occurred at the lower temperatures in reduced hydrogen sweep gases. This reverse conditioning in the Li_2O specimen may have been associated with a buildup of tritium inventory in the form of dissolved moisture. The occurrence of the large component of HTO in the recovery peaks during a return to the reference state is consistent with Tanaka et al. (1994) findings of the association of the phenomena with higher moisture levels.

Inverted Recovery Peaks

The observed peaks found during reactor shutdown in a helium sweep gas for Phase II confirm the behavior seen earlier in Phase I, although the Phase II peaks are much smaller. For the Phase I temperature-change canister, a major recovery peak was observed to start at about 470°C. A much smaller recovery peak was observed at the start of shutdown at a temperature of approximately 620°C, but it is believed that this was caused by temperature fluctuations in the specimen. In Phase II, the peaks observed at 580°C and 450°C are considerably smaller than the Phase I peak observed starting at 470°C. A comparison of the temperatures across the ring specimen indicated that the Phase II peak starting at a temperature of 450°C is consistent with the 470°C peak in Phase I.

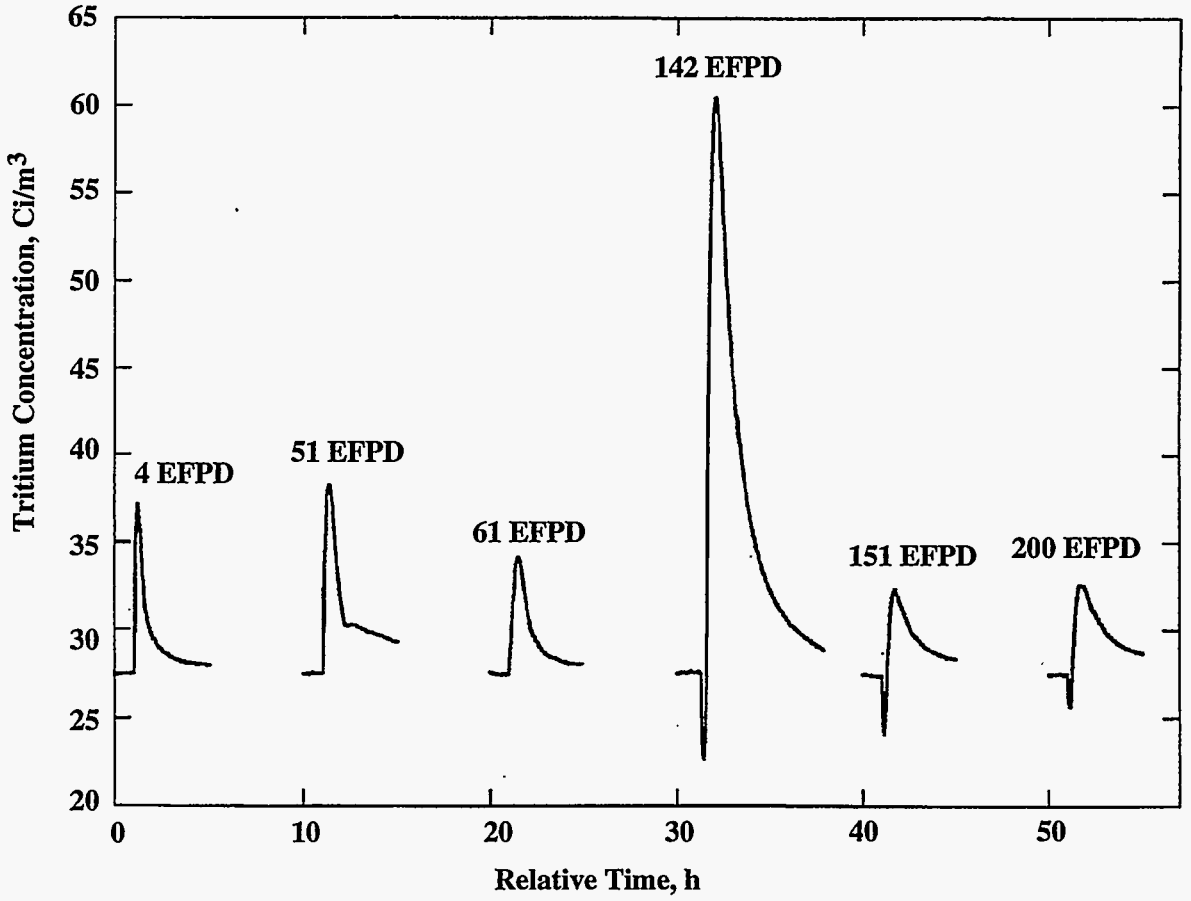

Figure 5.5. Tritium-Recovery Peaks for Temperature Transient 530 to 640°C at 4, 51, 61, 142, 151, and 200 EFPD

The Phase I specimen had a 40°C temperature difference across the specimen while the Phase II Specimen had a 20°C difference. An inner temperature of 450°C in Phase II was equivalent to a specimen temperature of 450 to 430°C. A 470°C temperature in Phase I was equivalent to a specimen temperature of 470 to 430°C. The temperature overlap between Phase I and Phase II suggests that the data are in very good agreement.

The tritium-recovery peaks that occurred during reactor shutdowns in helium suggest that if temperature transients had been carried out in the specific temperature regions associated with these peaks, temperature decreases would result in tritium-inventory decreases. The fact that such decreases were not seen during the temperature transients carried out from 640-590-530°C may have been because the temperature intervals were too broad and/or the decreases were masked by the overall increase. The Phase II shutdown peak in the vicinity of 580°C (Figure 5.8) was not a particularly large peak and could easily be overshadowed by a larger temperature drop. However, in Phase I, the shutdown peak in the 470 to 430°C temperature range was much larger, and one could expect to see such an "inverse" effect in temperature transients carried out at these lower temperatures. Because these lower temperatures were not achievable in BEATRIX-II, no data are available. However, the CRITIC-I experiment on Li_2O did carry out temperature transients at these lower temperatures. During the initial part of the experiment, low temperature transients in the range of 460 to 620°C resulted in inverted peaks. That is, a decrease in temperature resulted in a positive peak in the tritium-recovery curve. The CRITIC-I experimental observations included a temperature transient from 540

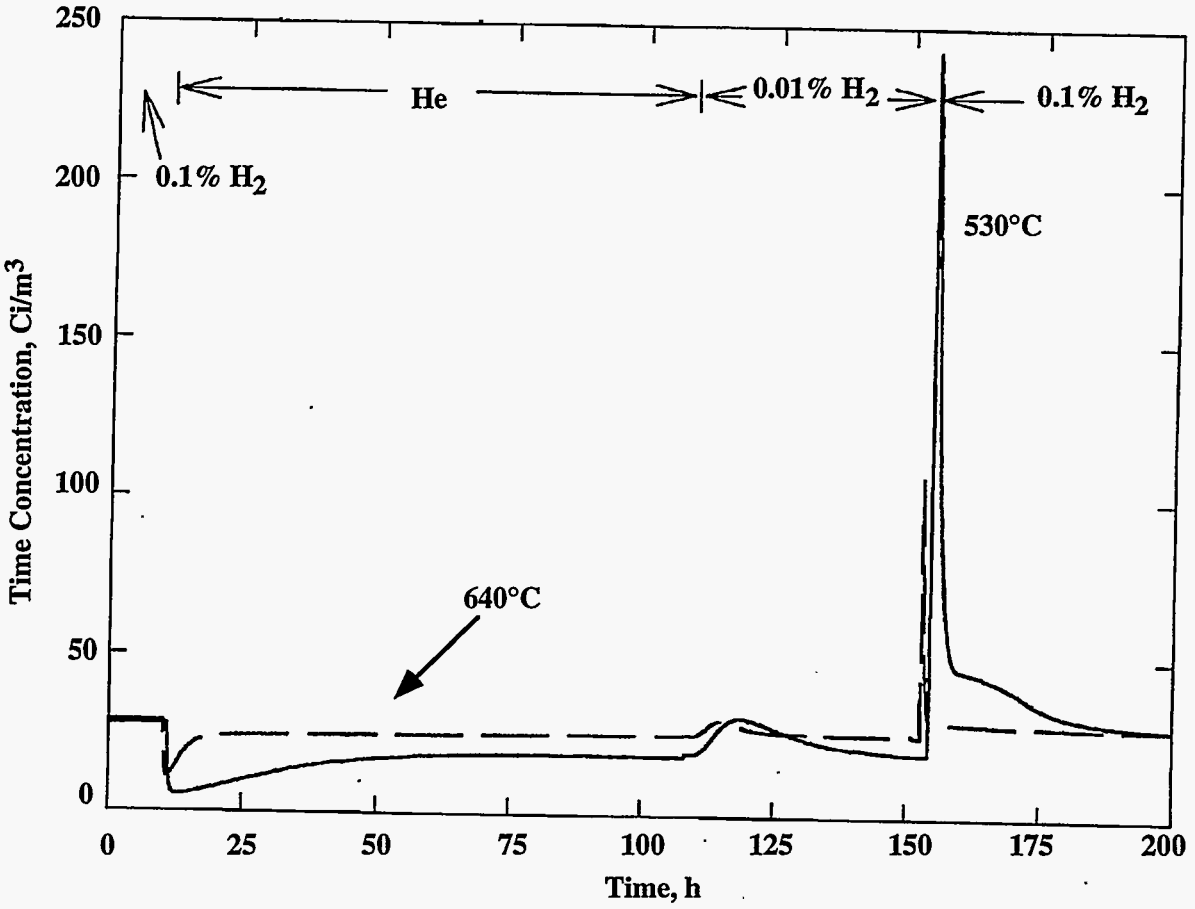

Figure 5.6. Tritium-Recovery Curves Measured at Temperatures of 640 and 530°C for the Gas-Composition Sequence of 4 Days in Helium Followed by 2 Days in 0.01% H_2

to 480°C in helium sweep gas that resulted in a positive tritium-recovery peak. This behavior is very consistent with the behavior seen in the BEATRIX-II, Phase I and II shutdown curves in helium. As noted above for the "negative" peaks, the inverted peaks in the CRITIC-I test occurred in the first part of the test and were not observed later on in the experiment after the 800 to 850°C conditioning. It was proposed that the inverted peaks were associated with the solubility of tritium in a surface layer that was decomposed or eliminated during conditioning.

The inverted tritium recovery peaks in the 470 to 430°C temperature range correspond to a temperature range where LiOT or dissolved moisture is an important factor in determining the tritium inventory in Li_2O (Billone et al. 1991; Tetenbaum and Johnson 1984). Because the moisture levels in the BEATRIX-II sweep gas are typically less than 0.1 Pa, the amount of moisture in the specimen is expected to remain below the LiOH solubility limit as the temperature is decreased. A previous discussion of the Phase I behavior (Slagle et al. 1992) suggested that the variation of water vapor pressure over LiOT dissolved in Li_2O may have contributed to the shutdown behavior. At the present time, the explanation of the inverse peaks is not complete. However, operation in helium and the subsequent buildup of tritium inventory does appear to be associated with a buildup of dissolved moisture in the specimen as suggested by the large HTO peaks observed when the specimen is returned to the reference condition. This buildup of tritium inventory in the Li_2O is one of the primary differences in the specimens operated in helium versus 0.1% H_2. The occurrence of these inverse peaks during the shutdown in helium and not in 0.1% H_2 suggests that the buildup of tritium

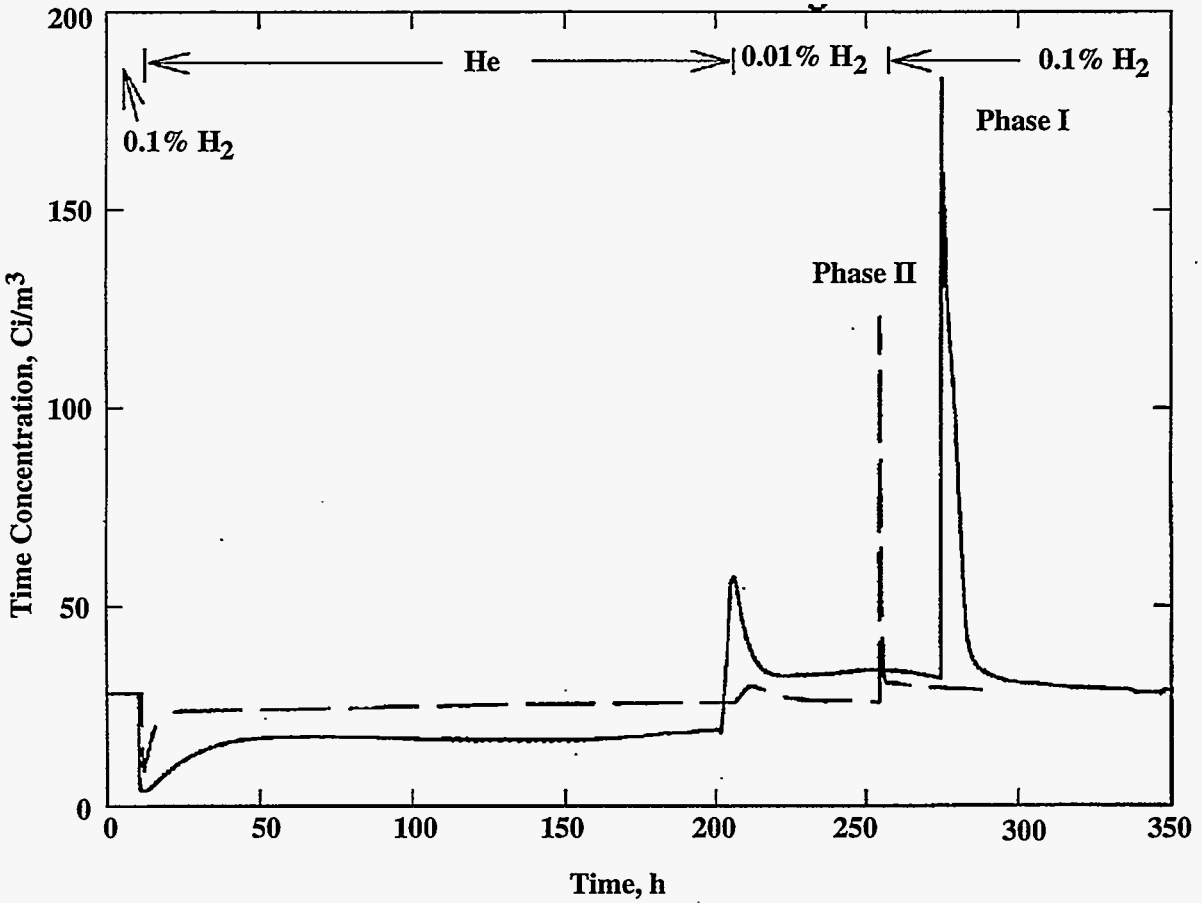

Figure 5.7. Comparison of 640°C Tritium Recovery Curves for the Phase I and II Sweep-Gas Composition Sequences of 8 Days in Helium Followed by 2 Days in 0.01% H_2

inventory during operation in helium, possibly in the form of dissolved moisture, may contribute to this behavior.

5.3 Temperature-Gradient Canister

The test plan for the irradiation of the Phase II temperature-gradient canister is detailed in Table 4.1. The primary parameter changes are sweep-gas composition and sweep-gas flow rate. The reference condition was selected to be a sweep gas of helium with 0.1% H_2, and a flow rate of 100 mL/min.

5.3.1 Centerline Temperatures

Figure 5.9 is a plot of center temperatures and sweep-gas moisture for the startup of the Phase II temperature-gradient canister. The center temperatures are the output of the two thermocouples in the center annulus of the specimen. The upper thermocouple was a Mo-Nb thermocouple designed to operate at higher temperatures than the lower thermocouple that was a Type K thermocouple as were the thermocouples used in the Phase I temperature-gradient canister. The upper thermocouple recorded consistently higher temperatures during startup with a final temperature at 100% power of 1115°C versus 1060°C for the lower thermocouples. After the power-reduction test carried out by reactor operations at 150 hours (Figure 5.9), the upper thermocouple had a 10°C lower reading while

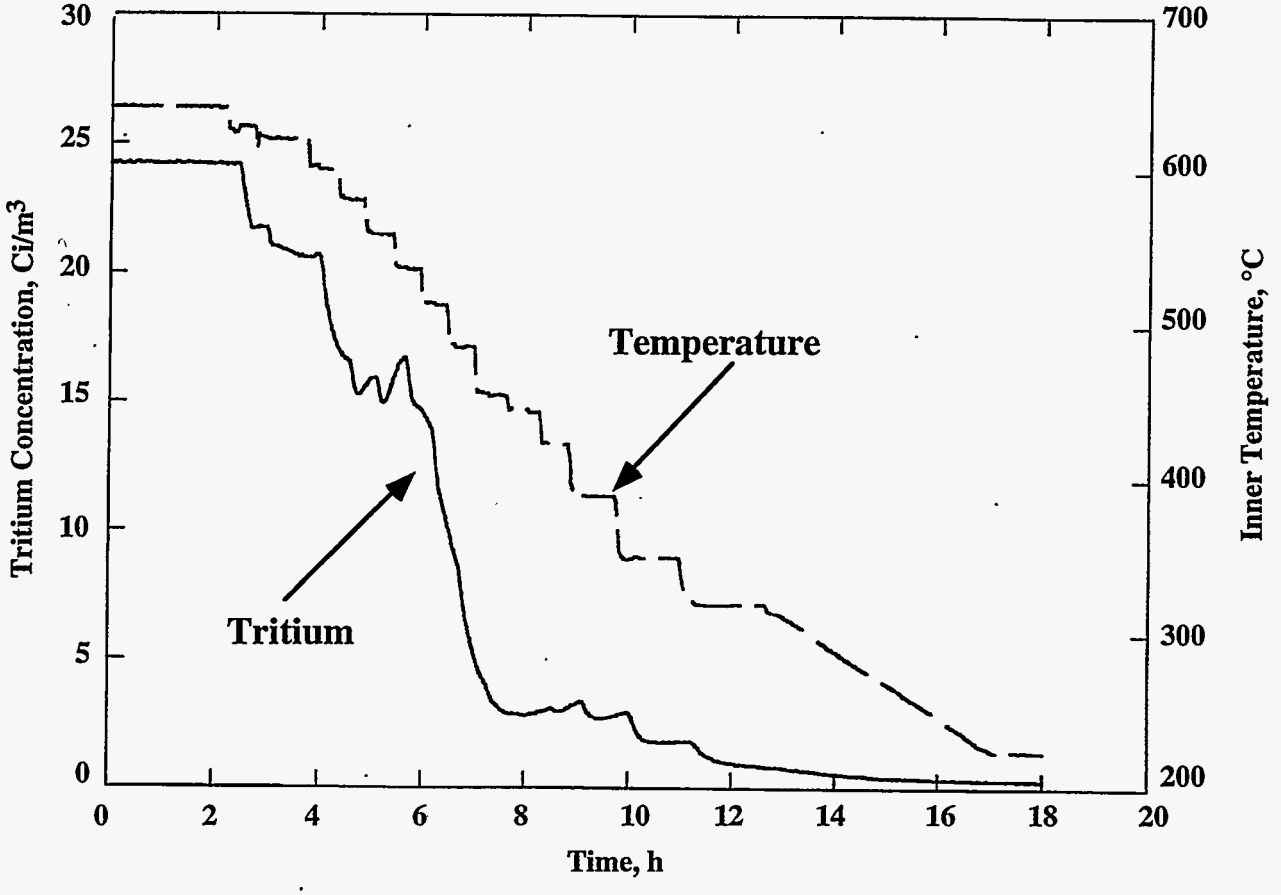

Figure 5.8. Recovered-Tritium Concentration and Inner Specimen Temperature During Shutdown in Helium Sweep Gas

the lower thermocouple remained the same. This difference of 45°C remained constant for the remainder of the operation shown in Figure 5.9. The higher reading for the upper thermocouple was attributed to the increase in neutron flux from the bottom to the top of the canister. The separation between the ends of the thermocouple sheaths from the pretest radiograph (Figure 2.8) was less than 1/3 cm, but the actual point of contact for the wires may have been as far apart as 2 cm.

The thermal and neutronic performance-analysis prediction (Section 2) carried out for the initial design of the canister had a predicted centerline temperature of 1095 ± 65°C. The temperatures found at the start of the irradiation lie within the predicted range. This range of predicted temperatures was due primarily to uncertainties in the thermal conductivity of the pebble bed. The good agreement of the predicted and measured temperature adds additional confidence in the ability to model the thermal properties of a Li_2ZrO_3 pebble bed.

Figure 5.10 is a plot of the readings from the two central thermocouples for the four irradiation cycles. The gradual decrease in temperature during each reactor cycle was attributed to burnup of the fuel and a decreasing flux at this position in the reactor. Similar thermal behavior was also observed in the Phase I irradiation of Li_2O, and the absence of drastic changes during irradiation was interpreted as an indicator of stable performance for the specimen. This stable performance is also confirmation of the physical stability of the Li_2ZrO_3 pebble bed and its suitability for use as a fusion blanket material.

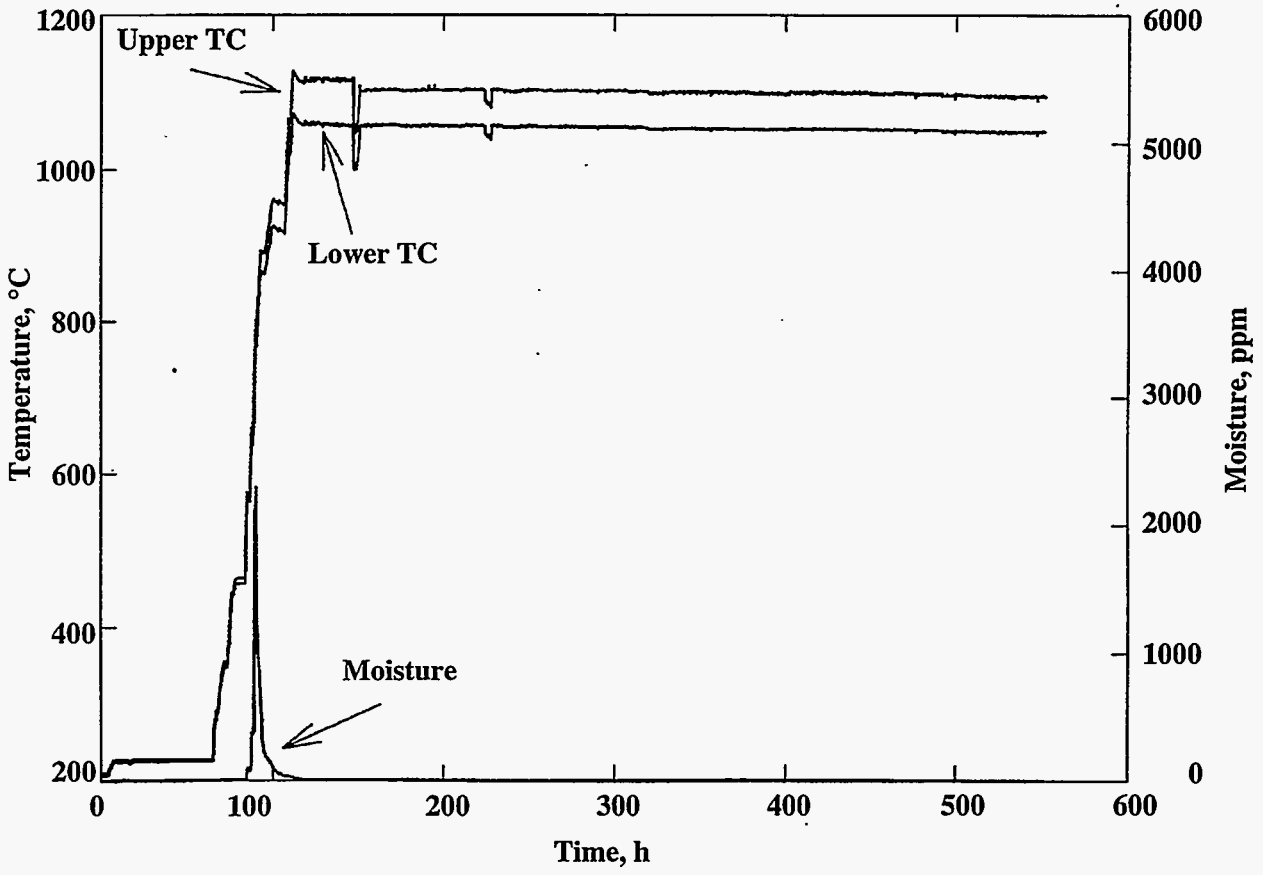

Figure 5.9. Center Temperatures and Sweep-Gas Moisture for the Startup of the Phase II Temperature-Gradient Canister

5.3.2 Sweep Gas Moisture

During the initial reactor startup at the beginning of the experiment, a 2400-ppm spike in the sweep-gas moisture concentration was observed (Figure 5.9). The moisture concentration then decreased to less than 1% of that value after 1 EFPD of operation. After 7 EFPD, the reading was less than 0.02 ppm (nominal), well below the instrument's limit of accuracy. Because sweep gas had been flowing for several days before reactor startup to dry all system components, it is assumed that the moisture release during startup emanated from the ceramic. This moisture release was much smaller than that observed in a similar experiment on Li_2ZrO_3 - CRITIC-II (Miller and Verrall 1994). In CRITIC-II, the specimen had been pre dried in air at 200°C. The source for the moisture for both experiments is believed to have been residual $(OH)^{-1}$ in the ceramic remaining after dry out. For the rest of the Phase II irradiation, the release of moisture was extremely low. During steady state operation, the meter output was zero. Following changes in sweep-gas composition when the hydrogen concentration was increased, small apparent peaks of moisture were recorded, but the indicated levels were less than 0.05 ppm. These small peaks in moisture release were consistently observed during sweep-gas-composition changes and coincided with a rise in both total tritium release and tritiated water release. Although the absolute accuracy of standard moisture meters does not extend to these low levels, these peaks probably indicated a real release of moisture. Low moisture release was a notable feature of the Phase II Li_2ZrO_3 test. Low levels of moisture were also released by Li_2O in the BEATRIX-II Phase I and Phase II tests, but not as low as Li_2ZrO_3.

5.3.3 Sweep Gas Composition Changes

Systematic changes in the sweep-gas composition were made to determine the effect of composition on tritium release. Observed changes in tritium recovery rate could potentially be due to inventory changes elsewhere in the system, e.g., the piping. However, laboratory tests at AECL have

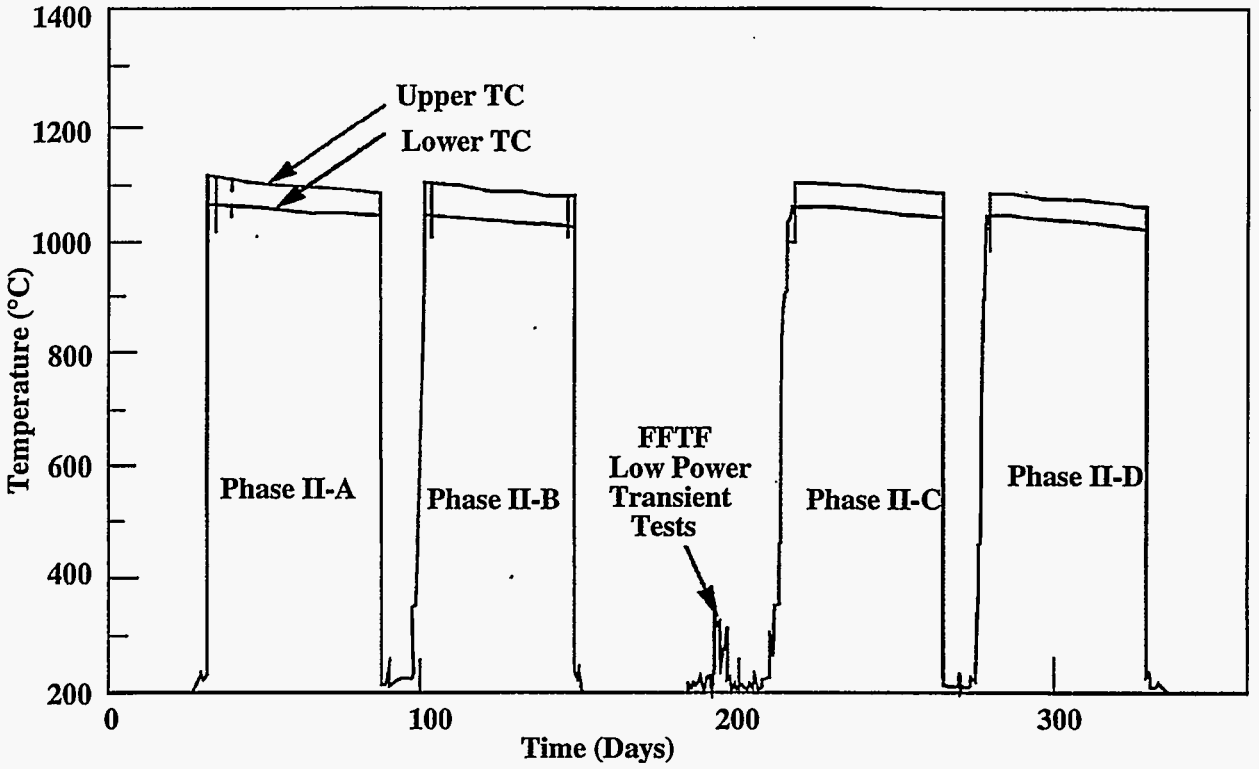

Figure 5.10. Center Temperatures of the Phase II Temperature-Gradient Canister for the Four Irradiation Cycles

shown that changes in inventory on piping do not readily occur from changes in hydrogen concentration in the sweep gas (Rodrigo et al. 1992). Moisture additions to the sweep gas are required to effect sizable inventory changes on the piping. For this reason, the observed tritium-recovery data can be expected to reflect the tritium release from the Li_2ZrO_3 pebbles.

Effect of Time in Helium

The buildup of tritium inventory with time in a helium sweep gas was investigated by switching to helium for varying lengths of time. Periods of 2, 4, and 8 days in helium were used. These tests are described in the test plan as A3.2, B1.2, and B1.3, respectively. The results are shown in Figure 5.11 and indicate the following:

- When switching from the reference sweep gas to pure helium, all tests showed a sharp transient drop in tritium recovery rate, followed by a return to a new steady-state rate, slightly lower than in the reference gas.

- All exhibited two distinct peaks or a "double" peak upon reintroduction of the reference sweep gas and a return to the same steady-state recovery rate as in the original reference condition.

- Following the He-0.1% H_2 transition, the peak height and integrated areas under the peaks increased with the duration in the helium sweep gas. The areas were 0.18 Ci (2 days), 0.77 Ci (2 days), and 1.63 Ci (8 days).

The double peak was thought to be due to a rapid HT peak and a slower HTO peak. The rapidity of the HT peak may reflect the kinetics of release from the ceramic or a more rapid transit through the piping to the ion chamber, due possibly to an "open-tube chromatographic" effect of the HTO gas. That is, the HTO continuously adsorbs and desorbs from the walls as it moves through the piping. The HT is less reactive with the walls.

After only a few hours in the helium sweep gas, the tritium recovery rate was approximately constant at a value that appeared to be slightly lower than the value in the reference sweep gas. This implies a steady buildup of tritium inventory in the specimen with time in helium. The steady-state recovery rates in the helium and 0.1% H_2 sweep gases have an uncertainty of 5 to 10% because of the uncertainty in the enhancement factors (Section 3.1) for the ion chambers. Despite this uncertainty, the tritium recovery rate in helium must be lower than the steady-state recovery rate in reference gas because of the tritium recovery peaks that occur after returning to 0.1% H_2. The size of these peaks does not appear to be approaching a limiting value after 8 days, suggesting that inventory buildup in the specimen is occurring even after 8 days in helium.

Tritium Recovery in 0.01% H_2 versus Helium

The tritium recovery for 4 days in 0.01% H_2 (B1.1) was compared to the recovery for 4 days in helium sweep gases (B1.2). The tritium-recovery curves are given in Figure 5.12. The steady-state recovery in 0.01% H_2 appears to be approximately equal to that in helium, but the smaller recovery peak for He-0.01% H_2 upon reintroduction of the reference gas is a clear indication that the inventory buildup in He-0.01% H_2 gas was less than in helium. This suggests that the recovery rate for helium may be slightly less than that for He-0.01% H_2.

Tritium Recovery in Helium Followed by 0.01% H_2

The inventory in helium versus 0.01% H_2 was investigated by following 4 days of operation in helium with 2 days in 0.01% H_2 (C3.1). The tritium-recovery curves in Figure 5.13 indicated that a 20% reduction of recovery rate occurred in helium (versus 0.1% H_2) followed by a recovery rate in

He-0.01% H_2 gas that was only 8% less than initial recovery rate in the reference gas. Upon re-introduction of reference gas, the recovery rate returned to its original value. One interesting feature of the recovery curve is the shape of the curve following the change from helium to 0.01% H_2. Instead of increasing to the new higher recovery rate, the curve first decreases. This type of "negative peak" was observed for temperature increases in the Phase I and Phase II temperature change canister and has been referred to as "negative peaks." Negative peaks were observed not only for Test Series C3.1, but also for similar Test Series C3.2 and A2.

Observations of the tritium recovery as a function of sweep-gas composition are consistent with a tritium release rate that decreases with decreasing hydrogen concentration in the helium sweep gas. In the reference gas, tritium was assumed to have been released and recovered at or near the generation rate in the ceramic. Residual tritium-inventory measurements during postirradiation examination (PIE) that confirm this will be discussed in Section 6. Measurements during PIE on Phase I Li_2O showed no large tritium inventory buildup, which was also consistent with this interpretation.

Tritium Recovery in 1.0% H_2

Decreasing hydrogen concentration from the reference sweep gas (0.1% H_2) resulted in an increase in the tritium inventory of Li_2O and Li_2ZrO_3. An obvious question is whether increasing the hydrogen concentration above 0.1% H_2 would result in a lower tritium inventory in the specimen. Figure 5.13 is the tritium recovery curve obtained for a 1-day change to 1.0% H_2. The total tritium, reduced tritium (HT) are plotted.

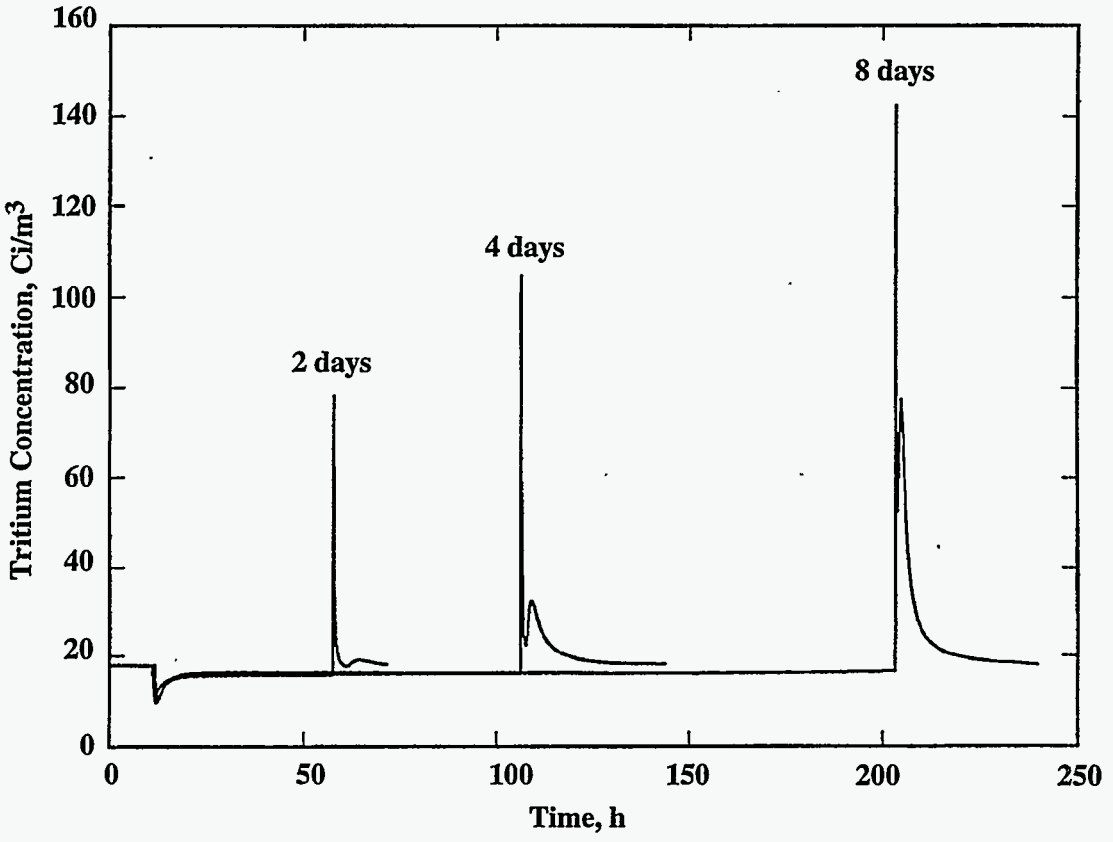

Figure 5.11. Superposition of the Results of Three Tests in Helium for 2, 4, and 8 Days in Helium Sweep Gas, Preceded and Followed by He-0.1%H_2

Compared to peaks recovered during transitions from helium and 0.01% H_2 to 0.1% H_2, the peaks for the transition from 0.1% H_2 to 1.0% H_2 are small. At the end of the one day period, the recovery rate in 1.0% H_2 appears larger than the steady-state recovery rate in 0.1% H_2. However, this larger recovery rate in 1.0% H_2 more likely results from the uncertainty of the ion-chamber correction factor used for 1.0% H_2. The same enhancement factor was used in this analysis as was used in Phase I:1.4.

The general shape of the total recovered tritium peak in Figure 5.14 is the same as that observed for the Phase I Li_2O temperature-gradient capsule after a transition to 1.0% H_2 sweep gas. The occurrence of the initial negative peaks in the transition from 0.1% H_2 to 1.0% H_2 is similar to that observed in the transition from He to 0.01% H_2 for the Phase II temperature-gradient canister (Figure 5.13).

Phase II Li_2ZrO_3 Versus Phase I Li_2O

Figure 5.15 is a superposition of the tritium recovery data for 4 days in helium for the Phase II temperature-gradient canister containing Li_2ZrO_3 pebbles (Test Series B1.2) and a very similar test series for the Phase I temperature-gradient canister containing solid Li_2O. The main difference in the recovery curves is in the integrated areas under the peaks. Both the negative peak at the introduction of He sweep gas and the positive peak at the return to helium-0.1% H_2 are smaller for Li_2ZrO_3. The inventory change for the large positive Li_2O peak is 14.4 Ci, while that for the Li_2ZrO_3 peak is 0.76 Ci. Centerline temperatures in the Phase I Li_2O were less than 1000°C, and the tritium generation rate was about 3 times as large in the Li_2O. Thus, tritium inventory increases in a helium sweep gas for

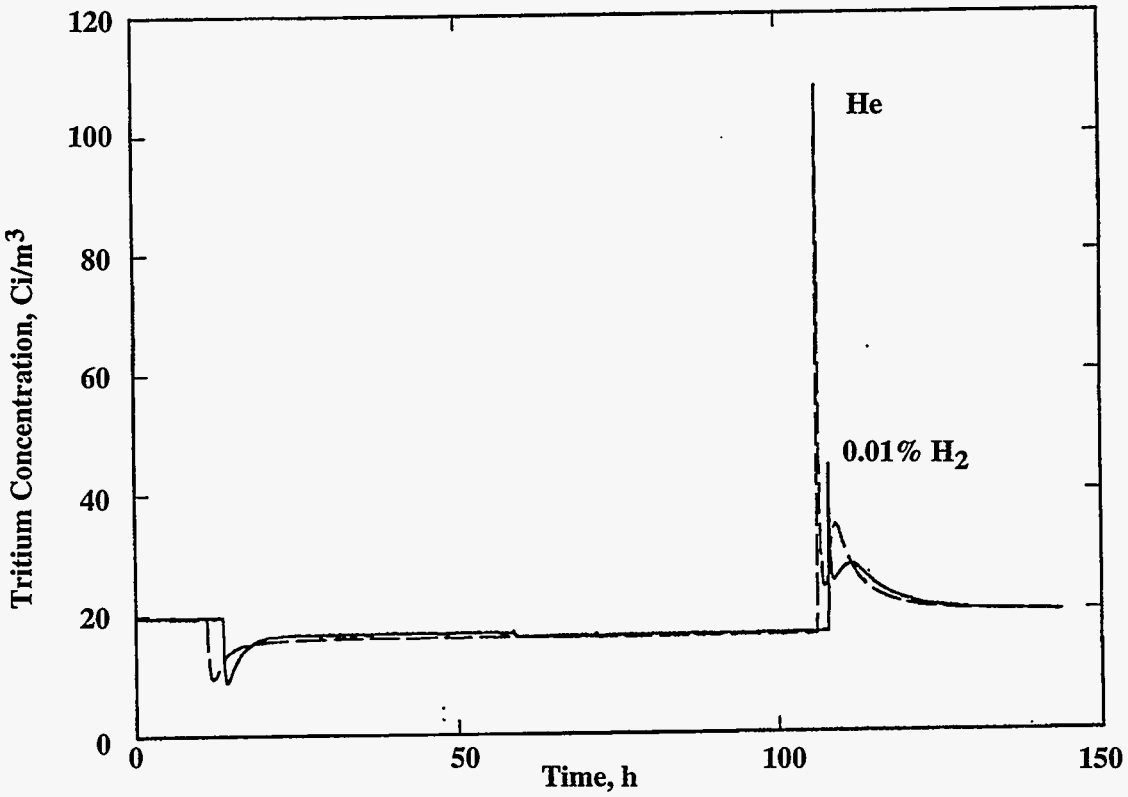

Figure 5.12. Superposition of the Results of Two Tests, One Using Helium and One Using He-0.01% H_2 Sweep Gas

both ceramics, but the buildup is smaller for the lithium zirconate. Note that a small secondary HTO peak does occur for Li_2O at reintroduction of He-0.1% H_2 but it is masked by the width of the large HT peak. These data indicate that, compared to Li_2O, the tritium inventory in Li_2ZrO_3 is less sensitive to the amount of hydrogen in the sweep gas.

5.3.4 Flow Rate

During the time periods when the ion chamber on the CEC flow stream for the temperature-change canister was being calibrated in helium sweep gas, the sweep-gas flow rate in the temperature-gradient canister was increased to 200 mL/min of 0.1% H_2 sweep gas. Immediately after the increase, the recovery rate increased about 3 to 4%, but then slowly decreased. Similarly, upon dropping the flow rate from 200 to 100 mL/min, the recovery rate decreased and then slowly increased. The data suggest that increasing the flow rate may cause a slight reduction in the inventory of the specimen or system. Such a reduction may have been associated with a "purging" effect due to the drop in tritium concentration in the sweep gas.

One of the difficulties in interpreting the changes in tritium recovery rates with changes in flow rate is that the effect of flow rate on the ion-chamber response is not known. Test Series B.2 for the temperature-gradient canister involved a change in flow rate through the CEC and the molecular sieve flow streams while keeping the total flow through the canister the same. The flow rate through the CEC was changed from 50 to 25 mL/min, and the flow rate through the molecular sieve was

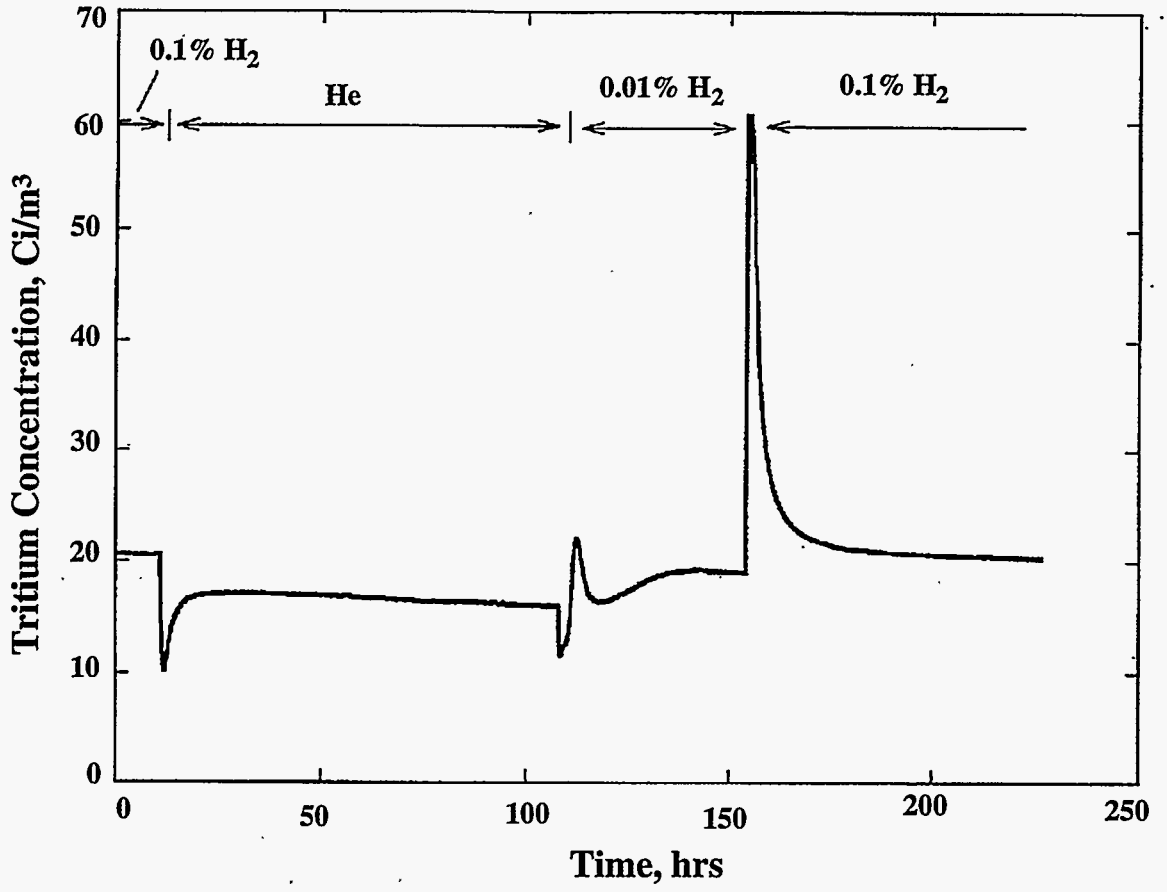

Figure 5.13. Recovered Tritium during Sweep Gas Composition Changes for 4 Days in Helium Followed by 2 Days in 0.01% H_2 for the Temperature-Gradient Canister

changed from 50 to 75%. No change occurred in the response of the ion chamber on the CEC flow stream, but the ion-chamber response on the molecular-sieve flow stream decreased 1.4% with the 50% increase in flow rate. These limited results suggest that for flow rates in the range of 25 to 75 mL/min, the effect of flow rate on the ion-chamber response was negligible.

5.3.5 Reactor Startup/Shutdown

The Phase II temperature-gradient canister was shutdown in helium at the end of Phase II-B and restarted in helium in Phase II-C. Temperature decreases were accompanied by decreases in the tritium recovery rate, and no unexpected behavior was observed as was seen in Phase I. This observation supports the conclusion reached from the comparison of Phase I and Phase II in Figure 5.15: compared to Li_2O, the tritium inventory in Li_2ZrO_3 is less sensitive to the amount of hydrogen in the sweep gas.

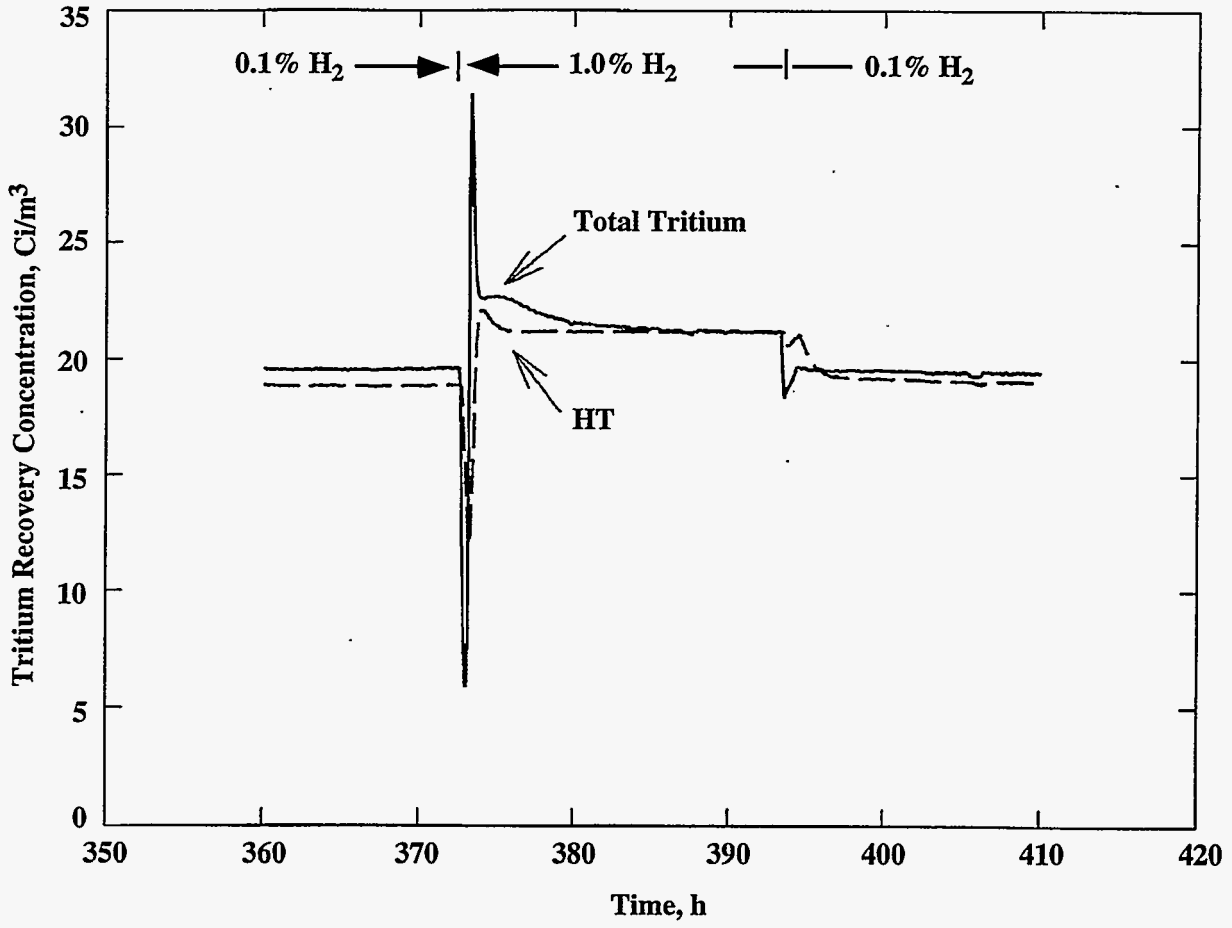

Figure 5.14. Tritium Recovery Curve for a 1-Day Change to 1.0% H_2

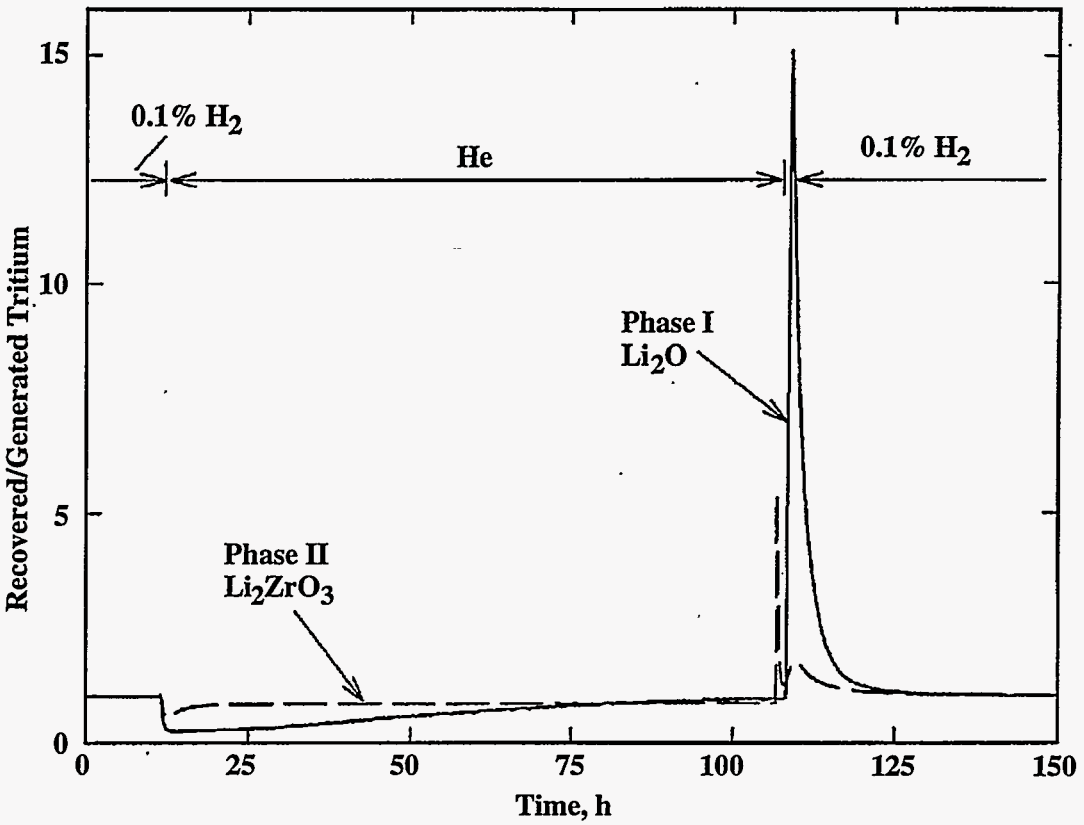

Figure 5.15. Superposition of the Results of Two Tests, both Using Helium Sweep Gas for 4 Days. One is for the BEATRIX-II, Phase II lithium zirconate, and one is for BEATRIX-II, Phase I Li_2O. The tritium-recovery-rate axis is normalized to the generation rates for the two materials.

6.0 Postirradiation Examination

Postirradiation examination of the lithium ceramics irradiated in BEATRIX-II was carried out to evaluate their physical and chemical stability during irradiation and to contribute to understanding the tritium/helium behavior. The final tritium inventory was used to establish a baseline at reference conditions that can be used to extrapolate to the tritium inventory at other testing temperatures and sweep-gas compositions. Postirradiation examination carried out after the Phase II *in situ* testing included the Phase II *in situ* canisters, the Phase I Li_2O single-crystal capsules, and the lithium ceramic-beryllium compatibility capsules irradiated in Phase I and II.

The chemical and physical integrity of the *in situ* Li_2O and Li_2ZrO_3 specimens were expected to be influenced by the temperature and sweep-gas compositions under which the materials operated. The irradiation was concluded by a reactor shutdown over 10 hours during which time approximately 0.6 Ci of tritium were generated in the Li_2O temperature-change specimen, and 0.5 Ci of tritium in the Li_2ZrO_3 temperature-gradient specimen. This generation of tritium at the lower temperatures may have contributed to a change in the tritium inventory in the specimen as compared to the steady-state inventory at the time of shutdown. After shutdown, the canisters remained at a temperature of 220°C for 9 months in a helium sweep gas until the irradiation vehicle was removed from the reactor.

Postirradiation examination of the *in situ* canisters included neutron radiography, lithium transport to the plenum, lithium isotopic, miscrostructural characterization, and tritium inventory. The results for the Li_2O single crystals include final lithium isotopic ratios and tritium/helium inventories. For the lithium ceramic-beryllium capsules, the postirradiation examination included microstructural examination and tritium/helium retention measurements.

6.1 Neutron Radiography

After removal from the irradiation test vehicle and before disassembly, the two vented canisters were shipped to Argonne National Laboratory, West (Idaho Falls, Idaho) for neutron radiography. Figures 6.1 and 6.2 include the resulting radiographs obtained for the temperature-change and temperature-gradient canisters, respectively. Because of the large neutron absorption cross section of ^6Li, the lithium ceramics are highlighted in the neutron radiographs (i.e., they appear dark in the prints). Two different exposures of the radiographs are shown. The radiograph on the left is lighter and shows the internal details of the specimen; the radiograph on the right shows the details of the metal canister.

The temperature-change-canister radiograph shows that the Li_2O ring specimen remained in its initial cylindrical geometry throughout the experiment. Although the neutron radiograph for the Phase I ring specimen had been found to contain a number of cracks, the Phase II specimen has no apparent cracks. Both the inlet and outlet gas plenums contain neutron absorbing residue, nominally lithium-containing material and likely Li_2O. Note that the capsule was radiographed in a vertical position, upside-down, so that the residue was in the bottom of the plenums at the time of radiography.

The low-contrast neutron radiograph (on the left) of the temperature-gradient canister after irradiation shows the pebble bed and the center thermocouple well. In the higher-contrast radiograph, the sweep-gas plenums at either end are clearly delineated, and no observable neutron absorbing residue is present. The pebble bed did not appear to have expanded or shrunk due to sintering during irradiation.

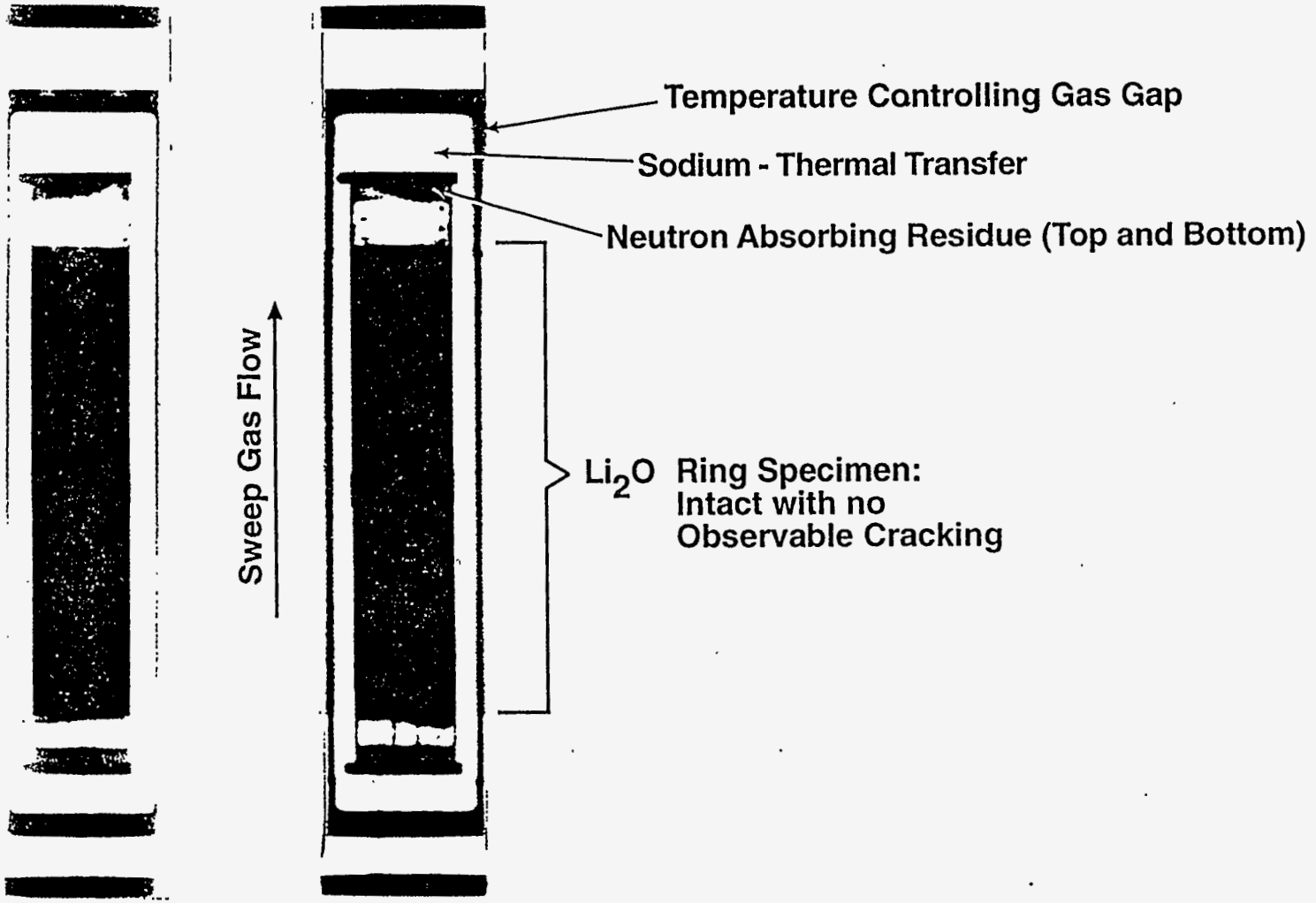

Figure 6.1. Neutron Radiograph of the Phase II Temperature-Change Canister after Irradiation

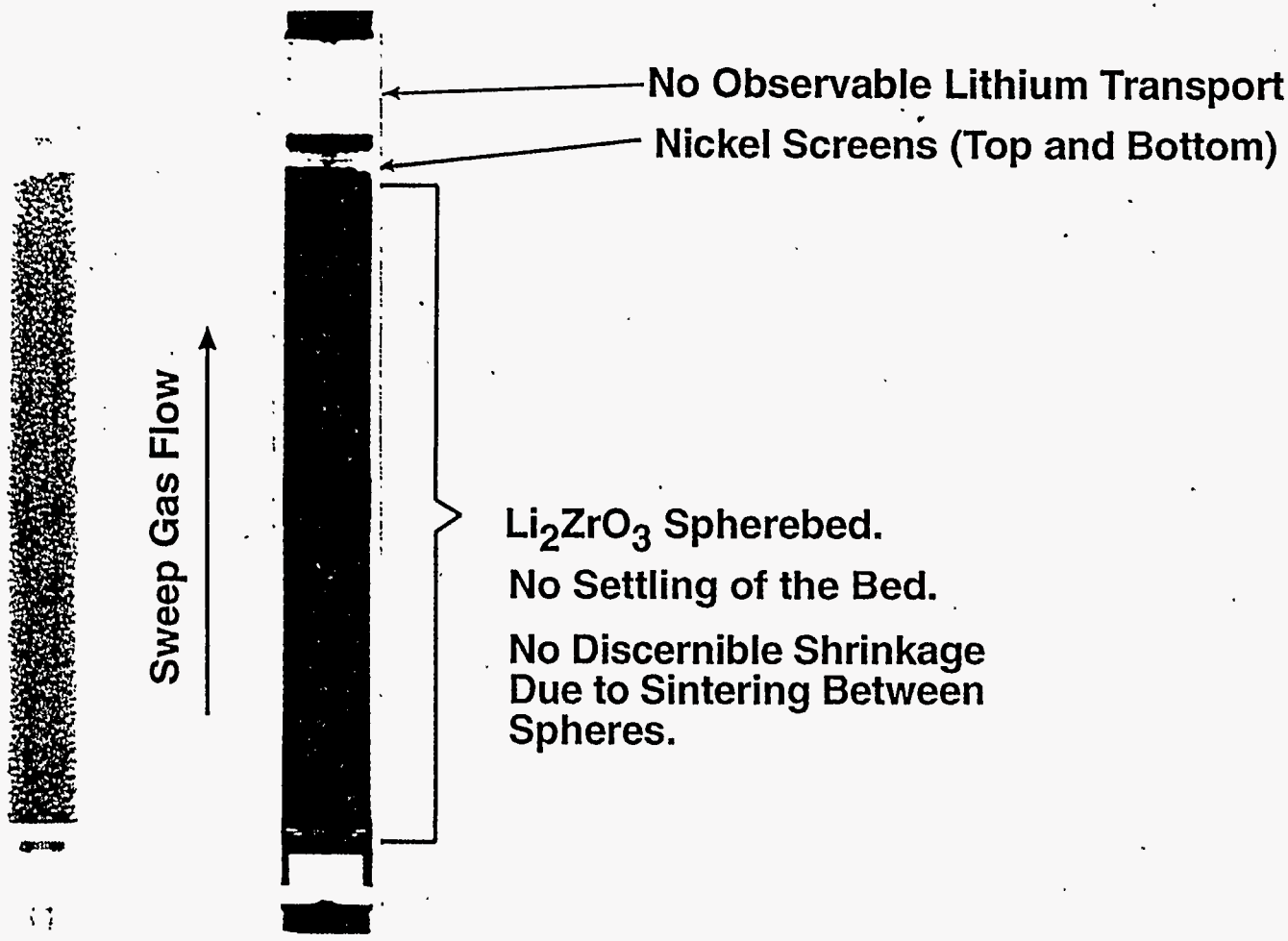

Figure 6.2. Neutron Radiograph of the Phase II Temperature-Gradient Canister after Irradiation

Neutron radiography was also carried out on the lithium ceramic-beryllium capsules. However, the size of these specimens was so small that whether or not the lithium migration had occurred could not be resolved.

6.2 Temperature-Change Canister

Postirradiation examination of the temperature-change canister was carried out at PNNL. This work involved canister disassembly, density measurements, microstructural examination, tritium transport to the plenums, final lithium isotopic ratios, and tritium retention in the Li_2O ring specimen.

6.2.1 Canister Disassembly

The canister was disassembled by slitting the inner capsule lengthwise adjacent to the specimens so that the cladding could be separated, resulting in as little disturbance to the specimens as possible. The ring specimen was found to be fragmented into pieces 1 cm^2 or smaller. Figure 6.3 is a photograph of typical specimen fragments removed from the temperature-change canister. Both surfaces of specimens from the bottom of the canister were light tan in color. Specimens taken from locations above this position had black inner surfaces and tan outer surfaces. Note that on the inner surfaces, a small circular region was lighter in color. These "dots" were thought to represent Li_2O that was extruded through the 1.5-mm holes in the stainless steel liner tube during irradiation.

6.2.2 Lithium Transport

In the operation of a solid-breeder fusion blanket, lithium in the vapor form should not transported out of the solid-breeder region into other components of the blanket. For this reason, it was useful to study the BEATRIX-II behavior and determine if lithium was transported from the Li_2O temperature-change specimens to the plenum regions of the capsule. For Phase II, the upper and lower plenums of the temperature-change canister consisted of the end caps and the diffuser plates separating the specimen from the plenums in the end caps. All four components were acid-washed and the resulting solutions analyzed for lithium. Table 6.1 lists the results of the analysis of the wash solutions. The results for the upper diffuser indicated considerably more lithium than the results from the other components. This observation was reasonable because the sweep gas passes through the upper diffuser immediately after passing along the inner diameter of the specimen. The 0.1% of lithium is much higher than the amount of lithium found for the Phase I canisters where the combined amount of lithium in the upper and lower end caps and on the associated diffuser was 0.0035% of the total lithium in the specimen.

Table 6.1 Amount of Lithium Found in the Analysis of Wash Solution from Selected Components of the Phase I Temperature-Change Capsule

Component	Total Lithium (mg)	Percent of Specimen Weight
Upper End Cap	0.05	0:001
Upper Diffuser	3.60	0.100
Lower End Cap	0.35	0.010
Lower Diffuser	0.31	0.010

6.2.3 Density and Microstructural Characterization

Density and microstructural characterizations of the specimen were carried out to determine the changes in microstructure that occurred during irradiation and to establish the microstructural parameters associated with the final tritium inventories. A more detailed description of the density and microstructural changes in the Phase II ring specimen was presented by Takahashi et al. (1995).

BEATRIX-II, Phase II
Li_2O Temperature-Change Specimen

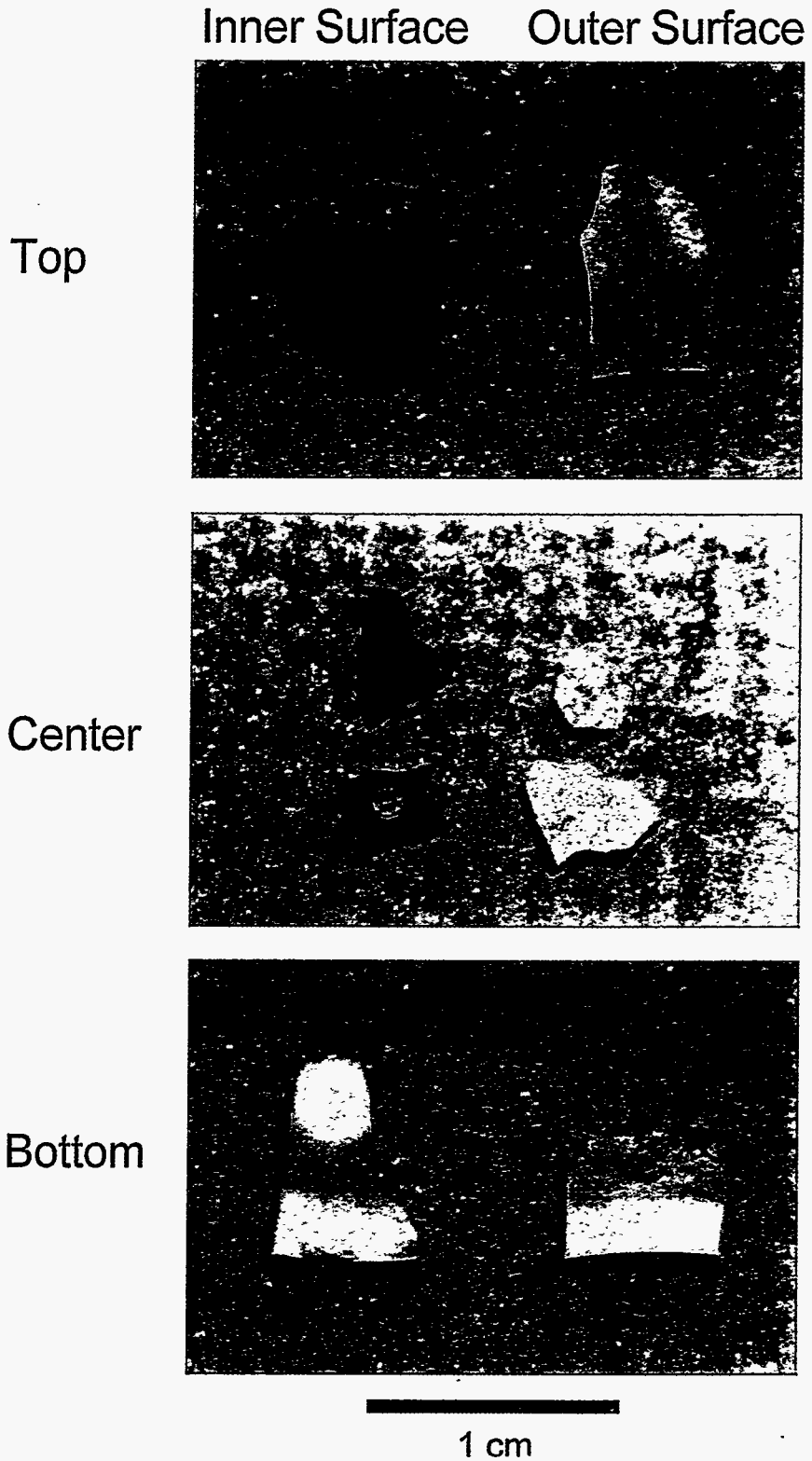

Figure 6.3. Typical Specimen Fragments Removed from Different Axial Locations of the Phase II Temperature-Change Canister after Irradiation

The postirradiation thickness of the ring specimen was measured and used to determine the radial swelling during irradiation. The thicknesses were measured for selected fragments from different axial locations along the ring specimen, and the resultant changes during irradiation are listed in Table 6.2. The wall-thickness swelling varied from 15.1 to 25.5 with an average value of 21.5%.

The density of the selected specimens was determined by immersion density measurements in xylene. Vacuum impregnation was used to determine the relative amounts of open and closed porosity. The densities and porosities are listed in Table 6.2. The initial densities ranged from 87 to 88% TD compared to final densities in the range from 61 to 66% TD. The main contribution to this decrease in density appears to be an increase in the open porosity from 3 to 30%.

Table 6.2. Wall Thickness Changes, Densities, and Porosities for the Postirradiation Phase II Ring Specimen. Densities and porosities for an unirradiated archive specimen are included for comparison.

Axial Location	Wall Thickness Swelling (%)	Bulk Density (%TD)	Open Porosity (%)	Closed Porosity (%)
Top	15.1	62.9	31.3	5.8
Near Top	25.5	61.3	26.2	12.5
Upper Center	21.2	65.7	25.0	9.3
Lower Center	20.4	61.6	33.2	5.1
Near Bottom	24.8	63.3	32.6	3.9
Bottom	22.1	63.3	32.5	4.2
Average	21.5	63.0	30.1	6.8
Unirradiated	—	88.4	2.6	8.9

Ceramographic examination was carried out on a series of fragments taken from axial locations similar to those in Table 6.2. Figure 6.4 is a cross section taken from a fragment near the center of the specimen. No large grains were visible, but rather the structure appeared to have an open overall "spongelike" appearance. The microstructure appeared coarser (larger porosity) toward the inner surface. This coarseness tended to be more apparent in the upper part of the specimen. Figure 6.5 includes SEM micrographs taken at two different magnifications of an area near the center of the specimen. This view shows in more detail the open "spongelike" microstructure. The individual grains in the network appeared to be platelets with cross sections on the order of 5 μm or less across and thicknesses of 0.1 μm. The platelets were arranged in stacks to make up the microstructure of the material. These small grains were characteristic of the majority of the ring sample, but specimens taken from the top of the ring specimen showed regions of larger grain size (Takahashi et al. 1995).

6.2.4 Lithium Isotopic Determinations

Mass spectroscopy was used to determine the relative amounts of ^{6}Li and ^{7}Li at selected locations along the ring specimen. These values were used to determine the total lithium burnup during the irradiation. The pre- and postirradiation amounts of ^{6}Li and the calculated burnups are listed in Table 6.3. The calculated lithium burnup varies from 2.1 to 3.8%. This is considerably less than the burnup value of 4.6% determined from the total amount of tritium recovered (Table 5.1). Because of the large uncertainties in the burnups calculated from the % of ^{6}Li and the fact that the initial ^{6}Li values were not made on the same specimen as the final measurements, the agreement is as good as can be expected. The primary conclusion to be reached here is that isotopic measurements on high-enrichment ceramics are not reliable methods for determining burnups.

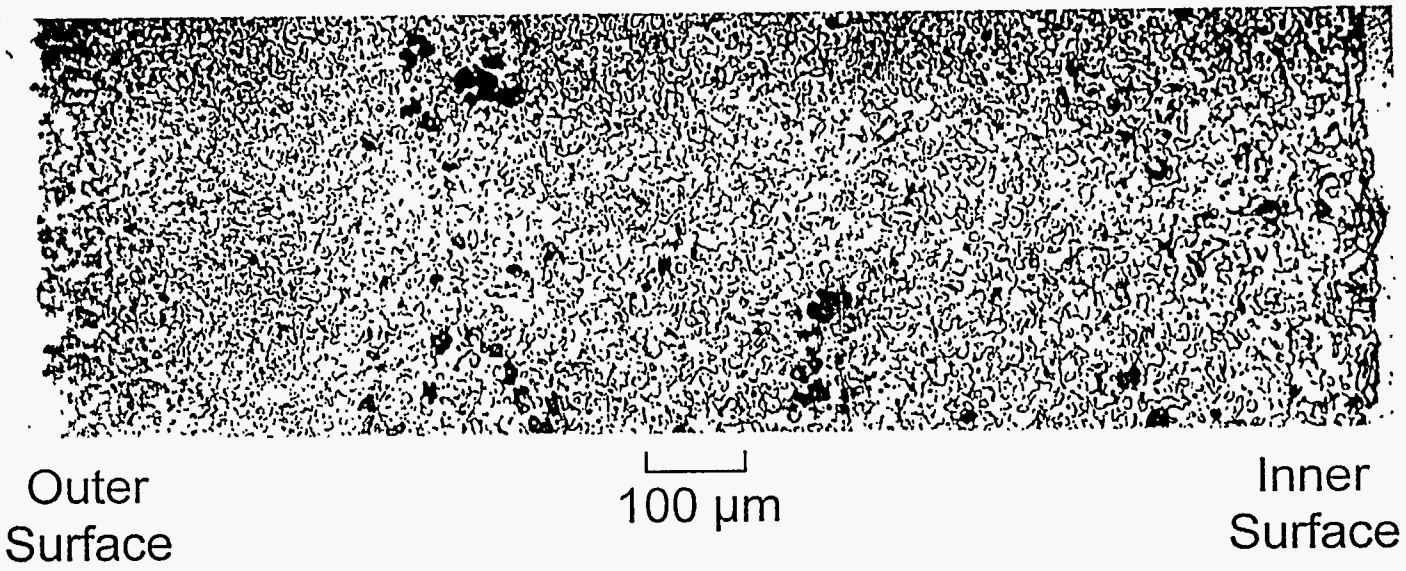

Figure 6.4. Ceramographic Cross Section from a Region near the Center of the Phase II Temperature-Change Specimen

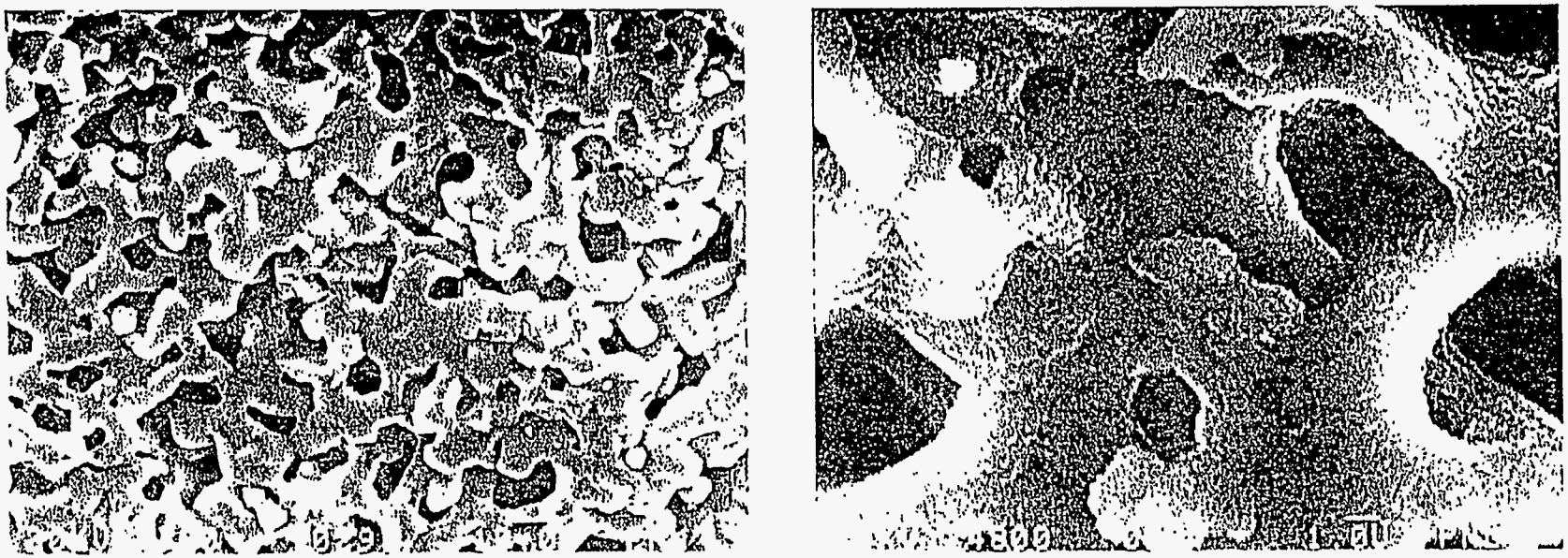

Figure 6.5. SEM Micrographs from an Area near the Axial Center of the Phase II Temperature-Change Specimen

Table 6.3. Pre- and Postirradiation Percentages of ^6Li in the Phase II Temperature-Change Specimen and the Resulting Lithium Burnup

Description	Initial ^6Li (%)	Final ^6Li (%)	Lithium Burnup (%)
Top	95.26 ± 0.02	95.12 ± 0.02	2.9 ± 0.8
Upper Center	95.26 ± 0.02	95.08 ± 0.03	3.7 ± 1.0
Lower Center	95.26 ± 0.02	95.16 ± 0.02	2.1 ± 0.8
Bottom	95.26 ± 0.02	95.07 ± 0.03	3.8 ± 1.0
Average	95.26 ± 0.02	95.11 ± 0.025	3.1 ± 0.9

6.2.5 Tritium Inventory Measurements

The tritium inventory along the length of the ring specimen was measured using specimens taken from four different axial locations. The top and bottom sections were selected on the basis of having an end surface and hence represented material within 1 cm from the end. Upper center and lower center are only approximate locations. The analysis was done by two different methods. In the first method, the selected specimens were melted, and the tritium released was determined using a variation of the method previously described (Baldwin and Hollenberg 1986). The present analysis technique used a gas sweep rather than vacuum extraction for obtaining the gas sample. In the second method, the Li_2O specimens were dissolved in heated water within a closed system that was swept by a sweep gas flowing through a copper oxidizer and into collection bubblers. Tritium was measured by liquid-scintillation counting both in the dissolution liquid and in the collection bubblers and then combined for the final result. Aliquots of the dissolution solutions were titrated with acid to determine the extent of hydrolysis at the time of specimen weighing, and the results were 0.068 ± 0.001 moles OH/g. Unhydrated Li_2O has 0.067 moles OH/g; fully hydrated Li_2O (LiOH) is expected to have 0.042 moles OH/g. The titration results indicate that the specimens were unhydrated.

The Phase II results of postirradiation tritium inventories for the temperature-change specimen in Table 6.4 are compared with results from Phase I. The Phase I inventories determined by melting have been reported previously (Slagle et al. 1994). The inventories determined by dissolution were carried out as an over check. Two differences in the data sets are significant: 1) the inventories for the Phase II specimens are smaller than for the Phase I specimens even though the Phase II shutdown occurred over a much longer time and 2) the measured tritium inventory for the Phase I specimens decreased from the top to the bottom of the specimen, but for the Phase II specimens, the inventory was essentially constant.

Table 6.4. Measured Tritium Inventories for the Phase I and Phase II Li_2O Temperature-Change Specimens. All inventories were corrected for tritium decay to represent the inventories at the time of shutdown.

	Tritium Inventory (wppm)			
	Phase I		Phase II	
Axial Position	Melt	Dissolution	Melt	Dissolution
Top	0.66	0.68	0.19	0.25
Upper Center	0.48	0.42	0.20	0.24
Lower Center	0.29	0.32	0.20	0.22
Bottom	0.25	0.21	0.22	0.23
Average	0.42	0.41	0.20	0.24

Because the Phase II experiment was shut down over a period of 10 hours versus the 2-minute controlled scram for Phase I, it was hypothesized that the Phase II inventory would be higher due to a buildup in the tritium inventory while the specimen was operated at the lower temperatures. The data in Table 6.4 suggest that this was not the case. One of the reasons why the Phase I and II data were analyzed by dissolution/titration was to ensure that the differences in the melt-determined inventories were not a result of weight changes during postirradiation handling.

The measured post-irradiation tritium inventories of the Phase II ring specimen were smaller than similar inventories measured previously for the Phase I specimen. Compared to Phase I, the *in situ* tritium recovery from the Phase II ring specimen was very similar to Phase I. During the first half of the Phase II irradiation period, the tritium recovery peaks following temperature transients were very similar to those observed at the end of the Phase I irradiation (Figure 5.3). During the second half of the Phase II experiment, after extended operation in sweep gases with a concentration of hydrogen less than 0.1%, the tritium recovery peaks after a temperature transient became broader and less sharp. However, the total peak size or change in tritium inventory remained essentially the same. On the basis of the *in situ* recovery results, no reason existed why the inventory of the Phase II specimen should have been significantly different than the Phase I specimen.

The measured tritium inventories in Table 6.4 for Phase I temperature-change specimen increase from bottom to top, but the currently measured Phase II inventories are essentially constant. In fact, the Phase II inventories are in very good agreement with the Phase I inventories from the bottom half of the specimen. Previously, the increasing inventories at the top of the Phase I specimen were thought to have resulted from the sweep gas flow from the bottom to the top of the canister (Slagle et al. 1994). At the top of the specimen, the sweep gas would have contained a higher partial pressure of HTO/HT, and this higher partial pressure would have tended to decrease the tritium recovery rate. The constancy of the Phase II inventories is inconsistent with the previous explanation, and therefore, the axial variation of the Phase I inventories remains an open question.

6.2.6 Tritium Retention Predicted from Shutdown Data

In situ tritium recovery data from the Phase I and Phase II temperature-change canisters indicated that decreasing temperatures during shutdown could have resulted in an increase in the tritium inventory in the specimen (see Section 5.2.2). It is possible that during the slow shutdown of Phase II, the inventory increased as the temperature decreased. As a check on whether such an increase may have occurred, a comparison was made between the recovered tritium and the amount of tritium generated during that time. Since the flux monitor was inoperable during shutdown, an alternative means of estimating the tritium generation was needed. The amount of tritium generated was estimated from the power or heat generation using two different methods:

1. Reactor power versus time during the shutdown. This is the average power for the reactor and not specifically for location of the temperature-change canister that was near the bottom of the core region.

2. Power or heat generation in the specimen. The temperature difference across the Li_2O ring specimen was assumed to reflect changes in the heat generation. For the Phase II temperature-change canister, the available temperature difference is between a thermocouple on the inner diameter of the specimen and a thermocouple outside the specimen subcapsule in the sodium thermal-bonding region. To better approximate the power generation in the specimen, the temperature difference across the specimen was corrected for the change in thermal conductivity of the Li_2O during shutdown (Takahashi and Kikuchi 1980; Hollenberg and Baker 1982). This approximation does not take into account specimen to capsule gaps forming/increasing during shutdown.

Figure 6.6 is a comparison of the recovered tritium for the temperature-change canister with the calculated tritium generation. The difference between the tritium recovery and the tritium generation curves gives a means of predicting the change in tritium inventory in the specimen from the start of shutdown to the end. Integrating over the recovery curve indicates that 0.607 Ci of tritium were recovered during the shutdown. For the reactor power case, 0.549 Ci were generated for an inventory decrease of 0.059 Ci (0.74 wppm). For the specimen temperature case, 0.637 Ci were generated to effect a 0.029 Ci (0.36 wppm) increase in specimen inventory. Because both of these cases represent an approximation to the tritium generation during cool down and because both predictions are opposite and within the 10% uncertainty of the tritium recovery measurements, an analysis of the shutdown curves does not provide conclusive evidence that the tritium inventory changed during shutdown.

6.3 Temperature-Gradient Canister

After neutron radiography, the Phase II temperature-gradient canister was shipped to AECL Research at Chalk River, Ontario, where the postirradiation examination was carried out. This report includes the results of post-irradiation examination of the Li_2ZrO_3 pebble bed, including neutron radiography, x-ray diffraction, tritium-inventory measurements, and SEM.

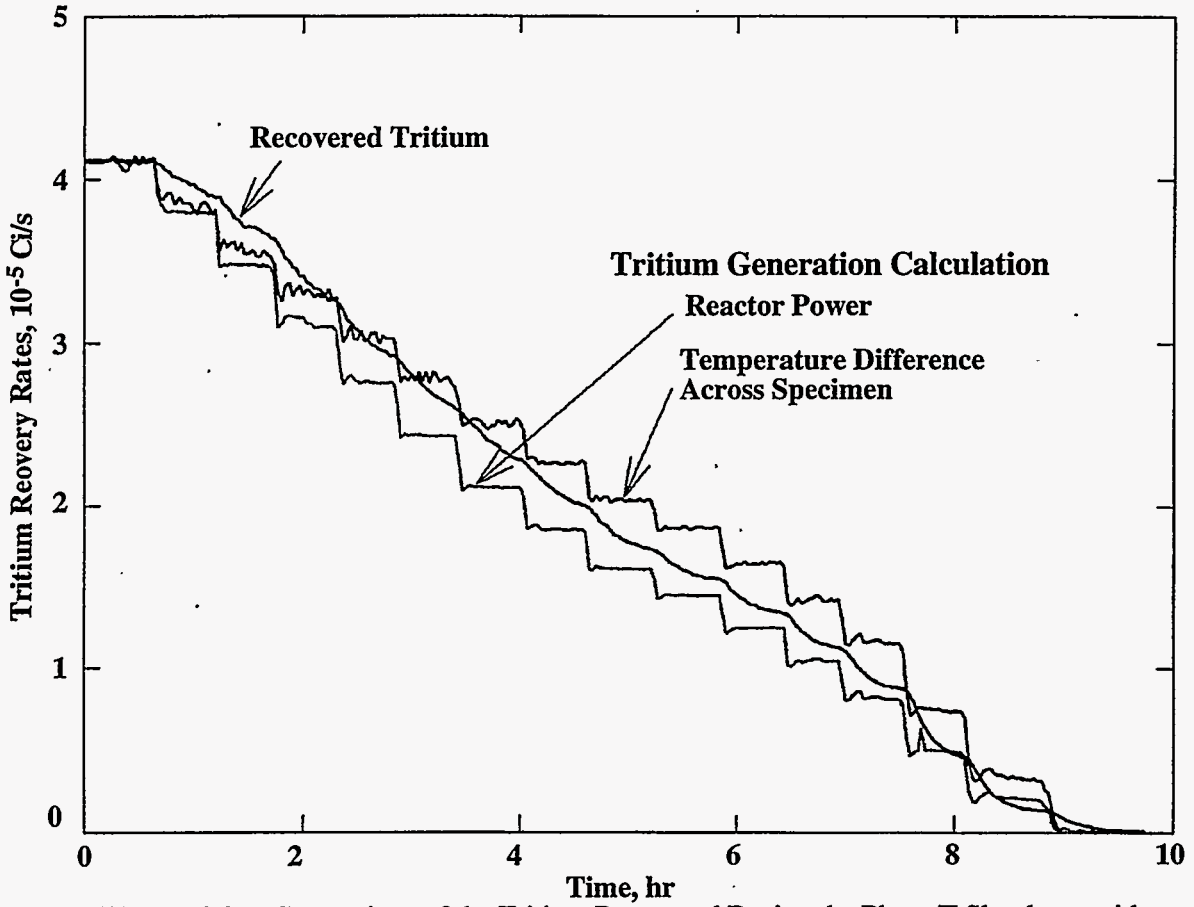

Figure 6.6 Comparison of the Tritium Recovered During the Phase II Shutdown with Two Different Assumptions for the Tritium Generated

6.3.1 Tritium-Inventory Measurements

Because of the large temperature variation from the edge of the specimen (400°C) to the center (>1000°C at shutdown), the tritium inventory was expected to vary significantly with radial position in the specimen. Determining the inventory as a function of radial position became the primary focus of the tritium-inventory measurements.

Disassembly Procedures

To obtain tritium inventory data as a function of temperature and location, the Li_2ZrO_3 pebbles were immobilized with a low-temperature curing resin, Castoglass®, to fix the position of the pebbles before removing the pebble bed from the irradiation canister. With the canister in a hot cell, the resin was added to the pebble bed through the purge-gas line. At various positions along the length of the solidified pebble bed, 2-mm-thick wafers were cut from the bed. Figure 6.7 shows the axial location of the 11 wafers. The wafers were designated A, B, and K with wafer A at the top. Figure 6.8 is the cutting diagram used to divide each of the wafers into 1.8- x 1.8-mm sections. The sections were cut from the wafers using a computerized numerical control (CNC) machine fitted with a diamond saw. To maintain wafer strength for subsequent cutting and handling, each saw cut was filled with Castoglass® resin and allowed to set.

The cutting diagram was designed to divide the 13.2-mm-diameter wafers from the pebble-bed into a fine grid of specimens that would minimize the temperature variation in any one section. Conversely, it was necessary to make the individual sections large enough to allow handling and provide sufficient section weight for carrying out the tritium-inventory measurements. The sectioning pattern allowed the tritium inventory to be determined as a function of the radial direction to distinguish possible angular differences in temperature or neutron flux.

The sectioned wafers were removed from the hot cell and placed in a fume hood. The stainless-steel sheath and inner thermocouple segment were removed using methylene chloride to dissolve the resin holding them in contact with the ceramic. The orientation of the wafer with respect to its position in the capsule was retained in the procedure. The 1.8- x 1.8-mm samples were also separated along the cut lines by dissolving the resin. Each section was then placed in methylene chloride to dissolve the resin from the pebbles. After approximately 24 hours, the methylene chloride was evaporated, and the resin was separated from the dry pebbles. The pebbles (and pebble-pieces cut by the CNC saw) for each section were weighed and then reweighed approximately 1 hour later to confirm the measured dry weights. Agreement within ± 0.1 mg was considered acceptable. Section weights ranged from 5 to 17 mg; the average for the 40 sections analyzed was 10.6 mg.

Several measurements of weight and tritium inventory were made on samples containing two or three sections. The sections were combined to give increased sample size and tritium inventory and therefore determine if sample size contributed to scatter.

To release the tritium from the Li_2ZrO_3 matrix, the samples were refluxed in a solution of 10 mL aqua regia/0.5 mL HF for approximately 90 minutes. A portion of the reflux solution was then neutralized and distilled. The tritium content of the distillate was measured by liquid-scintillation counting, and the inventory of the sample was calculated. This procedure was developed and tested using non-irradiated wafer samples from a mock-up capsule with a known quantity of tritium added to the samples. Procedures for refluxing, sampling, and counting were developed that gave an accuracy and repeatability to within ±10% for the mock-up samples. The distillation procedure removed gamma and beta contaminants, present mainly from handling in the hot cell. The liquid-scintillation counting procedures were selected to ensure that only tritium was being counted and measured.

Tritium inventory data were obtained for one wafer (A) at the top and for four wafers (B, C, D, and F) from the interior of the pebble bed. The axial locations of these wafers is shown in

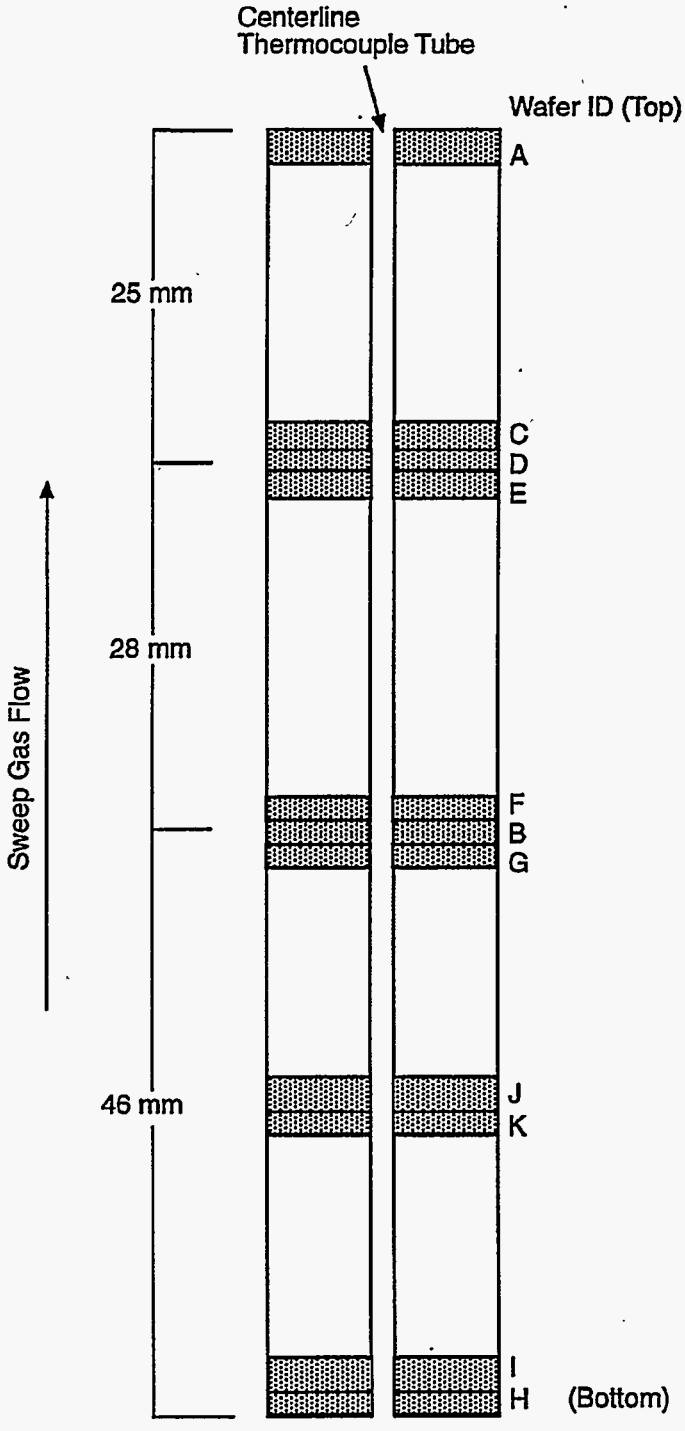

Figure 6.7. Axial Location of the 11 Wafers Cut from the Impregnated Li_2ZrO_3 Pebble Bed

Figure 6.7. The wafers from the interior of the pebble bed had similar in-reactor temperature profiles, and a comparison of their tritium inventories was expected to indicate if the inventory varied with vertical position in the capsule. The wafer cut from top of the pebble bed had a different radial temperature profile than the inner wafers because of end effects. The tritium-inventory measurement results are given in Figure 6.9. Measurements made on samples containing a single section are shown on the section. Measurements made on samples containing more than one section are given below the wafer and are identified using * and # symbols. These samples will be referred to as single-section and multi-section, respectively.

All measurements were assigned to one of three radial zones identified by the dotted lines. Wafer A at the top-left was cut from the top of the canister, and data from this wafer were not used, either in calculations of average values or in the histograms below. Comparing the inventory data from the four interior wafers indicates that no discernible variation in tritium inventory occurs with vertical position or radial direction in the capsule.

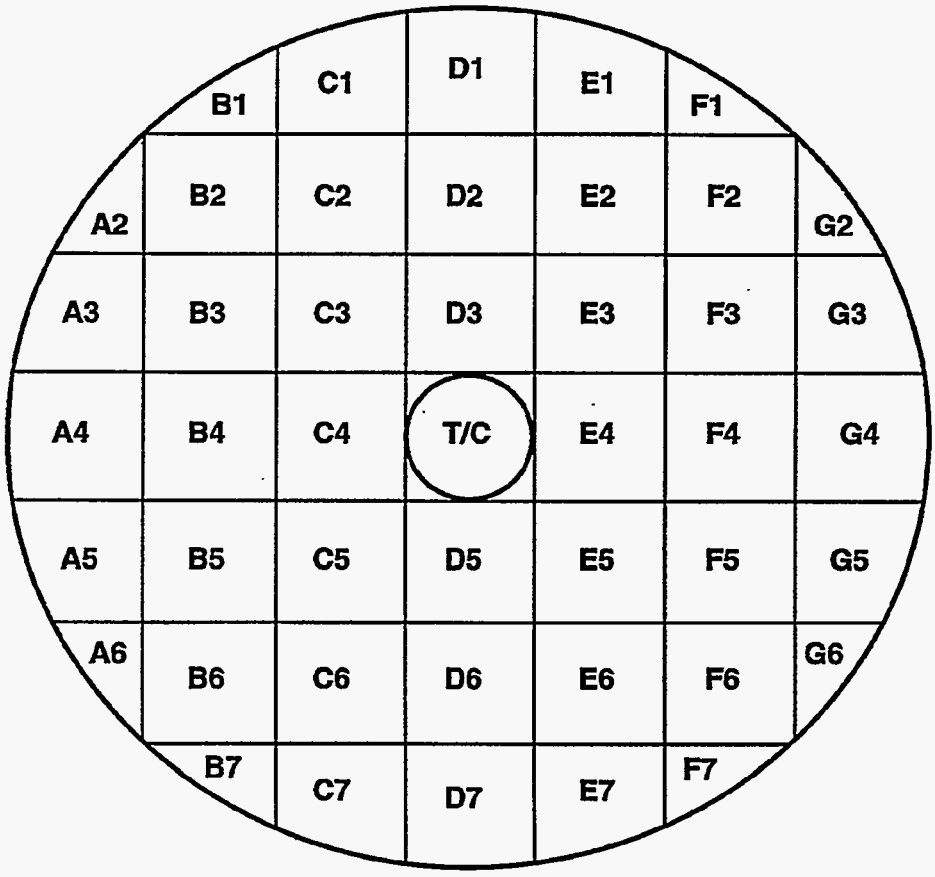

Figure 6.8. Cutting Diagram used to Divide the Wafers from the Li_2ZrO_3 Pebble Bed into 1.8- x 1.8-mm Sections.

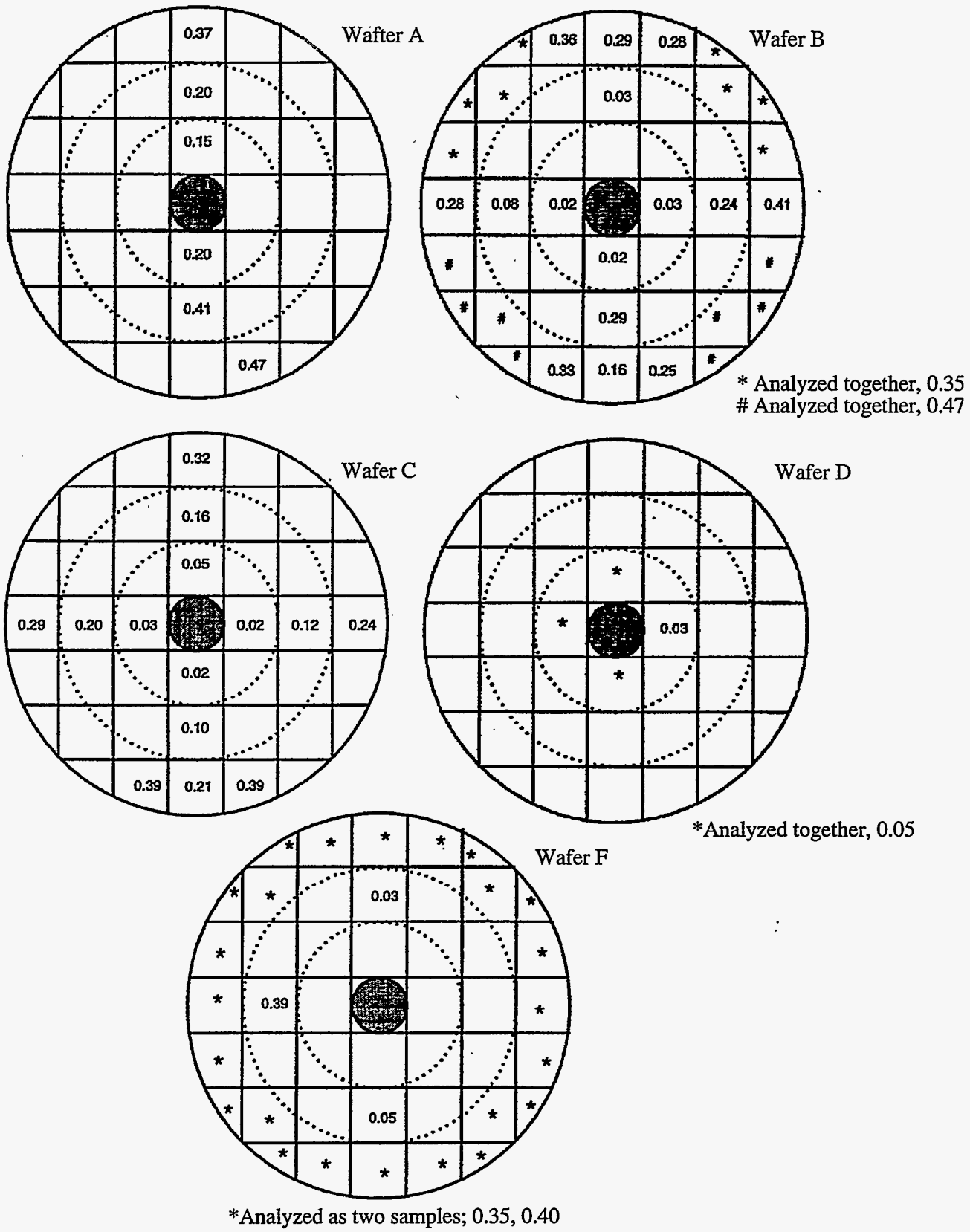

Figure 6.9. Tritium Inventory Measurements for the Sections from All Five Wafers

For comparative purposes, the radial position of the individual sections (distance from the canister centerline) were grouped into three zones: inner (1.15 to 2.95 mm), middle (2.95 to 4.75 mm), and outer (4.75 to 6.55 mm). For the outer zone, the four multi-section samples showed a smaller range of inventories (0.35 to 0.47 wppm), compared to the 14 single-section samples (0.167 to 0.47 wppm) at similar radii. The multi-section samples also had a higher average tritium inventory, 0.39 wppm versus 0.30 wppm for the single-section samples. However, since there were only four of the multi-sectioned samples, confidence in the statistics is low. Both the multi-section and single-section samples from the four interior wafers were used to determine the radial profile of tritium inventory.

Table 6.5 gives the average and standard deviation for the tritium inventories in each of the three radial zones, incorporating all data from single- and multi-section samples except those from the end wafer (see Figure 6.9). The average tritium inventory for the whole pebble-bed (weighting the data in Table 6.5 for the relative amounts of material in each radial range) is 0.22 ± 0.08 wppm. Figure 6.10 is a histogram of tritium inventories measured in the three radial zones, inner (1.15 to 2.95 mm), middle (2.95 to 4.75 mm) and outer (4.75 to 6.55 mm). The divisions on the x-axis demarcate the ranges in tritium inventory that are represented by the individual histogram's position between the divisions.

Table 6.5. Summary of Tritium Inventory Data

Radius	Temperature Range at time of Shutdown[a] (°C)	Tritium Inventory: No. of Average and Standard Deviation (wppm)	Measurements
Inner 1.15 to 2.95 mm	1025-945	0.032 ± 0.01	9
Middle 2.95 to 4.75 mm	945-770	0.15 ± 0.12	11
Outer 4.75 to 6.55 mm	770-395	0.32 ± 0.08	18

(a) See discussion below on effects of extended shutdown on tritium inventories.

Two points are evident from Table 6.5 and the histogram in Figure 6.10:

1. The scatter in the data is significantly larger than the 10% experimental error associated with the tritium-inventory measurements. The scatter is thought to be due mainly to pebble relocation that occurred during transfer of the canister from Richland, Washington, to Chalk River, Ontario, and during the procedure of flooding the pebble-bed with resin. An additional factor would be the variations in temperature within the bed due to the macroscopic nature of the pebble bed.

2. The distribution of tritium-inventory measurements for the middle zone (2.95 to 4.75 mm) is not a normal peaked distribution around the average value. Instead, they range from 0.03 to 0.39 wppm, with the peak of the distribution at the lowest values. Again, this is thought to be due to pebble relocation.

Tritium-inventory measurements of Li_2ZrO_3 after irradiation for SIBELIUS and EXOTIC-6 experiments at 485 to 550°C gave values by up to a factor of ten lower (Kopasz et al. 1995) than those in the outer zone (4.75 to 6.55 mm) of this test. Direct comparison is not simple, however, because the tritium generation rates in SIBELIUS were about a factor of 10 lower than in this BEATRIX-II lithium zirconate irradiation. In EXOTIC-6, there were self-shielding effects, and the local tritium generation rates were uncertain at the locations where the temperatures were in the range of 485 to 550°C.

Effects of Final Shutdown On Tritium Inventory

The Phase II experiment was terminated by a reactor shutdown that occurred over a period of 10 hours, and it is possible that during shutdown, a change in the tritium inventory in the lithium zirconate occurred so that the final inventory after shutdown was different than the steady-state values present at the start of the shutdown. A similar consideration for the temperature-change canister was given in Section 6.2.6. Gierszewski (1995b) has calculated the tritium generation for the Phase II temperature-gradient canister during shutdown by using thermal analysis and the measured temperatures across the pebble bed. He found that 0.43 Ci of tritium were generated during shutdown versus 0.40 recovered. With a 10% uncertainty in the amount recovered, the difference between generated and recovered becomes 0.03 ± 0.10 Ci or 0.10 ± 0.14 wppm. This means that it is possible that anywhere from none of to all of the average residual tritium inventory measured in the pebbles (0.22 wppm average) is due to inventory buildup during the shutdown. As was the case for

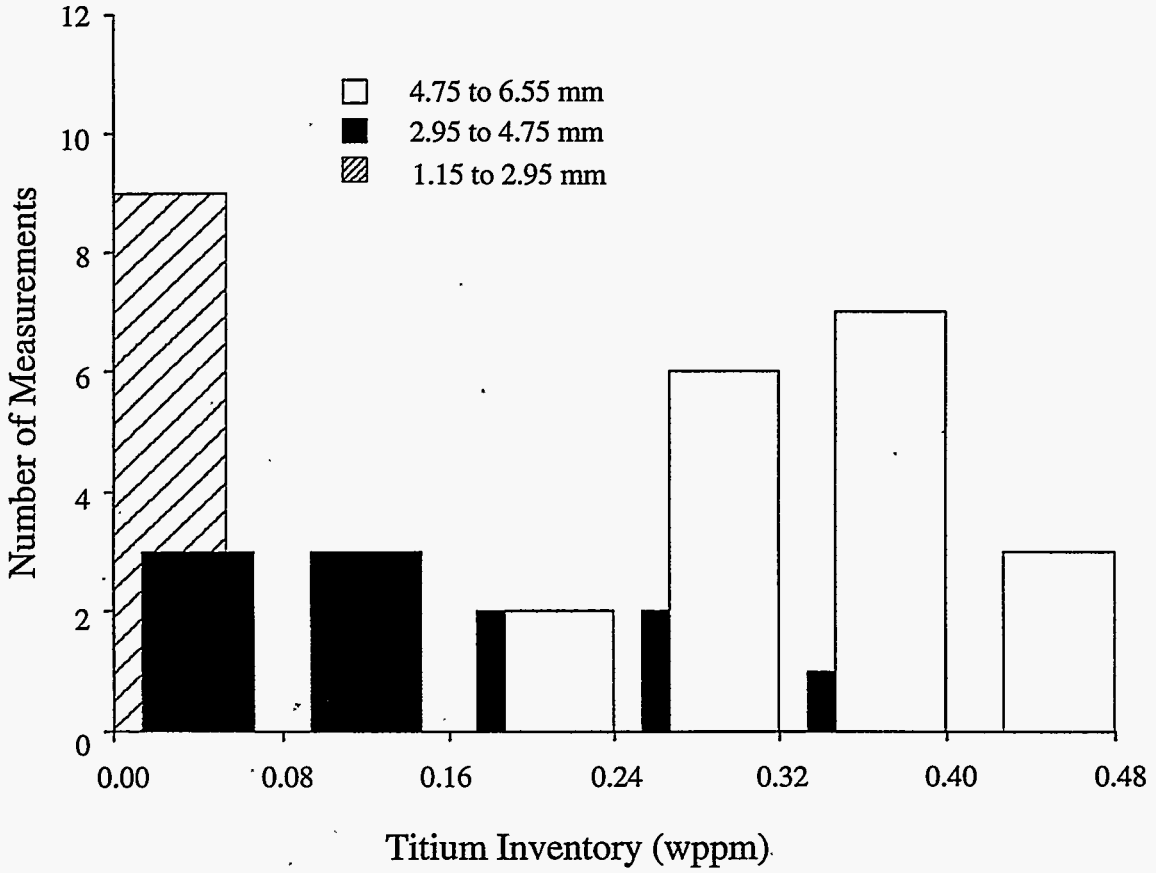

Figure 6.10. Histogram of Tritium Inventories Measured in the Three Radial Ranges, 1.15 to 2.95 mm, 2.95 to 4.75 mm, and 4.75 to 6.55 mm

the Phase II temperature-change canister, an analysis of the shutdown curves does not provide conclusive evidence that the tritium inventory changed during shutdown.

After the FFTF reactor had been shut down, the temperature-gradient canister remained at elevated temperatures in a helium sweep gas for an extended period of time: 8 hours at temperatures of over 220°C, and 6000 hours at 200°C. Gierszewski (1995b) has indicated that current models that predict *residence times* for tritium in lithium zirconate in 0.1% H_2[(a)] suggest that most of the tritium inventory could have been released from the zirconate during the extended period of time in the reactor after shutdown. However, no evidence existed for substantial tritium release during subsequent cool down and hold at 200°C for several months. The use of helium sweep gas during the extended period after shutdown seems to have prevented any significant reduction in the tritium inventory.

6.3.2 X-Ray Diffraction

An X-ray diffraction analysis was carried out on wafer G (see Figure 6.7) to determine if neutron irradiation of Li_2ZrO_3 resulted in the formation of other phases. The X-ray diffraction pattern (XRD) of unirradiated archive lithium zirconate contained all the lines for lithium zirconate and only the strongest line for monoclinic zirconium oxide. The line for zirconium oxide was for a d-spacing of 3.16 Å and had a peak height of only 1% of the strongest peak for lithium zirconate.

After irradiation, the XRD pattern contained two sets of lines: one for lithium zirconate and one for monoclinic zirconium oxide. The 3.16 Å peak for zirconium oxide was about 15% of the largest lithium zirconate peak. The radial dependence of these phases was determined by masking, alternatively, the central part of the lithium zirconate wafer and then the peripheral part of the wafer, and then qualitatively comparing the radial variation in the amount of zirconium oxide. The respective XRD patterns indicate that more zirconium oxide was in the central part of the pebble-bed than in the periphery (Table 6.6).

Table 6.6. Relative Ratio of Dominant XRD Peaks for an Irradiated Wafer

Sample Portion	Ratio of Dominant Peaks (ZrO_2/Li_2ZrO_3)
All	0.15
Edge	0.10
Center	0.28

6.3.3 Scanning Electron Microscopy

Both the polished surfaces and the fracture surfaces of the irradiated Li_2ZrO_3 pebbles, as well as samples of unirradiated archive pebbles, were subjected to SEM. Figure 6.11 is a micrograph of a polished surface of the unirradiated archive Li_2ZrO_3 pebble. Figure 6.12 is a polished surface of section through two pebbles of Li_2ZrO_3 located near the center of the pebble-bed (wafer G). The white phase is thought to be the ZrO_2 phase, both because it was found to be present from the XRD results and because the lighter appearance suggests a higher density of high-atomic-mass elements, i.e., zirconium. The occurrence of the ZrO_2 phase did not appear to give rise to any internal cracking. The contact point between the pebbles appeared to exhibit "necking" and grain growth. Both of these effects are associated with sintering phenomena between the two pebbles.

(a) M. C. Billone. "Algorithms for Estimating Tritium Inventory in ITER Solid-Breeder (Li_2O and Li_2ZrO_3) Blanket Designs." Letter to Y. Gohar, march 20, 1995.

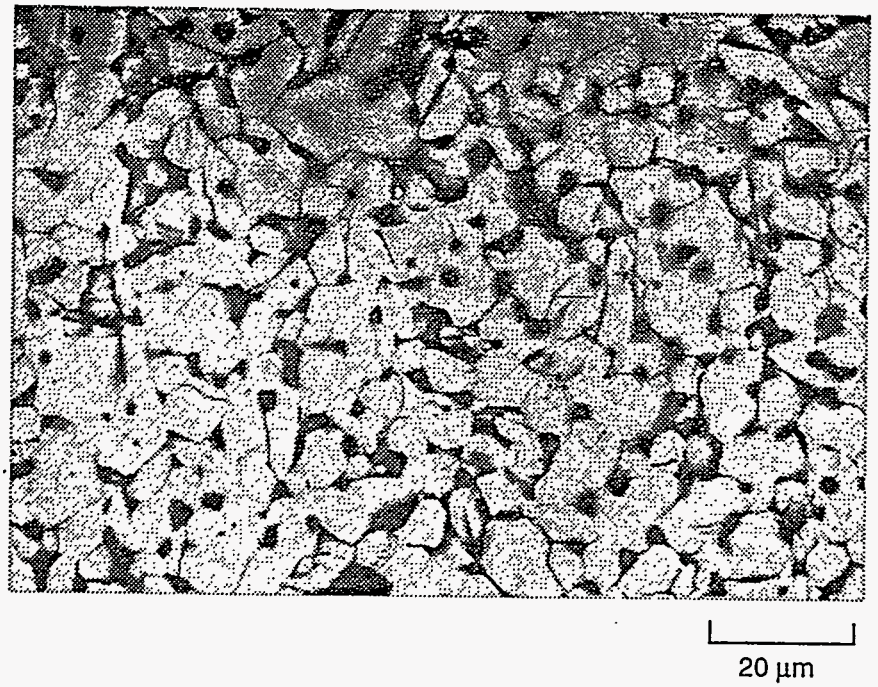

Figure 6.11. Polished Surface of the Unirradiated Archive Li_2ZrO_3 Pebble

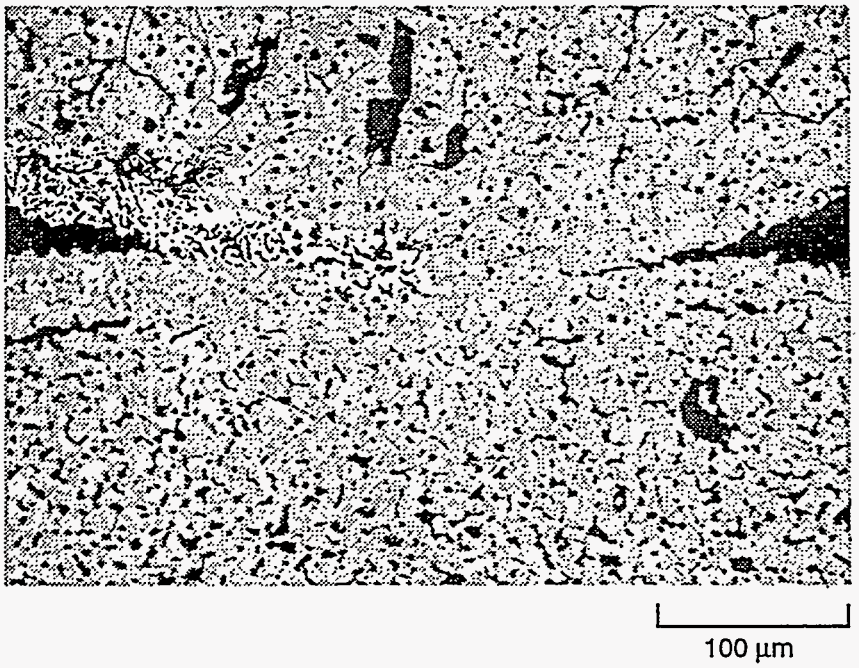

Figure 6.12. Polished Surface of Section Through Two Pebbles of Li_2ZrO_3 Located near the Center of Pebble-Bed (Wafer G). Note sinter-neck between particles and white phase throught to be ZrO_2.

Figure 6.13 is a micrograph of a fracture surface from wafer E near the center of the bed. A large number of small bubbles (<1 μm) appeared on the fractured grain surface and are most likely a result of helium generation. Helium bubbles in lithium ceramics were first seen in Li_2O (Verrall et al. 1989) and confirmed by Takahashi et al. (1995). At low magnification, the bubbles tended to form along lines (not necessarily straight lines) in the hot central zone, which is typical of helium bubbles in ceramics at high temperatures.

Figure 6.14 is a fracture surface of the center of the pebble in Wafer E, near the circumference of the bed. The grain near the center of the displays indicates the occurrence of microcracking. It is to be noted that severe damage in the form of extensive fracturing or friability that might be associated with second phase formation or anisotropic thermal expansion was lacking. Alvani et al. (1994) have proposed that extensive microcracking can originate from these phenomena.

6.4 Lithium Oxide Single Crystals

Single crystals of Li_20 were irradiated in BEATRIX-II, Phase I, to determine the fundamental mechanisms of radiation damage. The single crystals were grown by the floating zone technique at JAERI (Slagle et al. 1990) with ^6Li enrichments of 0.07, 1.8, and 61 at%. They were hand ground to an approximate uniform cylindrical shape and sized using a ring gauge. The 61 at% enriched crystals were ground to a 7-mm diameter, while the others were ground to an 8-mm diameter. Lengths ranged from 1 to 2.5 cm.

The radiation damage in the 0.07 and 1.8% enriched single crystals has been characterized by a series of electron spin resonance (ESR), optical absorption and microstructural characterization. Masaki et al. (1994) have reported the results of ESR and optical absorption and concluded that colloidal lithium metal was formed in Li_2O under fast neutron irradiation. Microstructural characterization was reported by Takahashi et al. (1994), and the results indicate that although extensive microstructural and density changes occur during irradiation, these changes had no significant impact on the integrity of Li_2O during irradiation. This report includes the postirradiation results of the tritium and helium retention measurements for all three enrichments. The plenum gas analysis, and the lithium isotopic analysis are also presented for the 61% ^6Li enriched single crystal.

6.4.1 Plenum Gas Analysis

A plenum gas analysis of the capsule containing the enriched single crystal (61% ^6Li) was carried out to determine the burnup incurred during irradiation. The gas was sampled by drilling through the top portion of the capsule and expanding the gas into a known volume at ambient temperature. Subsequent expansions into known volumes were used to determine the volume of the capsule. The amount of helium generated in the 0.7007 g Li_2O specimen and released to the plenum was 55.54 cc at standard temperature and pressure (STP) or 79.26 cc STP/g.

6.4.2 Capsule Disassembly

The capsules containing the lower enrichment single crystals (0.07 and 1.8%) were disassembled in a hot cell that had been purged with argon to minimize the moisture and prevent hydration of the Li_2O. One of the four 0.07%-enriched single crystals was intact, and several of the remaining sections had a full cross section. The two 1.8%-enriched single crystals were broken into pieces with dimensions smaller than 5 mm, and no fragment possessed a full cross section. Crystals of both enrichments were dark in color, but had the appearance on being single crystals. Archive crystals were transparent and colorless.

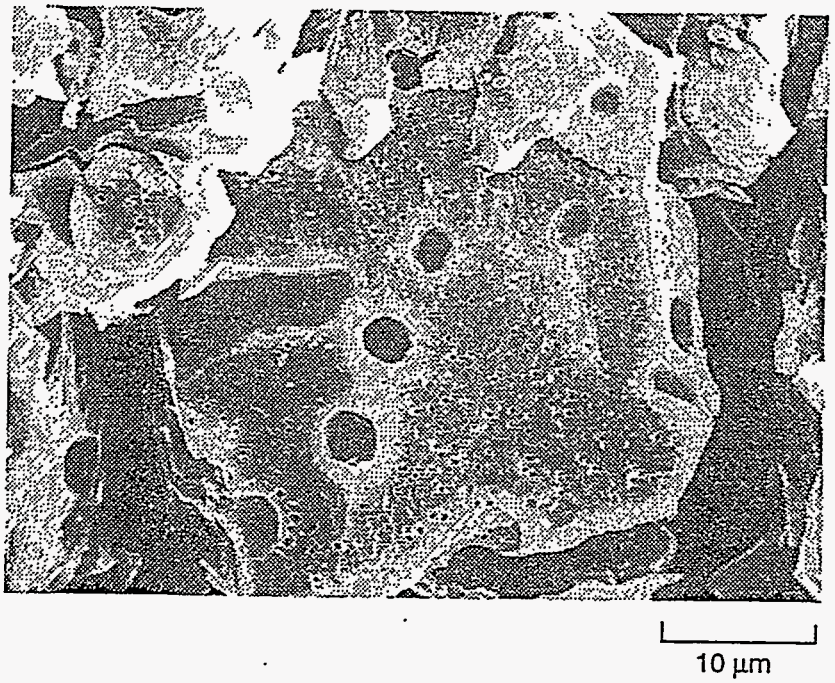

Figure 6.13. Fracture Surface from Wafer E near the Center of the Bed. Bubbles are clearly visible (small spots); large spots are probably residual sintering porosity.

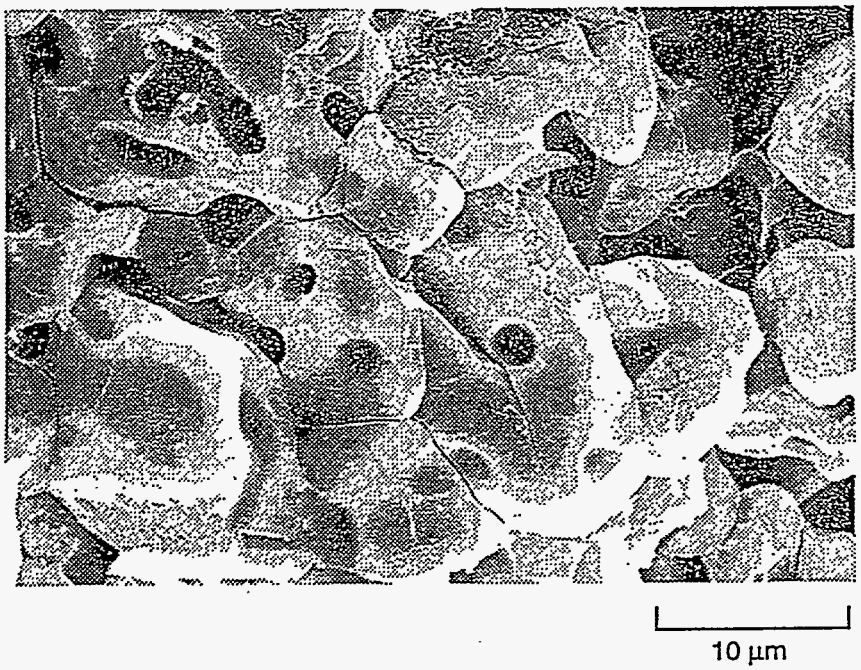

Figure 6.14. Fracture Surface of Center of Pebble in Wafer E, near the Edge (Radially) of the Bed. It shows signs of microcracking.

The enriched single-crystal capsule was disassembled in an air atmosphere. The capsule was cut above and below the specimen, and the specimen was pushed out. The specimen appeared to be intact upon removal, but subsequently broke into several smaller sections during subsequent handling. Figure 6.15 shows photographs of the specimen. During irradiation, the specimen had changed from a clear transparent crystal to an opaque white material resembling a polycrystal. The center of the material was black.

6.4.3 Lithium Isotopic Determinations

The change in the ^{6}Li enrichment during irradiation provides a means for determining the lithium burnup. Mass spectroscopy was used to determine the relative amounts of ^{6}Li and ^{7}Li in the enriched single crystal before and after irradiation. The pre- and postirradiation amounts of ^{6}Li are listed in Table 6.7 for several Phase I Li_2O single-crystal specimens. Also included in Table 6.7 are the results from two different isotopic measurements on the Phase I temperature-change specimen. The enriched single crystal and the Phase I temperature-change specimen were irradiated in Level 1 of cycle 11 of FFTF and hence are expected to have similar burnups. The Phase I temperature-gradient specimen was also irradiated in level 1, but inter-diffusion of ^{6}Li from the 61% enriched specimen to the depleted insulator pellets resulted in low final ^{6}Li values and predicted burnups that were too large.

The calculated lithium burnup for the single crystal is 5.5% with an uncertainty of ± 0.7%. This burnup is in agreement with the averages of the two series of measurements for the Phase I ring specimen, 6.3% and 5.8%, when the uncertainties of the individual measurements are considered. The average burnups of the Phase I ring specimen calculated from the lithium isotopic results are slightly larger than the burnup obtained from the recovered tritium, 4.8 ± 0.5% (Slagle and Hollenberg 1994), but again well within the uncertainty limits.

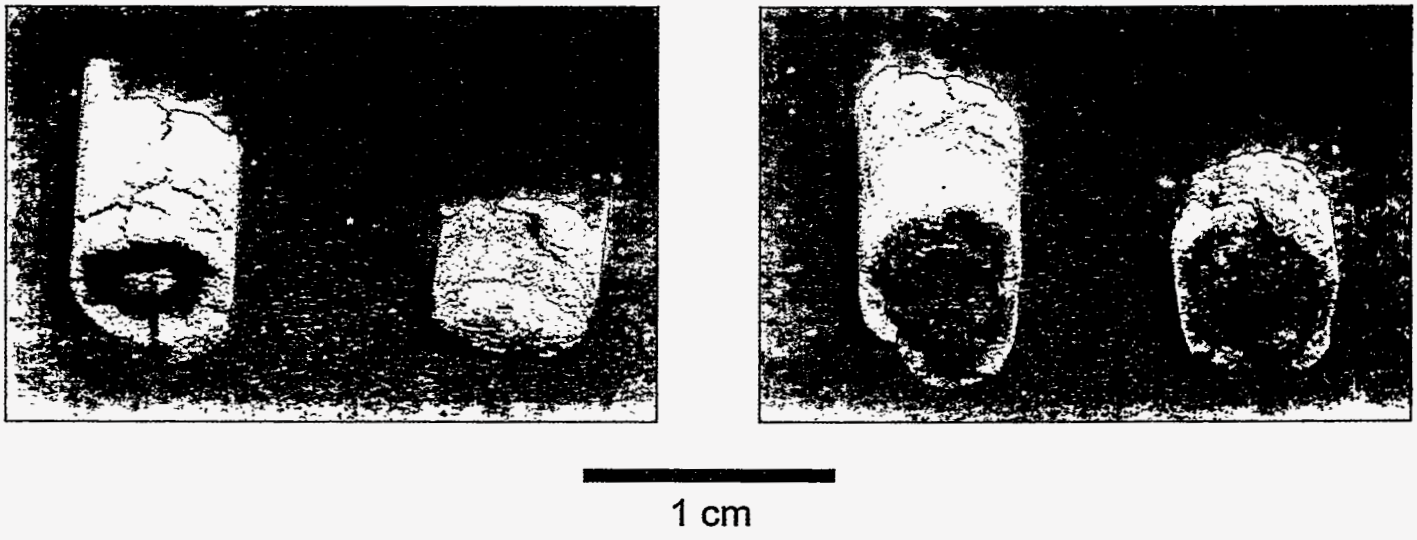

Figure 6.15. Photographs of the Enriched Single Crystal after Irradiation in Phase I

Table 6.7. Calculation of Lithium Burnups Based upon Pre- and Postirradiation Measurements of ^6Li%

Description	Initial ^6Li (%)	Final ^6Li (%)	Lithium Burnup (%)
	Phase I: Enriched Single Crystal		
	60.14 ± 0.2	57.84 ± 0.2	5.5 ± 0.7
	Phase I Temperature-Charge Specimen: September 1992		
Top	62.23 ± 0.6	58.6 ± 0.5	8.8 ± 2.5
Upper Center	62.23 ± 0.6	60.1 ± 0.5	5.3 ± 2.7
Lower Center	62.23 ± 0.6	60.0 ± 0.5	5.6 ± 2.7
Bottom	62.23 ± 0.6	59.7 ± 0.5	6.3 ± 2.7
Average			6.3
	Phase I Temperature-Change Specimen: July 1993		
Top	62.23 ± 0.6	59.86 ± 0.6	5.9 ± 2.9
Upper Center	62.23 ± 0.6	59.93 ± 0.6	5.7 ± 2.9
Lower Center	62.23 ± 0.6	60.09 ± 0.6	5.4 ± 2.9
Bottom	62.23 ± 0.6	59.98 ± 0.6	5.6 ± 2.9
Average			5.6

6.4.4 Tritium/Helium Retention

The retained tritium and helium in the single crystals after irradiation was determined by melting the specimens and determining the amounts of gases released. The procedure for determining the retained tritium was described in Section 6.2.5. The procedure for helium analysis involved the injection of ^3He and measurement of the $^3He/^4He$ ratio (Baldwin and Hollenberg 1986).

The tritium/helium retention results for the single crystals irradiated in Phase I are given in Table 6.8 The tritium/helium retention increased with increasing enrichment. The two tritium-inventory measurements for the 1.8% enriched specimen differed by a factor of 2. Such a difference could be related to temperature differences within the specimen. Higher temperatures could be expected to lead to lower inventories. For the 61% enriched specimen, samples representing a full cross section (Edge + Center) had higher inventories (both tritium and helium) than samples having only the edge portion. This suggests that the center had a higher inventory than the edge. Since the center is expected to be at a higher temperature than the edge, this result implies a higher inventory for a higher temperature. This observation is opposite to the behavior found from *in situ* testing (Section 5) and the Phase I Li_2O temperature-gradient specimen (Slagle et al. 1994).

The retained tritium and helium results in Table 6.8 were used to calculate the amount of lithium burnup, assuming no tritium and helium had been released from the 0.07 and 1.8% enriched crystals. In the case of the enriched single crystal, the amount of helium in the plenum gas was added to the retained helium to give the total generated. Table 6.9 lists the resulting burnup calculated in this manner. The total burnup calculated for the enriched single crystal is 5.6%, which is very good agreement with the 5.5% burnup found from the isotopic analysis. The burnup for the 0.07% enriched crystal is higher than the 61% enriched crystal on a proportioned basis. The calculated burnups indicate that 1/3 of the ^6Li in the 0.07% enriched crystal has been converted to tritium while 10% of the ^6Li in the 1.8% enriched single crystal has been converted. The 10% conversion is in good agreement with what occurred in the 61% enriched crystal, that is, 9%. The relatively high burnup in the 0.07% crystal suggests that the initial enrichment may have been higher than 0.07%.

Table 6.8. Tritium/Helium Retention in Single Crystals Irradiated in Phase I. The uncertainties in the tritium-retention measurements are 6% and for the helium measurements are 2%.

ID	Location	Tritium wppm	Helium ccSTP/g
	Depleted Single Crystals (0.07% ^6Li)		
1	NA	38.4	
2	NA	39.6	
3	NA		0.376
4	NA		0.300
	Depleted Single Crystals (1.8% ^6Li)		
1	NA	86.2	
2	NA	163.6	
3	NA		2.79
4	NA		2.87
	Enriched Single Crystals		
1	E + C	134.7	
3	E + C		7.2
4	E + C		7.1
5	E	86.4	
6	E		0.94
7	E		1.35

E = Edge, C = Center

Table 6.9. Lithium Burnup Calculated for the Tritium/Helium Retention Results for the Phase I Single Crystals. The uncertainties are the same as the uncertainties in Table 6.8

	Tritium Retention		Helium Retention	
Single Crystal Enrichment	Tritium (Ci/g)	Burnup (% Total Li)	Helium (ccSTP/g)	Burnup (% Total Li)
0.07	0.38	0.019	0.034	0.023
1.8	0.83	0.043	2.83	0.19
1.8	1.57	0.081	—	—
61	1.22	0.060	86.4	5.6 ± 0.6

6.5 Lithium Ceramic-Beryllium Compatibility Capsules

A series of 20 capsules was irradiated to test the compatibility of lithium ceramics and beryllium, which is a candidate neutron multiplier for blanket applications. The lithium ceramics specimens fabricated for this experiment included depleted and enriched Li_2O, $LiAlO_2$, Li_2ZrO_3, and Li_4SiO_4. The ceramic specimen size was 0.325 +.000/-.005 cm in diameter and 0.3 ± 0.025 cm thick. The target density was 85 ± 3% TD. The beryllium specimens were 0.30-cm-diameter discs punched from 0.035-cm-thick foil obtained from Brush-Wellman Inc. (Wellman, Ohio). A more detailed description of the specimens is given in the Phase I Data Summary Report (Slagle and Hollenberg 1994). Figure 6.16 is a schematic diagram of the lithium ceramic-beryllium capsules

showing the arrangement of the specimens and the nomenclature used to identify the specimens. The capsules contained no cerium getters as the single crystal capsules had. The outer beryllium disks on either end were in contact with 316 stainless steel.

The specimen matrix included depleted and enriched Li_2O, $LiAlO_2$, Li_2ZrO_3, and Li_4SiO_4. Table 6.10 lists the respective ^6Li enrichments. There were five different groups of capsules. Each group is characterized by the type of lithium ceramics (depleted/enriched) and the irradiation history. The five different groups are described in Table 6.11 with a description of the ^6Li enrichment of the lithium ceramics, the irradiation history, the tritium/helium retention measurement carried out and the calculated tritium/helium generation in the beryllium. The irradiation history includes the position of the capsule in the irradiation vehicle and whether it was irradiated in Phase I or Phase I and II. The position of the capsule in the irradiation vehicle refers to the position in the reactor core. Level 5 is at the top of the core, and level 8 is the highest level above the core. The tritium/helium measurement indicates whether tritium- or helium-retention measurements were included in the postirradiation examination. The last column is the calculated tritium or helium generated in the specimen for comparison with the postirradiation examination measurements.

6.5.1 Capsule Disassembly

The capsules were disassembled by cutting the capsule above and below the specimen stack between the outer beryllium disk and the stainless steel end cap. The beryllium lithium-ceramic specimen stack was then pushed into a vial using a specially designed fixture. The purpose of the disassembly was to remove the specimen stack from the highly radioactive stainless steel capsule so that postirradiation examination could be done in an unshielded glovebox. The disassembly procedure was designed to maintain the specimen order during push-out so that the positions of the individual disks could be identified and assigned as Be-1, Be-2, or Be-M, according to Figure 6.16.

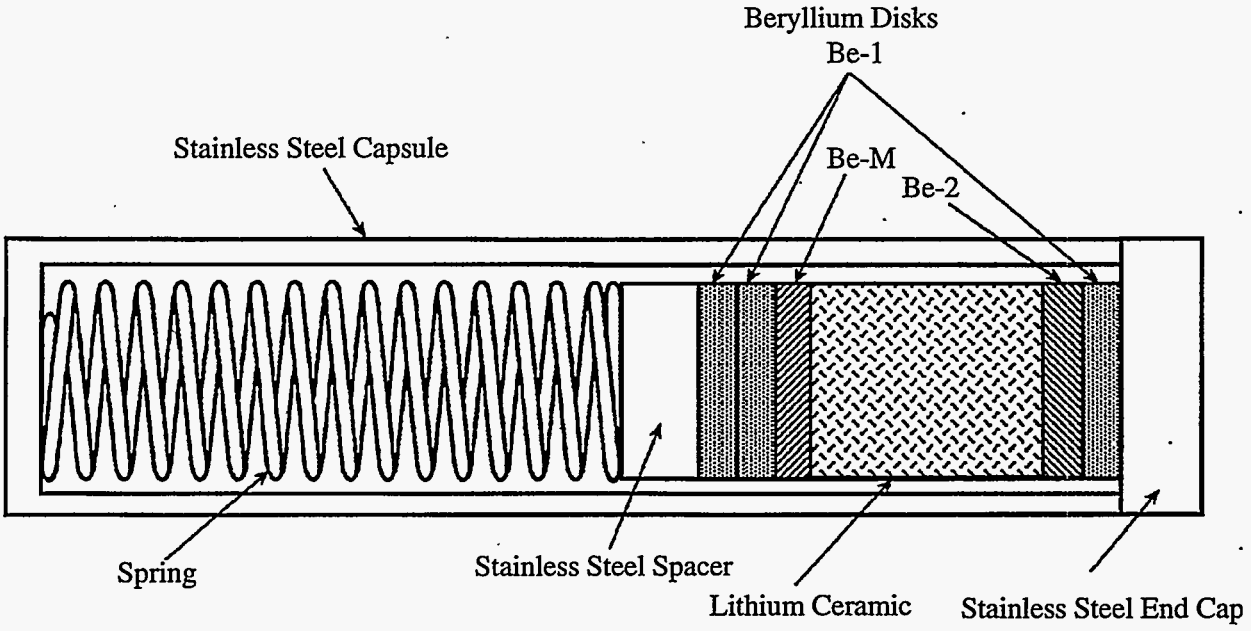

Figure 6.16. Schematic Diagram of the Lithium Ceramic-Beryllium Compatibility Capsules

Table 6.10. ^6Li Enrichments of the Lithium Ceramics in the Lithium Ceramic-Beryllium Compatibility Canisters

	Depleted (% ^6Li)	Enriched (% ^6Li)
Li_2O	0.2	61
Li_2ZrO_3	2.0	69
$LiAlO_2$	2.0	95
Li_4SiO_4	2.0	68

Table 6.11. Description of the Group I - V Lithium Ceramic-Beryllium Compatibility Capsules

			Tritium/Helium in Be	
Group	Lithium Ceramic	MOTA Level, B-II Phase	Retention Measurements	Calculated Generation (appm)
I	Enriched	Level 5, Phase I	Helium	1750
II	Depleted	Level 5, Phase I	Helium	930
III	Depleted	Level 5, Phases I & II	Tritium	45
IV	Enriched	Level 8, Phase I	—	—
V	Depleted	Level 8, Phases I & II	—	—

Observations made during disassembly indicated that, in general, the individual disks were not stuck to each other, to the lithium ceramic, or to the stainless steel end caps. The small size of the beryllium disks made handling in the hot cell difficult, and in several instances, the positions for the individual disks were lost. This resulted in some uncertainty in the specimen identification as specified in Figure 6.16.

The general appearance of the beryllium discs was bright and shiny. Some of the beryllium disks appeared bluish; others appeared bronze-colored. Several of the surfaces had small regions of white-colored residues. Although it was inferred that this residue was from the lithium ceramics, the occurrence of these regions was not always on surfaces adjacent to the ceramics.

6.5.2 Metallography

The beryllium disks identified as Be-M were adjacent to the ceramic and were chosen for ceramography. These disks were broken in half, mounted in resin, ground on SiC paper, and polished with 1-μm diamond. No discernible interaction layer could be seen between the beryllium and the lithium ceramic. The only observable phenomena was that in the beryllium surface adjacent to the ^6Li enriched ceramics, a region of fine bubbles was seen along the surface. Group I and Group IV capsules contained enriched ceramics (See Table 6.11). Figures 6.17 through 6.20 are a combination of low- and high-magnification micrographs of beryllium adjacent to enriched ceramics: Li_2O (Group IV), Li_2ZrO_3 (Group I), $LiAlO_2$ (Group I), and Li_4SiO_4 (Group I). The low-magnification micrographs show the complete disk cross section and the absence of any gross change in microstructure adjacent to the lithium ceramic. The high-magnification micrographs show the occurrence of small bubbles in the surface region adjacent to the ceramic. These bubbles lie within a 20-μm band adjacent to the surface. These bubbles are most likely helium bubbles formed by helium recoiled from the lithium ceramics into the beryllium disks. There was no apparent gray surface layer as found in the SIBELIUS experiment by Roux et al. (1992). The absence of a gray layer is consistent with the bright, shiny appearance of the disks.

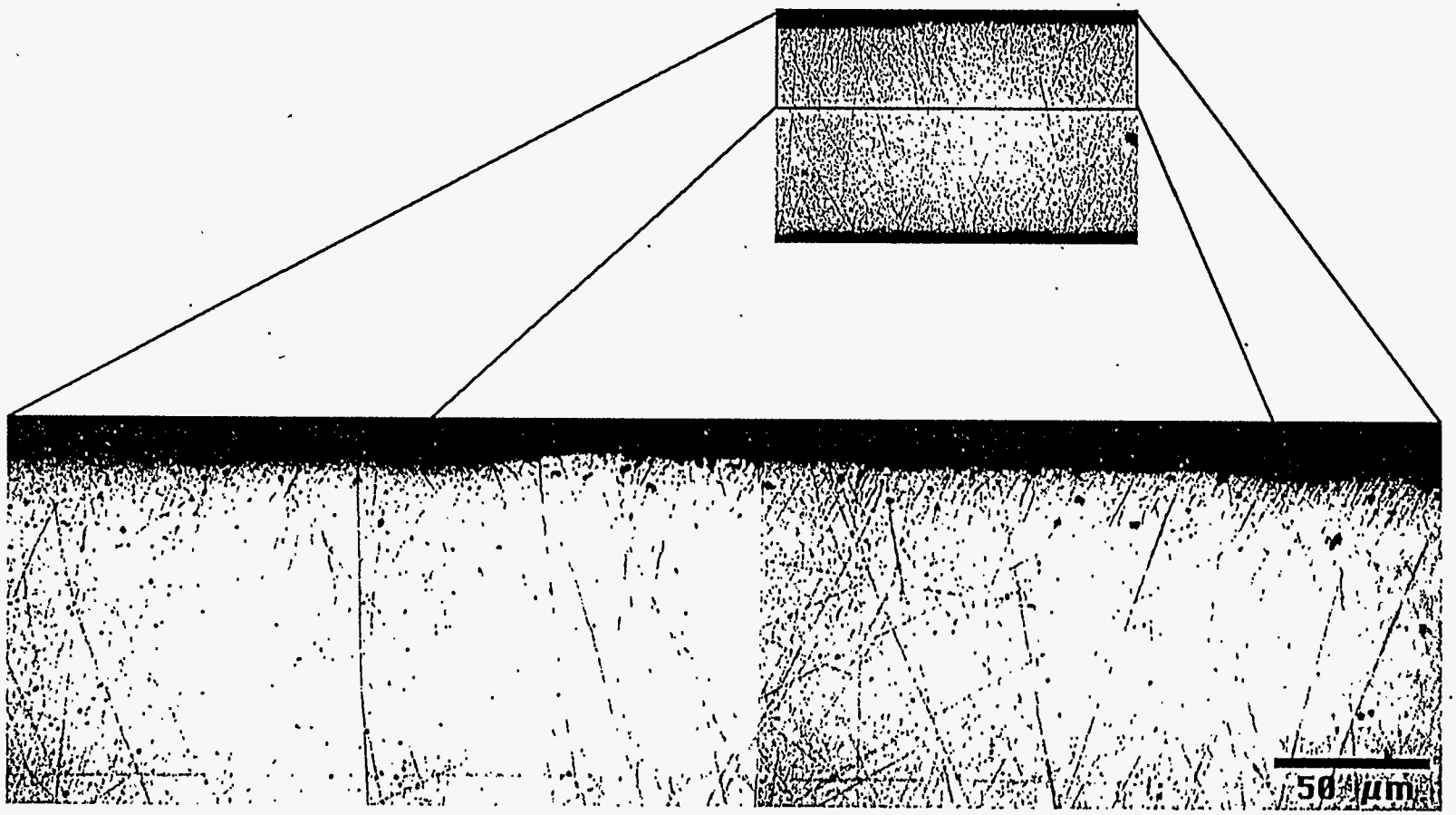

Figure 6.17. Micrographs of a Beryllium Disk Adjacent to Li_2O (Group IV) after Polishing on 1-µm Diamond

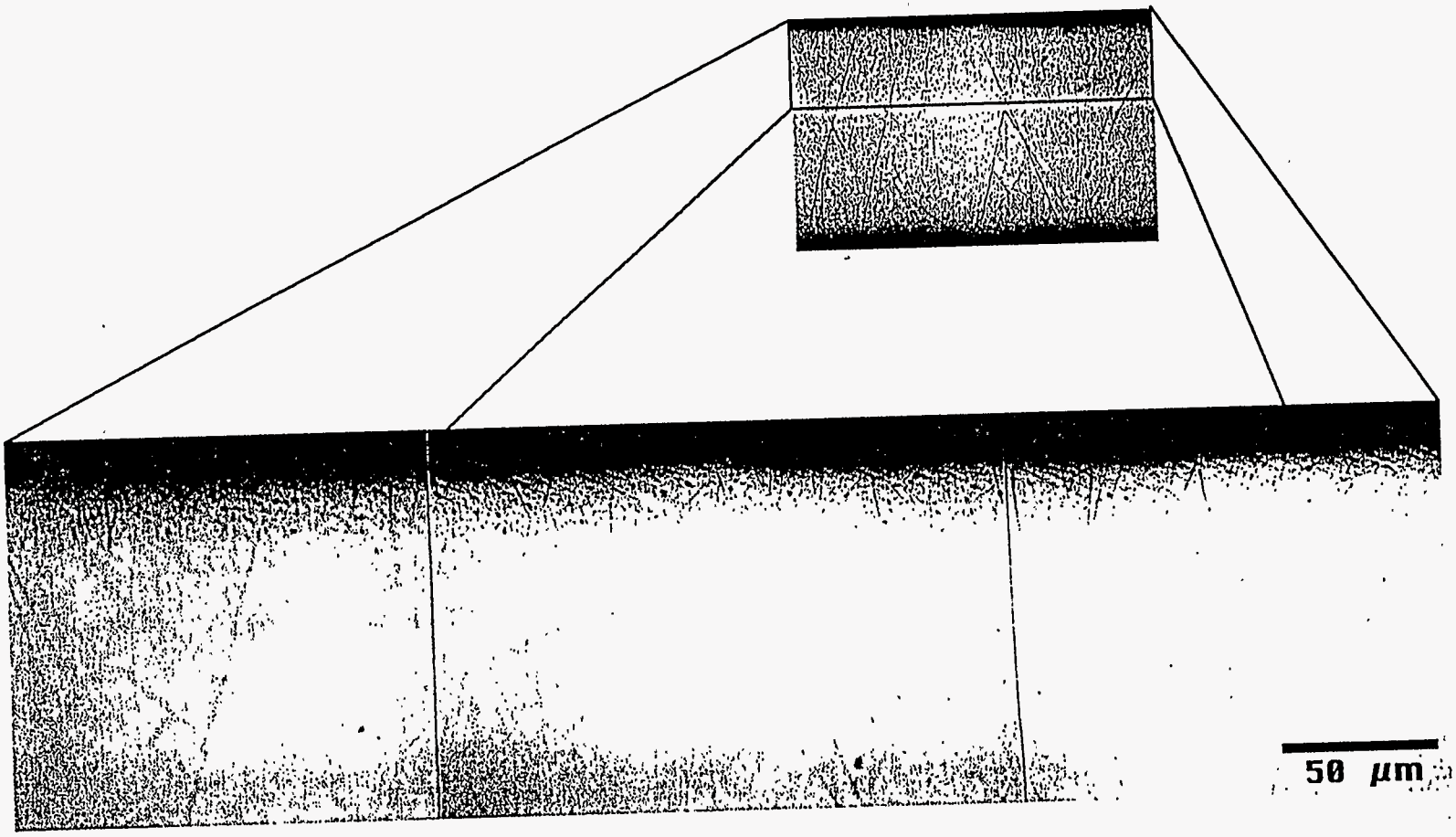

Figure 6.18. Micrographs of a Beryllium Disk Adjacent to Li_2ZrO_3 (Group I) after Polishing on 1-µm Diamond

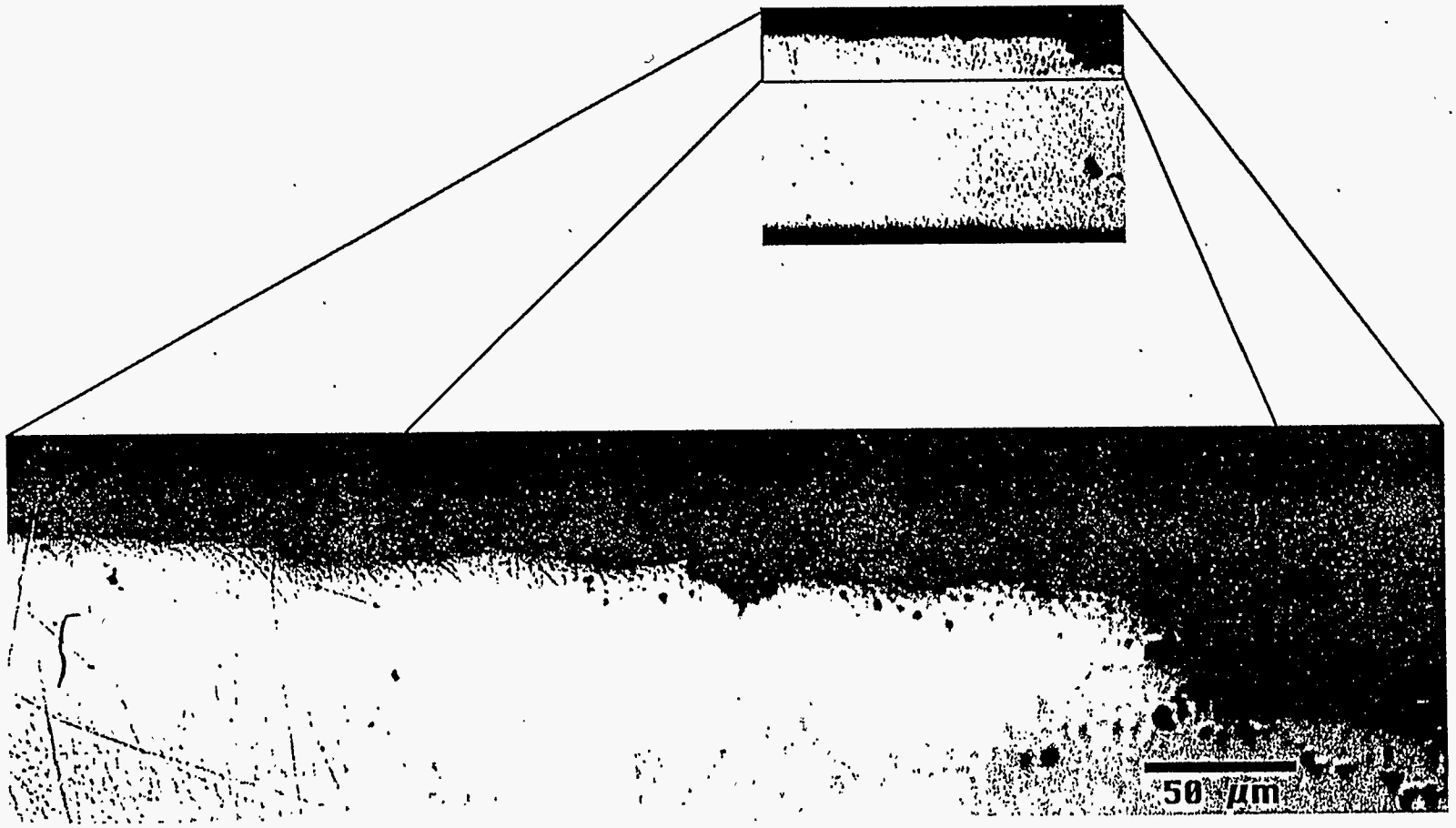

Figure 6.19. Micrographs of a Beryllium Disk Adjacent to $LiAlO_2$ (Group I) after Polishing on 1-µm Diamond

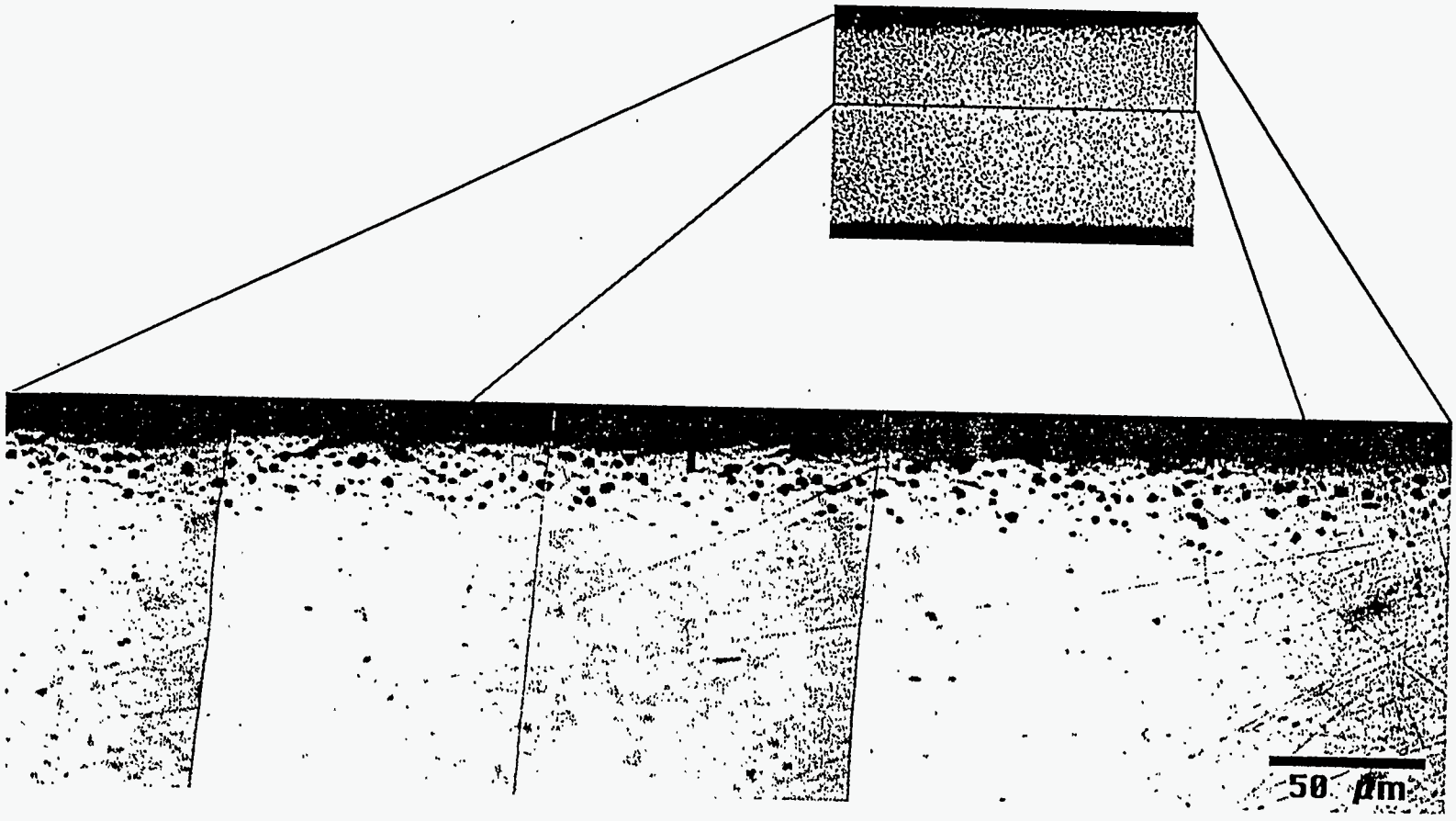

Figure 6.20. Micrographs of a Beryllium Disk Adjacent to Li_4SiO_4 (Group I) after Polishing on 1-µm Diamond

6.5.3 Tritium/Helium Retention

Tritium/helium assay measurements were carried out on the beryllium disks Be-1 and Be-2 (Figure 6.16) as indicated in Table 6.11. The measurements were carried out in a manner similar to that described in Section 6.2.5; that is, the disks were melted to effect gas release, followed by an analysis of the associated gases (Baldwin and Hollenberg 1986).

The results of the helium-assay measurements for the beryllium disks in Group I and II capsules are given in Table 6.12. It was expected that the helium retention in disks adjacent to the lithium ceramics (Be-2), particularly for the ^{6}Li-enriched ceramics, would be higher than in those disks adjacent to metal (Be-1) because of the bubbles observed in the metallography that were attributed to recoiled helium (Figures 6.17 through 6.20). In three of the four cases, the helium assay results confirmed that helium retention was higher in the disks adjacent to the ^{6}Li enriched ceramics (Be-2). For the ^{6}Li depleted ceramics, the effect was opposite, and even though a smaller effect would have been expected, an opposite effect was not. It is believed that the difficulty in correctly identifying the positions of the individual disks may have contributed to the inconsistent results. To eliminate the problem of disk identification, the helium-assay results were averaged by taking into account the difference in sample weights. These weighted averages were compared to the calculated values of helium generation in the last column of Table 6.12. For the Group I capsules, the helium retained tended to be larger than the calculated generation rate. For the Group II capsule, the opposite tendency was observed. Such inconsistencies were thought to be due to uncertainties in the calculation of generated tritium.

Table 6.12. Tritium/Helium Assay for Beryllium Disks in the BEATRIX-II Lithium Ceramic-Beryllium Compatibility Capsules

Ceramic	Tritium/Helium Assay BE-1	BE-2	Average	Average Retained/ Generated
Group I		*Helium*		
Li_2O	1226	2002	1518	0.87
Li_2ZrO_3	1870	1850	1864	1.07
$LiAlO_2$	1870	2135	1954	1.12
Li_4SiO_4	1898	2022	1922	1.10
Group II		*Helium*		
Li_2O	1166	784	1070	1.15
Li_2ZrO_3	716	635	692	0.74
$LiAlO_2$	663	—	663	0.71
Li_4SiO_4	804	—	804	0.86
Group III		*Tritium*		
Li_2O	22.1	43.0	29.1	0.85
Li_2ZrO_3	18.8	31.0	21.7	0.64
$LiAlO_2$	19.3	29.3	24.0	0.71
Li_4SiO_4	20.6	48.5	34.0	1.00

The tritium-assay measurements for the discs in the Group III capsules are given in Table 6.12. In all cases, the disk next to the ceramic (Be-2) has a larger amount of retained tritium than the disk adjacent to metal (Be-1). This higher value suggested that some of the tritium produced in the ceramic has recoiled into the adjacent beryllium disk. As was done for the helium result, a weighted average of the retained tritium was calculated and compared with the calculated amount of tritium generation. The values of retained versus generated tritium tended to be low. This low value may

indicate that some tritium release has occurred or it may reflect the uncertainty in the tritium generation.

7.0 Data Transfers to Modelers and Code Developers

The BEATRIX-II results represent a significant expansion of the design database for fusion solid-breeder blankets. An interface between the BEATRIX-II experiment and the solid-breeder design groups was established to ensure an efficient transfer of data from BEATRIX-II to individuals involved in formulating models for solid-breeder performance. This interface also provided a means for the solid-breeder modelers and code developers to comment on the irradiation test plan and the postirradiation characterization of the BEATRIX-II experiment. Participants in this interface were from Japan, Canada, and the United States and were called the BEATRIX-II Modelers and Code Developers (MCD). The Phase I Data Summary Report (Slagle and Hollenberg 1994) described the first three data transfers that were held: November 1991, October 1992, and October 1993.

The fourth and final data transfer occurred at a meeting of the MCD on October 1995 in Tokyo, Japan. At this meeting, the complete *in situ* data set of Phase I and Phase II and the results of the Phase II postirradiation examination were transferred to the MCD. The *in situ* data set consisted of the complete data compilations from Phase I (Slagle and Hollenberg 1994) and Phase II (Appendix B). These data were supplied in the form of LOTUS 1-2-3 spreadsheets (*.WK3) on 150-MB Bernoulli disks. The data were later distributed on CD disks, which were more universally compatible with the MCD members. The postirradiation examination results included tritium retention and microstructural characterization of the Phase II temperature-change and temperature-gradient specimens.

8.0 Conclusions

The purpose of the BEATRIX-II experiment was to evaluate the performance of ceramic solid-breeder materials in a fast neutron environment at extended burnup levels. In addition, the BEATRIX-II experiment provided an excellent testbed for developing methods for monitoring and safely handling tritium during an *in situ* tritium-recovery experiment that was in operation for over 500 EFPD.

The BEATRIX-II experiment generated an extensive database on the tritium recovery from Li_2O and Li_2ZrO_3 in a fast-neutron environment to extended burnups. The Li_2O in Phase I and Phase II of the experiment was irradiated to lithium burnups in excess of 4% while operating at temperatures from 400 to 1000°C The Li_2ZrO_3 in Phase II was irradiated to burnups in excess of 5% while operating at temperatures from 400 to 1100°C. Both Li_2O and Li_2ZrO_3 were operated in helium sweep gases with additions of 0 to 1.0% H_2. Many of the fusion-blanket design issues pertaining to Li_2O and Li_2ZrO_3 were addressed during this experiment:

- *Reference database*: The results of the *in situ* tritium recovery provide a reference database that can be used for predicting the effects of temperature and sweep-gas composition on the tritium release inventories of Li_2O and Li_2ZrO_3 over a wide range of operating conditions.

- *Burnup effects on tritium inventory*: Tritium-retention measurements at the end of irradiation indicated a very low tritium inventory for both Li_2O (<0.3 wppm) and Li_2ZrO_3 (<0.3 wppm). In addition, the low tritium inventory changes found in both Phase I and Phase II for the Li_2O temperature-change specimens after temperature changes indicated that the tritium inventory remained low throughout the test.

- *High temperature physical stability at extended burnup*: The long-term thermal stability of the Phase I and Phase II temperature-gradient specimens together with the postirradiation microstructure verified the high-temperature physical stability of Li_2O and the Li_2ZrO_3 pebble bed.

- *Lithium transport at high temperatures*: Only minimal vapor transport of lithium to the plenum regions of the Li_2O canisters was measured during postirradiation examination (<0.1 wt%).

- *Tritium transport due to grain growth at high temperatures*: The large-grained columnar regions of the Phase I temperature-gradient Li_2O solid specimen were found to have extremely low tritium inventories (<0.06 wppm).

- *Microstructural changes in Li_2O*: Changes were observed after irradiation to depend upon the local temperature and temperature gradient. At these burnups, the microstructural changes did not interfere with the functionality of the ceramic breeder.

- *Interaction of lithium ceramics and beryllium*: Lithium ceramics (Li_2O, Li_2ZrO_3, $LiAlO_2$, and Li_4SiO_4) in contact with beryllium resulted in no observable chemical interaction for lithium burnups up to 4% and irradiation times up to 500 EFPD.

Based on these results, it was confirmed that Li_2O and Li_2ZrO_3 should be considered as leading candidates for use in a solid-breeder fusion-blanket application.

9.0 References

Alvani, C., M. R. Mancini, F. Alessandrini, and S. Casadio. 1994. "Environmental Attack Effects on Li_2ZrO_3 and Properties Evolution as a Function of the Fabrication Route." In: *Proceedings of the International Workshop on Ceramic Breeder Interactions*, Ed. by N. Roux, pp. 369-378, September 22-24, 1993. Commissariat A L'Energie Atomique, Paris France.

Asaoka, Y., H. Moriyama, and Y. Ito. 1992. "Production Behavior and Its Modeling of Irradiation Defects in Lithium Oxide under Ion Beam Irradiation." *Fusion Tech.*, 21:1944-1948.

Baldwin, D. L., and G. W. Hollenberg. 1986. "Measurement of Tritium and Helium in Fast Neutron Irradiated Lithium Ceramics Using High Temperature Vacuum Extraction." *J. Nucl. Mater.* 305:141-143.

Billone, M. C., C. C. Lin, H. Attaya, and Y. Gohar. 1991. "Tritium Retention and Release Analysis for the U.S.-ITER Blanket." *Fusion Tech.,* 19:976-983.

Billone, M. C., W. Dienst, T. Flament, P. Lorenzetti, K. Noda, and N. Roux . 1993. *TER Solid Breeder Blanket Materials Database.* Argonne National Laboratory, ANL/FPP/TM-263 (November 1963).

Briec, M., J. J. Abassin, C. E. Johnson, M. Amasson, N. Roux, and H. Watanabe. 1988. "The MOZART Experiment: In-Pile Tritium Extraction from Lithium Oxide, Aluminates' Zirconates," In: *Proceedings of the 15th Symposium on Fusion Technology*, Ed. by A. M. Van Inger, A. Nigsen-Vis, and H. P. Kippel, pp 1105-1111, September 19-23, 1988, Utrecht, Elsevier, The Netherlands..

Gandhi, J. M., and S. C. Saxena. 1968. "Correlated Thermal Conductivity Data of Rare Gases and their Binary Mixtures at Ordinary Pressures," *J. Chem. Eng. Data,* 13:357-361.

Hall, R. A. O., and D. G. Martin. 1981. "The Thermal Conductivity of Powder Beds: A Modell. Some Measurements on UO_2 Vibro-Compacted Microspheres and their Correlation." *J. Nucl. Mater.*, 101:172-183.

Hollenberg, G. W., and D. E. Baker. 1982, "Thermal Properties of Lithium Ceramics for Fusion Applications," presented at the American Ceramic Society Meeting, May 2-5, 1982, HEDL-SA-2674-FP.

Hollenberg, G. W., and D. L. Baldwin. 1985. "The Effect of Irradiation on Four Solid Breeder Materials." *J. Nucl. Mater.*, 133 and 134: 242-245.

Kennedy, P., K. Gilchrist, D. Walker, and S. Broughton. 1986. "The Preparation, Characterization and Properties of Lithium Oxide and Lithium Meta-Zirconate Irradiated in the HFR Petten in the Second and Third Exotic Experiment." In: *Proceedings 14th Symposium on Fusion Technology,* Vol. 2. pp. 1013-1018. Avignon, France.

Knight, R. C., and D. L. Greenslade. 1991. *Irradiation Testing of a Niobium-Molybdenum Thermocouple*, WHC-SA-1256-FP, Westinghouse Hanford Company, Richland Washington.

Kopasz, J. P., A. K. Fischer, and C. E. Johnson. 1990. "Multiple Activation Energies For Tritium Release from Ceramic Breeders." In: *Fabrication and Properties of Lithium Ceramics II: Advances in Ceramics,* Vol. 27, Eds. G. W. Hollenberg, and I. J. Hastings, pp. 317. The American Ceramic Society, Westerville, Ohio.

Kopasz, J. P., C. E. Johnson, and D. L. Baldwin, 1995. "Performance of Ceramic Breeder Materials in the SIBELIUS Experiment." *J. Nucl. Mater.*, 219:259-264.

Masaki, N. M., K. Noda, H. Watanabe, R. G. Clemmer, and G. W. Hollenberg. 1994. "Spectroscopic Study of Lithium Oxide Irradiated by Fast Neutrons." *J. Nucl. Mater.,* 212-215:908-911.

Miller, J. M., R. A. Verrall, D. S. MacDonald, and S. R. Bokwa. 1988. "The CRITIC-I Irradiation of Li_2O-Tritium Release and Measurement." *Fusion Tech.* 14:649-656.

Miller, J. M., and R. A. Verrall. 1994. "Performance of a Li_2ZrO_3 Sphere-Pac Assembly in the CRITIC-II Irradiation Experiment." Presented at the Sixth International Conference of Fusion Reactor Materials, *J. Nucl. Mater.*, 212-215:897-901.

Porter, D. L., J. R. Krsul, M. T. Lang, L. C. Walters, and M. Tetenbaum. 1984. "Neutron Irradiation and Compatibility Testing of Li_2O." *J. Nucl. Mater.*, 122 and 123:923-933.

Rodrigo, L., J. M. Miller, S. R. Bokwa, R. E. Johnson, B. M. MacDonald, and J. Senohrabek. 1992 "Tritium Measurement and Monitoring in Experimental and Process Systems with Ionization Chambers." *Fusion Tech.*, 21:629-635.

Rodrigo, L., and D. Yin. 1993. *Effect of Impurities on the Measurement of Tritium with Ionization Chambers*. AECL-10764, AECL Research, Chalk River, Ontario, Canada.

Roux, N., J. J. Abassin, M. Briec, D. Cruz, T. Flament, and I. Schuster. 1992. "Compatibility Behavior of Beryllium with $LiAlO_2$ and Li_2ZrO_3 Ceramics with 316L and 1.4914 Steels in SIBELIUS," *J. Nucl. Mater.,* 191-194:168-172.

Slagle, O. D., K. Noda, and T. Takahashi. 1990. "Fabrication of Lithium Ceramic Pellets, Rings and Single Crystals for Irradiation in BEATRIX-II." In: *Fabrication and Properties of Lithium Ceramics II: Advances in Ceramics,* Vol. 27, Ed. by G. W. Hollenberg and I. J. Hastings, The American Ceramic Society, Westerville, Ohio.

Slagle, O. D., G. W. Hollenberg, and D. L. Baldwin. 1991. "The FUBR-1B Experiment - Tritium Release and Physical Stability of Solid Breeder Materials," *J. Nucl. Mater.,* 843:179-181.

Slagle, O. D., G. W. Hollenberg, D. E. Baker, and T. Kurasawa. 1992. "Effect of Sweep Gas Composition on Ionization Chamber Response in the BEATRIX-II In Situ Tritium Recovery Experiment." In: Proceedings *of the International Workshop on Ceramic Breeder Interactions,* Ed. by M. Yamawaki, pp. 204-212. October 26-29, 1992, University of Tokyo, Tokyo, Japan.

Slagle, O. D., T. Kurasawa, R. A. Verrall, and G. W. Hollenberg. 1992. "In-Situ Tritium Recovery from Li_2O Irradiated in Fast Neutron Flux—BEATRIX-II Temperature Change Specimen." *J. Nucl. Mater.,* 191-194:23-29.

Slagle, O. D., and G. W. Hollenberg. 1994. "BEATRIX-II, Phase I: Data Summary Report." PNL-10279, Pacific Northwest Laboratory, Richland, Washington.

Slagle, O. D., T. Takahashi, D. L. Baldwin, F. D. Hobbs, K. Noda, G. W. Hollenberg, and R. A. Verrall. 1994. "Postirradiation Examination of BEATRIX-II, Phase I." *J. Nucl. Mater.,* 212-215:902-907.

Takahashi, T., and T. Kikuchi. 1980. "Porosity Dependence on Thermal Diffusivity and Thermal Conductivity of Lithium Oxide Li_2O from 200 to 900°C." *J. Nucl. Mater.*, 91:93-102.

Takahashi, T., and H. Watanabe. 1989. "Preparation and Characterization of Lithium Oxide." *Fusion Eng. Des.,* 8:399-405.

Takahashi, T., K. Noda, O. D. Slagle, and F. D. Hobbs. 1994. "Microstructure and Density Changes of Li_2O during Irradiation in BEATRIX-II, Phase I." *Fusion Eng. Des.*, 28:271-277.

Takahashi, T., K. Noda, O. D. Slagle, F. D. Hobbs. 1995. "Microstructure and Density Changes of Li_2O During Irradiation in BEATRIX-II, Phase I and II." Presented at the International Workshop on Ceramic Breeder Blanket Interactions, October 9-11, 1995. Kyoto, Japan.

Tanaka, S., D. Yamaki, and M. Yamawaki. 1994. "Effects of Surface Heterogeneity on Tritium Release." In: *Proceedings of the International Workshop on Ceramic Breeder Blanket Interactions,* Ed. by N. Roux, pp. 257. September 22-24, 1993. Commissariat A L'Energie Atomique, Paris, France.

Tetenbaum, M., and C. E. Johnson. 1984. "Partial Pressures of H_2O Above the Diphasic Li_2O(s)-LiOH(s,l) System." *J. Nucl. Mater.,* 126:25-29.

Verrall, R. A., J. M. Miller, S. R. Bokwa. 1989a. "CRITIC-I - Instrumented Lithium Oxide Irradiation: Part 2 - First Results." In: *Fabrication and Properties of Lithium Ceramics: Advances in Ceramics,* Vol. 25, Eds. G. W. Hollenberg and I. J. Hastings, pp. 41. The American Ceramic Society, Westerville, Ohio.

Verrall, R. A., D. H. Rose, J. M. Miller, I. J. Hastings, and D. S. MacDonald. 1989b, "Bubble formation in irradiated Li_2O." In: *Proceedings of the Fourth International Conference on Fusion Reactor Materials* (ICFRM-4) Kyoto, Japan, December 4-8, 1989. *J. Nucl. Mater.,* 179-181 (1991) 855-858.

Appendix A

BEATRIX-II, Phase II Experimenter Log

Appendix A

BEATRIX-II, Phase II Experimenter Log

Experimenter Log - Phase II

PCN No.	Date (m-d-y)	Ring Specimen Temperature Initial	Ring Specimen Temperature Final	Ring Specimen Flow Rate/Gas Comp Initial	Ring Specimen Flow Rate/Gas Comp Final	Solid Specimen Flow Rate/Gas Comp Initial	Solid Specimen Flow Rate/Gas Comp Final	Remarks
1	5-11-91			He		He		Parameter Adjustment
2	5-14-91			He		He purge of CEC		Purge RE-52771-1
3	5-15-91			He		Secure Purge		
4	5-18-91	He Purge of CEC-IC		He				Purge RE-52270-1
5	5-19-91	Secure Purge		He		He purge of CEC		
6	5-20-91			He		Secure Purge		
7				He	0.1 H_2	He	0.1 H_2	
Reactor startup on May 27, 1991								
8	5-29-91			Increase CEC volts		0.1 H_2		
9	5-31-91	100 to 75% He		0.1 H_2		0.1 H_2		
10	5-31-91	75% to 10% He		0.1 H_2		0.1 H_2		
11	6-2-91	645	590	0.1 H_2		0.1 H_2		
12	6-3-91	590	535	0.1 H_2		0.1 H_2		
13	6-4-91	535	645	0.1 H_2		0.1 H_2		
14	6-6-91	645		Purge CEC IC -0.1		0.1 H_2		Purge RE-52270-1
15	6-7-91	645		Take Calib Sample		0.1 H_2		CEC Cell Failed
16	6-8-91	645		Purge CEC IC -0.1		0.1 H_2		
17	6-10-91	645		Take Calib Sample		0.1 H_2		t=16:58
18	6-10-91	645		0.1 H_2	He	100	200	
19	6-12-91	645		Purge CEC IC -He		200		
20	6-13-91	645		Take Calib Sample		200		t=14:53
21	6-14-91	645		He	0.1 H_2	200	100	
22	6-17-91	645	590	0.1 H_2		0.1 H_2	He	
23	6-18-91	590	535	0.1 H_2		He		50 mL He
24	6-19-91	535		0.1 H_2		He		50 He + 3 1% H_2
25	6-19-91	535		0.1 H_2		He		50 He + 6 1% H_2
26	6-19-91	535		0.1 H_2		He		50 He + 13 1% H_2
27	6-19-91	535		0.1 H_2		He		50 He + 50 1% H_2
28	6-19-91	535	645	0.1 H_2		He		50 mL He
29	6-21-91	645		0.1 H_2	0.01 H_2	He	0.01 H_2	
30	6-23-91	645		0.01 H_2		0.01 H_2	0.1 H_2	
31	6-24-91	645	590	0.01 H_2		0.1 H_2		
32	6-26-91	590	535	0.01 H_2		0.1 H_2		
33	6-28-91	535	645	0.01 H_2		0.1 H_2		
34	6-30-91	645		0.01 H_2	0.1 H_2	0.1 H_2	0.01 H_2	
35	7-2-91	645		0.1 H_2	He	0.01 H_2	0.1 H_2	
36	7-6-91	645	590	He		0.1 H_2		
37	7-8-91	590	535	He		0.1 H_2		
38	7-9-91	535		He		0.1 H_2	He	
39	7-10-91	535	645	He		He		
40	7-11-91	645		He		He	0.1 H_2	
41	7-12-91	645		He	0.01 H_2	0.1 H_2		t0=10:47
42	7-14-91	645		0.01 H_2	0.1 H_2	0.1 H_2		
43	7-16-91	645	590	0.1 H_2				
44	7-17-91	590	528	0.1 H_2				

Experimenter Log - Phase II (contd)

PCN No.	Date (m-d-y)	Ring Specimen Temperature Initial	Ring Specimen Temperature Final	Ring Specimen Flow Rate/Gas Comp Initial	Ring Specimen Flow Rate/Gas Comp Final	Solid Specimen Flow Rate/Gas Comp Initial	Solid Specimen Flow Rate/Gas Comp Final	Remarks
End of cycle 12A.1: Reactor shutdown on July 20, 1991								
45	7-18-91	528	645	0.1 H_2				
46	7-22-91	N/A		0.1 H_2	He	0.1 H_2	He	
47	7-23-91			He		Purge #9,1% H_2		0.057% H_2
48	7-24-91			He				0.107% H_2
49	7-25-91			He				0.5% H_2
50	7-25-91			He				0.206% H_2
51	7-26-91			He				0.107% H_2
52	7-26-91			He				0.057% H_2
53	7-27-91			He		Purge Stopped		
54	7-29-91	100% Helium		He	0.1 H_2	He	0.1 H_2	
Start of Cycle 12-A.2; July 30, 1991								
55	8-5-91	530	645	0.1 H_2		0.1 H_2		
56	8-6-91	645	645	0.1 H_2		0.1 H_2		Temperature adjustment
57	8-7-91	645	590	0.1 H_2		0.1 H_2		
58	8-8-91	590	530	0.1 H_2		0.1 H_2		
59	8-9-91	530	645	0.1 H_2		0.1 H_2		
60	8-10-91	645	530	0.1 H_2		0.1 H_2		
61	8-11-91	530	645	0.1 H_2		0.1 H_2		
62	8-13-91	645		0.1 H_2	He	0.1 H_2		
63	8-15-91	645		He	0.01 H_2	0.1 H_2	0.01 H_2	t0R=11:35, t0S=13:08
64	8-17-91	645		0.01 H_2	0.1 H_2	0.01 H_2		
65	8-19-91	645		0.1 H_2		0.01 H_2	0.1 H_2	
GetterBed XX-52280-2 Changeout								
66	8-21-91	645		0.1 H_2	He	0.1 H_2	He	
67	8-25-91	645		He	0.01 H_2	He	0.1 H_2	
68	8-27-91	645		0.01 H_2	0.1 H_2	0.1 H_2		146 Ci/m^3
69	8-28-91	645		0.1 H_2		0.1 H_2	He	
70	8-31-91	645		0.1 H_2	He	He		
71	9-5-91	645		He		He	0.1 H_2	187 Ci/m^3
72	9-8-91	645		He	0.01 H_2	0.1 H_2		t0R=9:46
73	9-9-91	645		0.01 H_2		25 CEC:75 MS		Flow Rate Test
74	9-10-91	645		0.01 H_2	0.1 H_2	25 CEC:75 MS		
75	9-11-91	645		0.1 H_2		50 CEC:50 MS		
76	9-12-91	645		0.1 H_2		0.1 H_2		Purge RE-52270-1
77	9-13-91	645		0.1 H_2		50 IG 0.1 H_2 to CEC IC		Calibrate RE-52270-1
78	9-14-91	645		0.1 H_2		0.1 H_2		Purge RE-52270-2
79	9-15-91	645		0.1 H_2		0.1 H_2		Calibrate RE-52270-2
80	9-16-91	645		0.1 H_2		Purge CEC IC		
81	9-17-91	645		0.1 H_2		Purge MS IC		
82	9-18-91	645		0.1 H_2		0.1 H_2		Secure Purges
83	9-19-91	645		0.1 H_2	He	0.1 H_2	He	

Experimenter Log - Phase II (contd)

PCN No.	Date (m-d-y)	Ring Specimen Temperature Initial	Ring Specimen Temperature Final	Ring Specimen Flow Rate/Gas Comp Initial	Ring Specimen Flow Rate/Gas Comp Final	Solid Specimen Flow Rate/Gas Comp Initial	Solid Specimen Flow Rate/Gas Comp Final	Remarks
Reactor Shutdown on September 21, 1991								
84	9-22-91	N/A		He	0.01 H_2	He	0.01 H_2	
85	9-23-91	N/A		0.01 H_2	0.1 H_2	0.01 H_2	0.1 H_2	
86	9-24-91	N/A		0.1 H_2	He	0.1 H_2	He	CEC voltage to -0.9 V
87	9-25-91	N/A		He	0.1 H_2	He	0.1 H_2	
88	10-15-91			He		0.1 H_2	He	
89	10-17-91			He		He @ 100 ml/min		Purge RE-52271-1(He)
90	10-18-91			He		He @ 50 ml/min		Stop Purge
91	10-21-91			He		He	0.1 H_2	
92	10-22-91			He		0.1 H_2	He	Purge RE-52271-1(0.1 H_2)
93	10-23-91			He		He		Purge RE-52271-2(0.1 H_2)
94	10-24-91			He		He		Stop Purge
95	10-28-91			He	0.1 H_2	He		
96	10-29-91			0.1 H_2	He	He		Purge RE-52270-1(0.1 H_2)
97	10-30-91			He		He		Purge RE-52270-2(0.1 H_2)
98	10-31-91							Stop Purge
99	11-15-91	Injection Gas changed to 1.0% H_2						
Reactor Startup Cycle 12-B.1: November 21,1991								
100	11-22-91	Voltage for electrolysis cell increased for restart						
101	11-26-91	480	580	He		He		Reactor Power @ 75%
102	11-27-91	630	525	He		He		Reactor Power @ 90%
103	11-29-91	535	645	He		He	0.1 H_2	
104	11-30-91	645		He	0.1 H_2	0.1 H_2		
105	12-2-91	Gas Bottle changed for upcoming purge						
On December 2, 1991 the instrumentation lost power at 9:00 - Data interruption Expected								
106	12-3-91	645		0.1 H_2		0.1 H_2		Purge RE-52270-1(0.1% H_2)
107	12-4-91	645		0.1 H_2		0.1 H_2		Gas Sample XN-7-2
108	12-5-91	645		0.1 H_2	He	200 ml/min		
109	12-7-91	645		He		200 ml/min		Purge RE-52270-1(He)
110	12-8-91	645		He		200 ml/min		Gas Sample XN-7-2
111	12-9-91	645		He	0.1 H_2	0.1 H_2		
112	12-11-91	645	535	0.1 H_2		0.1 H_2		
113	12-12-91	535		0.1 H_2	He	0.1 H_2	He	
114	12-14-91	535		He	0.01 H_2	He	0.01 H_2	
115	12-16-91	535		0.01 H_2	0.1 H_2	0.01 H_2	0.1 H_2	
116	12-17-91	535						
117	12-18-91	535		0.1 H_2	He	0.1 H_2	He	
118	12-22-91	535		He	0.01 H_2	He	0.01 H_2	
119	12-24-91	535		0.01 H_2	0.1 H_2	0.01 H_2	0.1 H_2	
120	12-27-91	535		0.1 H_2	0.01 H_2	0.1 H_2	0.01 H_2	
121	12-29-91	535		0.01 H_2	He	0.01 H_2	He	
122	12-31-91	535		He		He	0.1 H_2	

Experimenter Log - Phase II (contd)

PCN No.	Date (m-d-y)	Ring Specimen Temperature Initial	Ring Specimen Temperature Final	Ring Specimen Flow Rate/Gas Comp Initial	Ring Specimen Flow Rate/Gas Comp Final	Solid Specimen Flow Rate/Gas Comp Initial	Solid Specimen Flow Rate/Gas Comp Final	Remarks
123	1-2-92	535		He	0.1 H_2	0.1 H_2		
124	1-4-92	535	645	0.1 H_2		0.1 H_2		
125	1-6-92	645		0.1 H_2		0.1 H_2		Purge RE-52270-1
126	1-7-92	645		0.1 H_2		0.1 H_2		Purge RE-52270-2
127	1-8-92	645		0.1 H_2		0.1 H_2		Purge RE-52271-1
128	1-9-92	645	590	0.1 H_2		0.1 H_2		Calibration RE-52271-1
129	1-10-92	590	535	0.1 H_2		0.1 H_2		Purge RE-52271-2
130	1-11-92	535	645	0.1 H_2		0.1 H_2		Calibration RE-52271-2
131	1-12-92	645	535	0.1 H_2		0.1 H_2		
132	1-13-92	535	645	0.1 H_2		0.1 H_2		
Reactor shutdown January 15, 1992 at 0000 hrs								
133	1-16-92	N/A		0.1 H_2	He	0.1 H_2	He	
134	1-23-92	N/A		He		He		Remove Calibration Sample
135	1-25-92			He	0.1 H_2	He	0.1 H_2	Getterbed Replacement
Reactor Startup on January 29, 1992								
136	1-29-92	535	645	0.1 H_2		0.1 H_2		
137	1-31-92	645		0.1 H_2		0.1 H_2		Purge RE-52270-1
138	2-1-92	645		0.1 H_2		0.1 H_2		Calibration Sample
139	2-2-92	645		0.1 H_2	He	200 cc/min		
140	2-4-92	645		He		200 cc/min		Purge RE-52270-1
141	2-5-92	645		He		200 cc/min		Calibration Sample
142	2-6-92	645		He	0.1 H_2	0.1 H_2		
143	2-8-92	645	590	0.1 H_2		0.1 H_2		
144	2-10-92	590	535	0.1 H_2		0.1 H_2		
145	2-12-92	535	590	0.1 H_2		0.1 H_2		Purge RE-52271-1
146	2-12-92	Replace gaskets in calibration sampler on solid specimen						Abort Purge
147	2-13-92	590		0.1 H_2		0.1 H_2		Purge RE-52271-1
148	2-14-92	590	645	0.1 H_2		0.1 H_2		Purge RE-52271-2
149	2-15-92	645		0.1 H_2		0.1 H_2		Secure Purge
150	2-16-92	645	535	0.1 H_2		0.1 H_2		
151	2-18-92	535	645	0.1 H_2		0.1 H_2		
152	2-19-92	645		0.1 H_2		50 cc/min		Locate Leak
153	2-20-92	645		0.1 H_2	He	0.1 H_2		
154	2-22-92	645	590	He		0.1 H_2		
155	2-24-92	590	535	He		0.1 H_2		
156	2-26-92	535	590	He		0.1 H_2		
157	2-28-92	590	645	He		0.1 H_2		
158	3-1-92	645	535	He		0.1 H_2		
159	3-3-92	535	645	He		0.1 H_2		
160	3-5-92	645		He	0.01 H_2	0.1 H_2		
161	3-7-92	645		0.01 H_2	0.1 H_2	0.1 H_2		
162	3-8-92	645		0.1 H_2		0.1 H_2	1.0 H_2	
163	3-9-92	645		0.1 H_2		1.0 H_2	0.1 H_2	Purge RE-52270-2
164	3-10-92	645		0.1 H_2		0.1 H_2		Purge RE-52270-1
165	3-11-92	645		0.1 H_2		0.1 H_2		Secure Purge

Experimenter Log - Phase II (contd)

PCN No.	Date (m-d-y)	Ring Specimen Temperature Initial	Ring Specimen Temperature Final	Ring Specimen Flow Rate/Gas Comp Initial	Ring Specimen Flow Rate/Gas Comp Final	Solid Specimen Flow Rate/Gas Comp Initial	Solid Specimen Flow Rate/Gas Comp Final	Remarks
166	3-12-92	645	590	0.1 H_2		0.1 H_2		
167	3-13-92	590	535	0.1 H_2		0.1 H_2		
168	3-14-92	535	645	0.1 H_2		0.1 H_2		
169	3-15-92	645	535	0.1 H_2		0.1 H_2		
170	3-16-92	535	645	0.1 H_2		0.1 H_2		
Reactor Shutdown 0830 March 19, 1992								
171	3-21-92	N/A		0.1 H_2	He	0.1 H_2	He	
172	4-6-92	N/A		He		He		

Appendix B

Corrected/Compiled Database

Appendix B

Corrected/Compiled Database

An overall summary of the BEATRIX-II, Phase II, experimental database was compiled to form two smaller, more manageable databases. The original 26 prime data channels that formed the experimental database of the irradiation phase of the Phase I experiment were reduced to the most important 20. The data set was condensed further by increasing the time interval of the data from 2 minutes to 6 minutes. The dataset was then segregated into two separate spreadsheets, one containing the data for the temperature-change canister and one for the temperature-gradient canister. Each of these canister spreadsheets included only the data applicable to the respective canister, i.e., 15 of the total 20 data channels. Table B.1 lists the 15 columns (A through O) included in each spreadsheet and the distribution of the data between the temperature-change canister (ring) and temperature-gradient canister (solid) spreadsheets.

The data compilation is very similar to the data compilation carried out in the Phase I Data Summary Report. One notable difference is a slight change in notation that was made in Phase II in an attempt to clarify the data-correction process. The tritium associated with the tritium generation rate is denoted G in this report (see Equation 3.7) but in the Phase I report is was denoted as G_{EX}.

The relationships used in correcting the ion-chamber response for sweep-gas composition and ion-chamber background are described in Section 3.1 of this report. The apparent tritium concentrations determined from the measured ion-chamber response in a sweep gas of x% hydrogen and the ion-chamber calibration curves (T_{IC} in Equation 3.4 of this report) are listed in Columns N and O of the spreadsheets (Table B.1), respectively, for the ion chambers after the ceramic electrolysis cell (CEC) and the molecular sieves. Columns P through AE in Table B.2 list the additional spreadsheet columns that were calculated and used in the interpretation of the tritium recovery results. Columns T and U are the final tritium concentrations for the CEC (T_{He}) and the molecular-sieve ionization chambers after correction for sweep-gas composition and background (Equation 3.5). The sweep-gas enhancement factors of 0, 1.1, 1.3, and 1.4 were entered in Columns P and Q of the spreadsheet and corresponded to hydrogen additions of 0, 0.01, 0.1, and 1.0%. The CEC ion-chamber backgrounds (Column R) are deduced from a comparison of the tritium concentration in Column T (T_{He}, Equation 3.5 of this report) with the tritium concentration extrapolated from the ion-chamber calibration in Column AC (G, Equation 3.7 of this report). The background for the molecular-sieve ion chamber in Column S was set qualitatively on the basis of keeping a constant value of HTO (Column V) concentration in the reference condition and maintaining a positive quantity of HTO during off-reference operation. The tritium recovery rate (Column W) and the total recovered tritium (Column X) were used to compile the total tritium recovered during the experiment (Table 5.1). Column AB is the correction term to correct measured tritium concentration at calibration (G_C) to other times in the irradiation cycle (G). This correction term takes into account changing neutron flux and lithium burnup. The relationship between G_C and G is given in Equation 3.7, Section 3.1.5 of this report. The extrapolated calibration concentration is given in Column AC. Column AE is the ratio of recovered tritium (Column T) to that generated (AD).

The final compiled data for the ring and solid specimen were plotted for each reactor cycle. Two plots were made to describe a given specimen in a given cycle. The first plot contains the total tritium concentration, T_{He} (Column T), the sweep-gas enhancement factor (Column P), and the ion-chamber background (Column R). The second plot includes the ratio of recovered/generated tritium (Column AE) and the average inner-specimen temperature (Column M). The sweep-gas

compositions are indicated on both plots. The two plots for each canister in each of the four cycles are included in Figures C.1 through C.16.

The complete database in the form of spreadsheets as described in Tables B.1 and B.2 have been compiled in LOTUS 1-2-3 format (**.WK1) and stored on a compact disk (CD) and on 150 MB Bernoulli disks. Bernoulli disks are compatible with "BERNOULLI BOXES" that are available from Iomega Corporation, 1821 West 4000 South, Roy, Utah 84067. The database is available, and requests for the data should be addressed to the BEATRIX-II Task Manager (G. W. Hollenberg, Pacific Northwest National Laboratory P. O. Box 999, Richland, Washington 99352).

Table B.1. Data Channels Selected for Final Compilation

Description	Spreadsheet Column in Data Compilation Ring	Solid
Elapsed Time from Start of Spreadsheet (hour)	A	A
Date	B	B
Time of Day (Fraction)	C	C
Ring Specimen Sweep Gas Moisture (ppm)	D	
Moisture after the Ring Specimen IC (ppm	E	
Solid Specimen Sweep Gas Moisture (ppm)		D
Moisture after the Solid Specimen IC (ppm)		E
Ring Specimen Sweep Gas Flow (CEC) (mL/min)	F	
Ring Specimen Sweep Gas Flow (MSD) (mL/min)	G	
Solid Specimen sweep Gas Flow (CEC) (mL/min)		F
Solid Specimen Sweep Gas Flow (MS) (mL/min)		G
Self-Powered Neutron Detector (Relative)	H	H
Temperature of the Glovebox (°C)	I	I
Solid Specimen Outer Temperature (°C)		J
Solid Specimen Center Temperature - Top (°C)		K
Solid Specimen Center Temperature - Bottom (°C)		L
Ring Specimen Outer Temperature (°C)	J	
Ring Specimen Inner Temperature No. 1 (°C)	K	
Ring Specimen Inner Temperature No. 2 (°C)	L	
Average Inner Ring Temperature (°C)	M	
Average Inner Solid Temperature (°C)		M
Ring Specimen Sweep Gas Tritium (CEC) (Ci/m^3)	N	
Ring Specimen Sweep Gas Tritium (MS) (Ci/m^3)	O	
Solid Specimen Sweep Gas Tritium (CEC) (Ci/m^3)		N
Solid Specimen Sweep Gas Tritium (MS) (Ci/m^3)		O

CEC = the sweep gas line through the CEC
MS = the line for the molecular sieve
IC = the ion chamber

Table B.2. Calculated Columns in the Data Compilation Spreadsheet

Spreadsheet Column	Description
P	CEC Ion Chamer Enhancement Factor (Ci/m^3)
Q	MS Ion Chamber Enhancement Factor (Ci/m^3)
R	CEC Ion Chamber Background (Ci/m^3)
S	MS Ion Chamber Background (Ci/m^3)
T	Total Tritium Concentration, T_{He} - Corected (Ci/m^3)
U	HT Tritium Concentration - Corrected (Ci/m^3)
V	HTO Tritium - Corrected (Ci/m^3)
W	Total Tritium Recovery Rate (Ci/s)
X	Tritium Recovered in Time Interval (Ci)
Y	Approximate EFPD
Z	Relative Flux Level (Equation 3.7)
AA	Effective Full Power Days in Present Cycle (Days)
AB	Generation Rate Correction for Flux and Burnup
AC	Generated Tritium Concentration, G (Ci/m^3)
AD	Tritium Generation Rate (Corrected) (Ci/s)
AE	Recovered/Generated Tritium

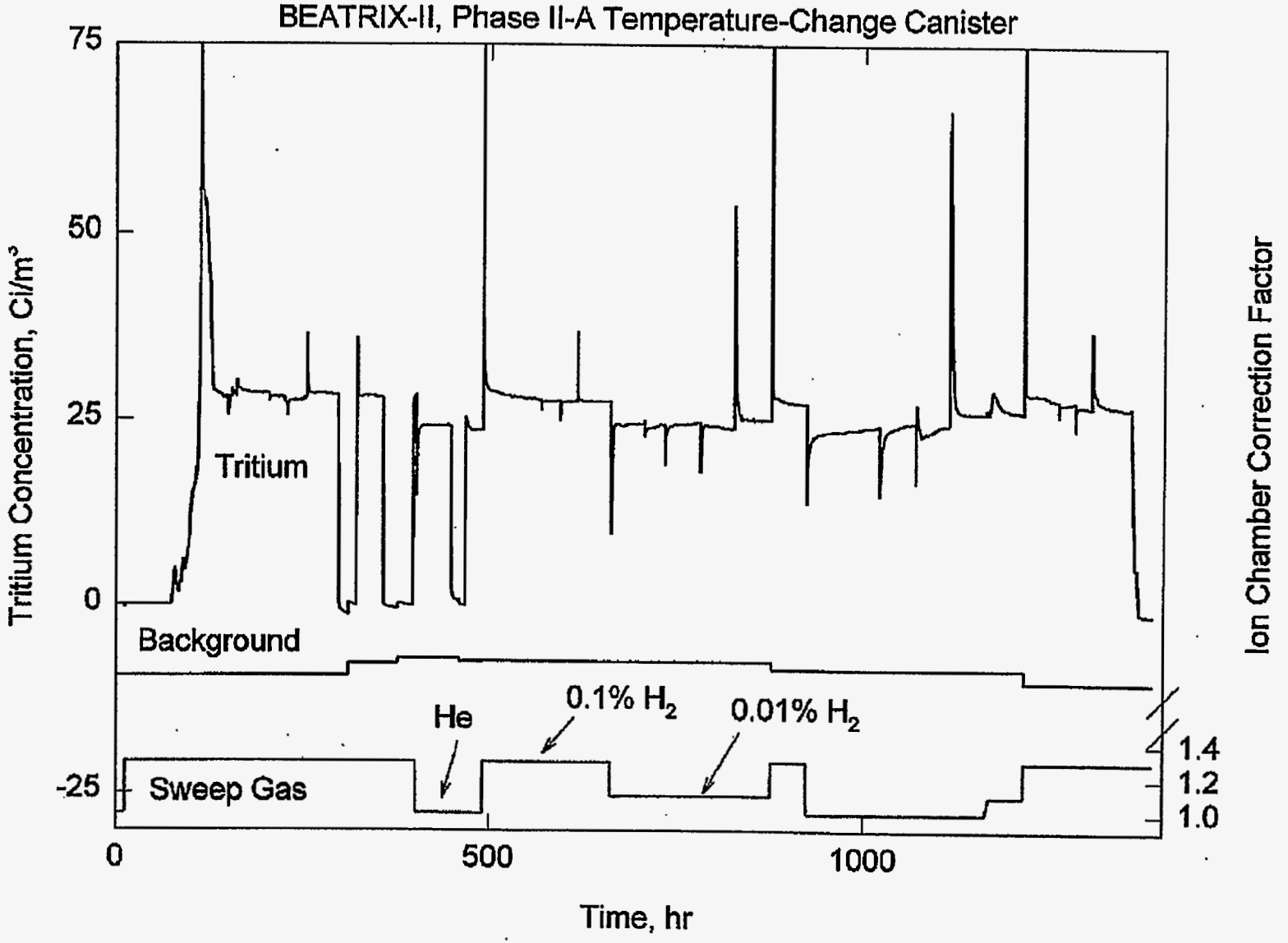

Figure B.1. Corrected Tritium Concentration and the Ion-Chamber Correction Factors Applied to the As-Measured Data for the Temperature-Change Canister in Phase II-A.

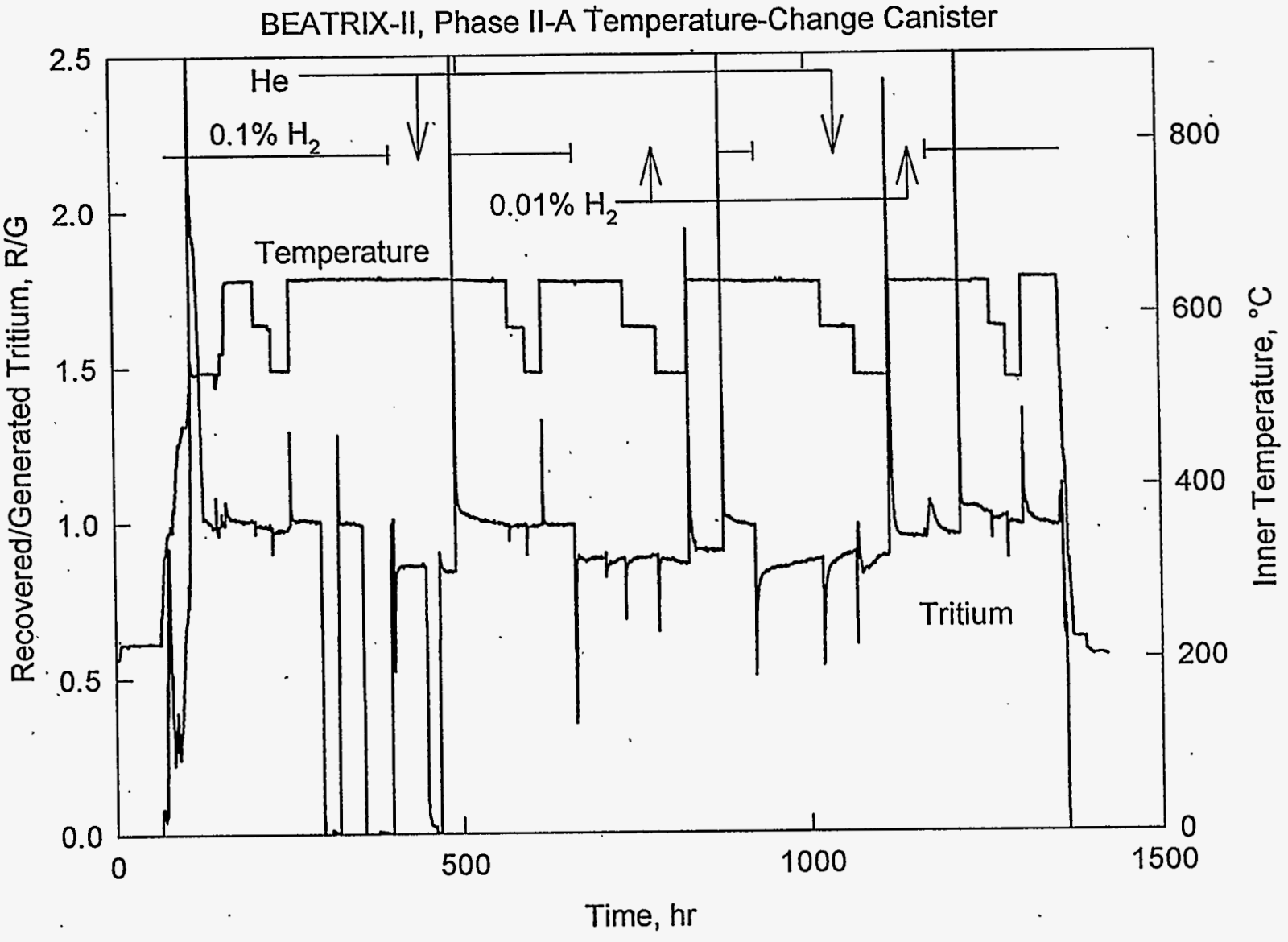

Figure B.2. Ratio of Recovered/Generated Tritium and the Average Inner Temperature for the Temperature-Change Canister in Phase II-A

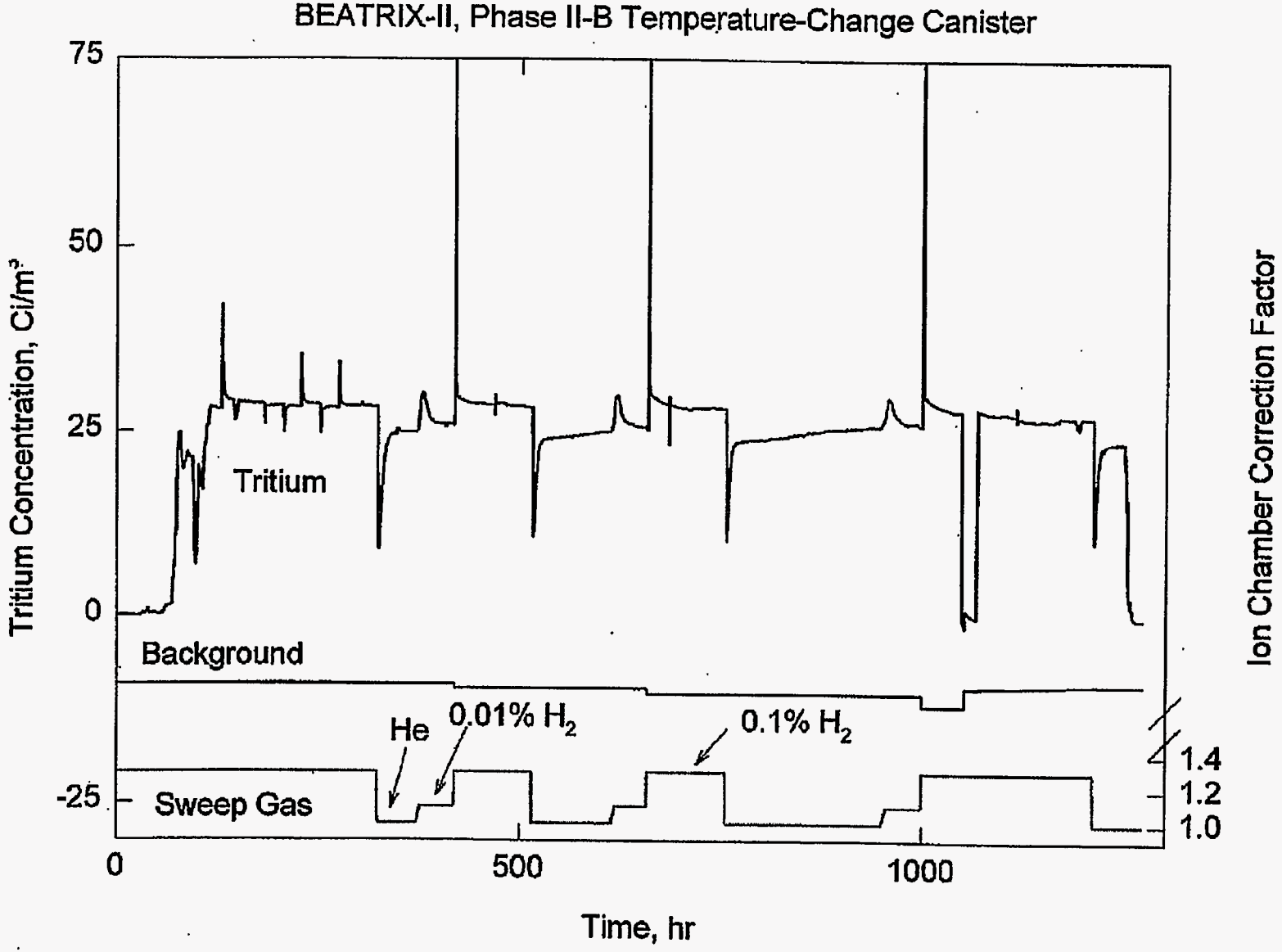

Figure B.3. Corrected Tritium Concentration and the Ion-Chamber Correction Factors Applied to the As-Measured Data for the Temperature-Change Canister in Phase II-B

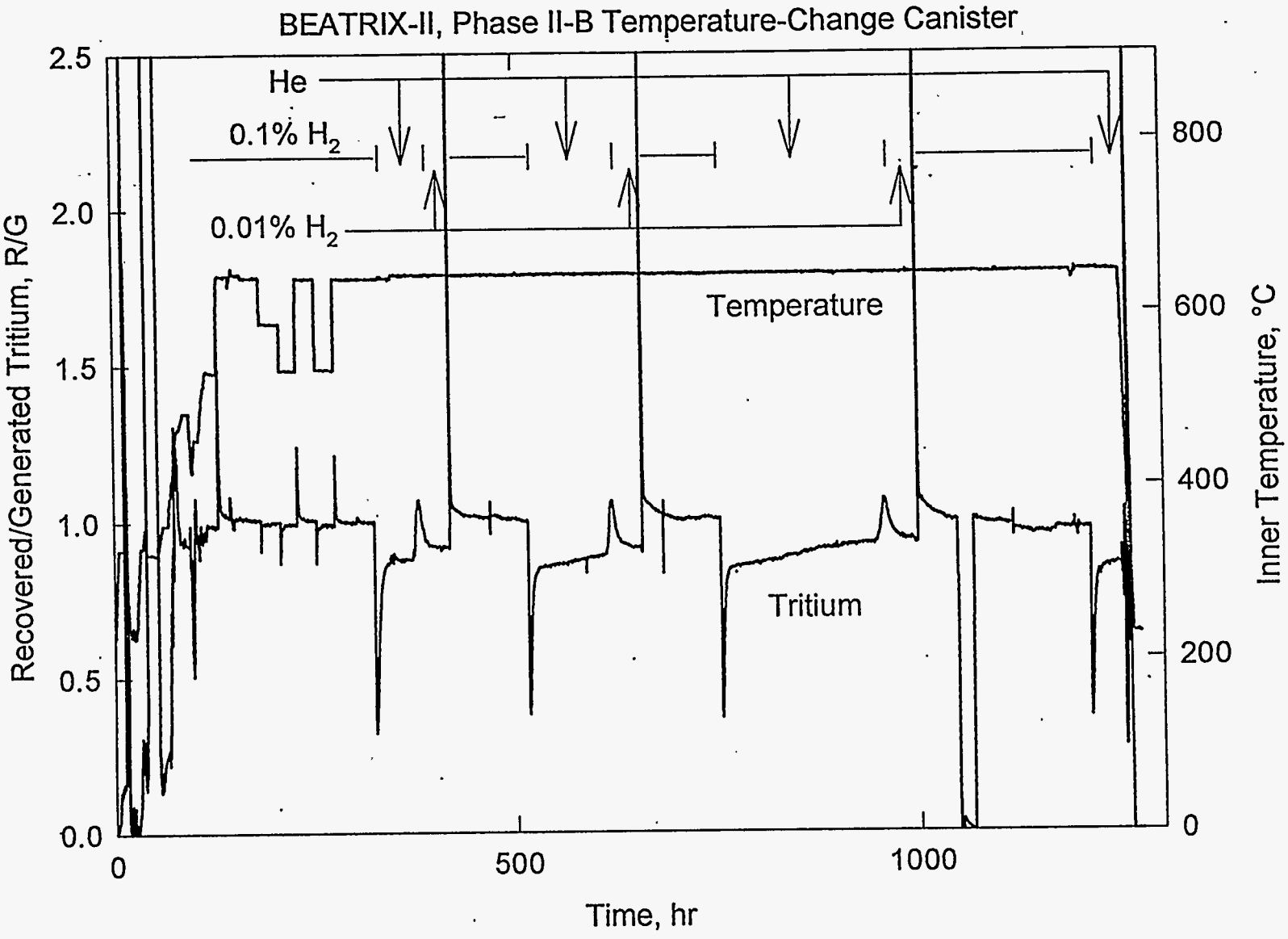

Figure B.4 Ratio of Recovered/Generated Tritium and the Average Inner Temperature for the Temperature-Change Canister in Phase II-B

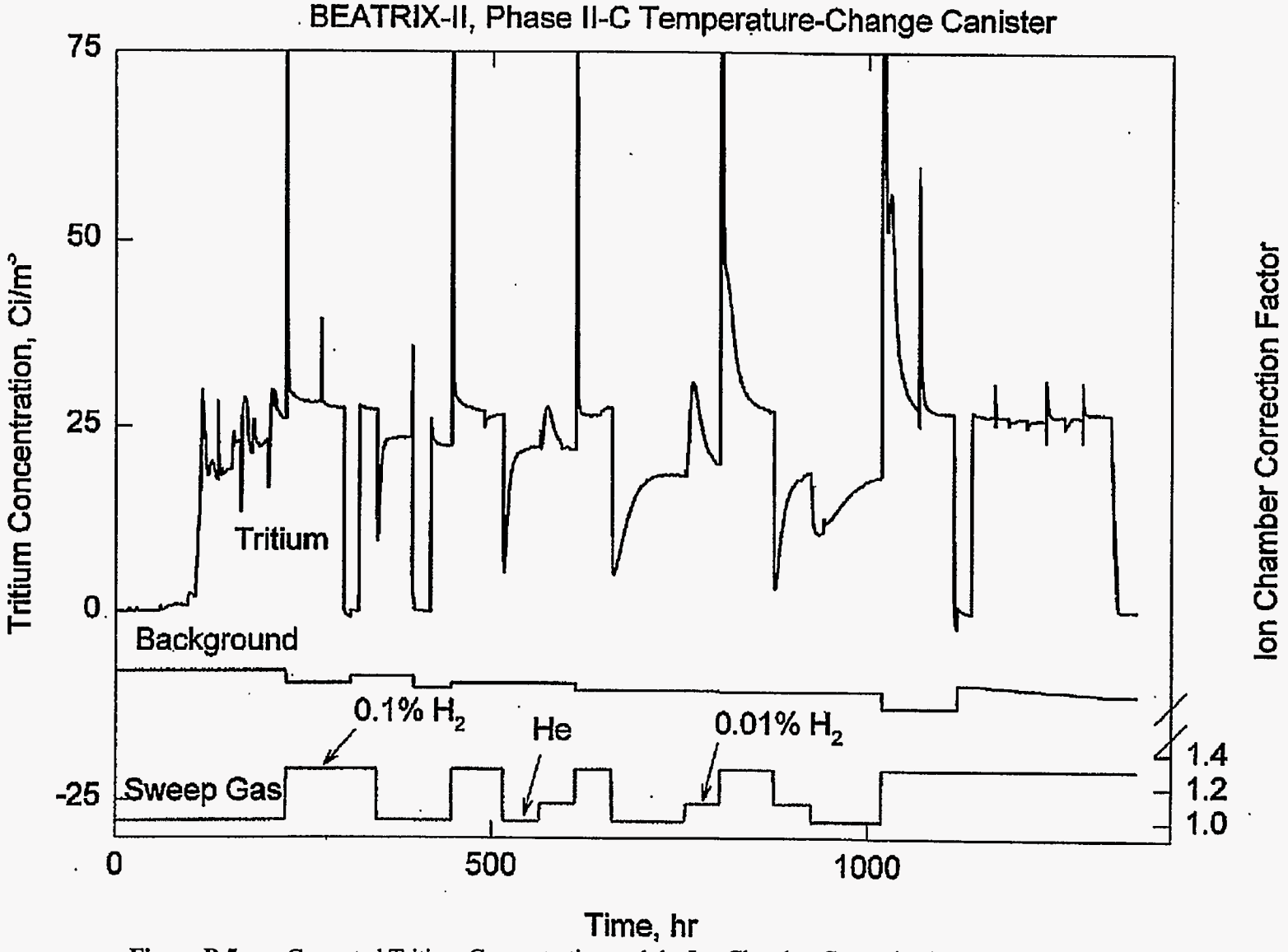

Figure B.5. Corrected Tritium Concentration and the Ion Chamber Correction Factors Applied to the As-Measured Data for the Temperature-Change Canister in Phase II-C

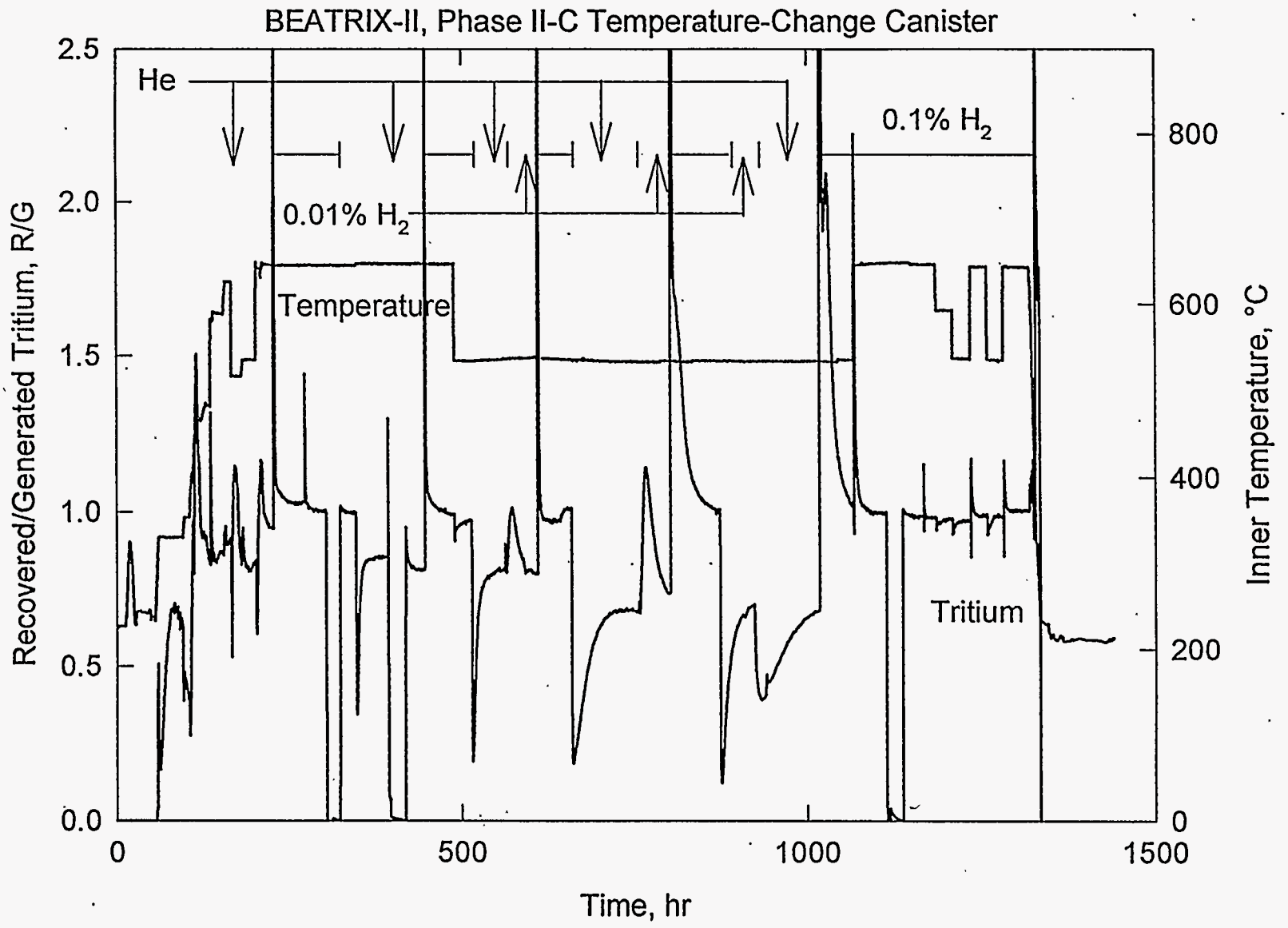

Figure B.6 Ratio of Recovered/Generated Tritium and the Average Inner Temperature for the Temperature-ChangeCanister in Phase II-C

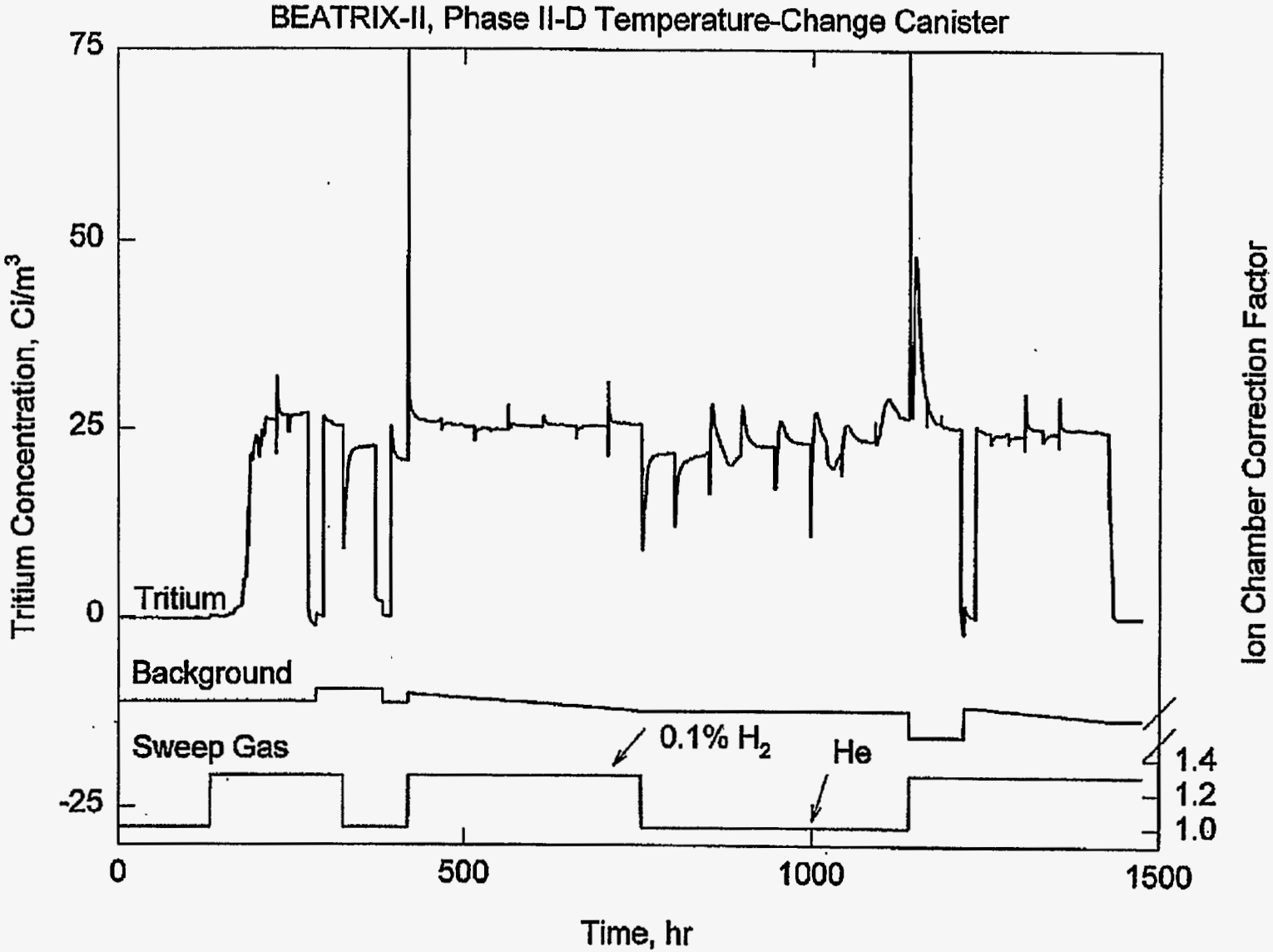

Figure B.7. Corrected Tritium Concentration and the Ion-Chamber Correction Factors Applied to the As-Measured Data for the Temperature-Change Canister in Phase II-D

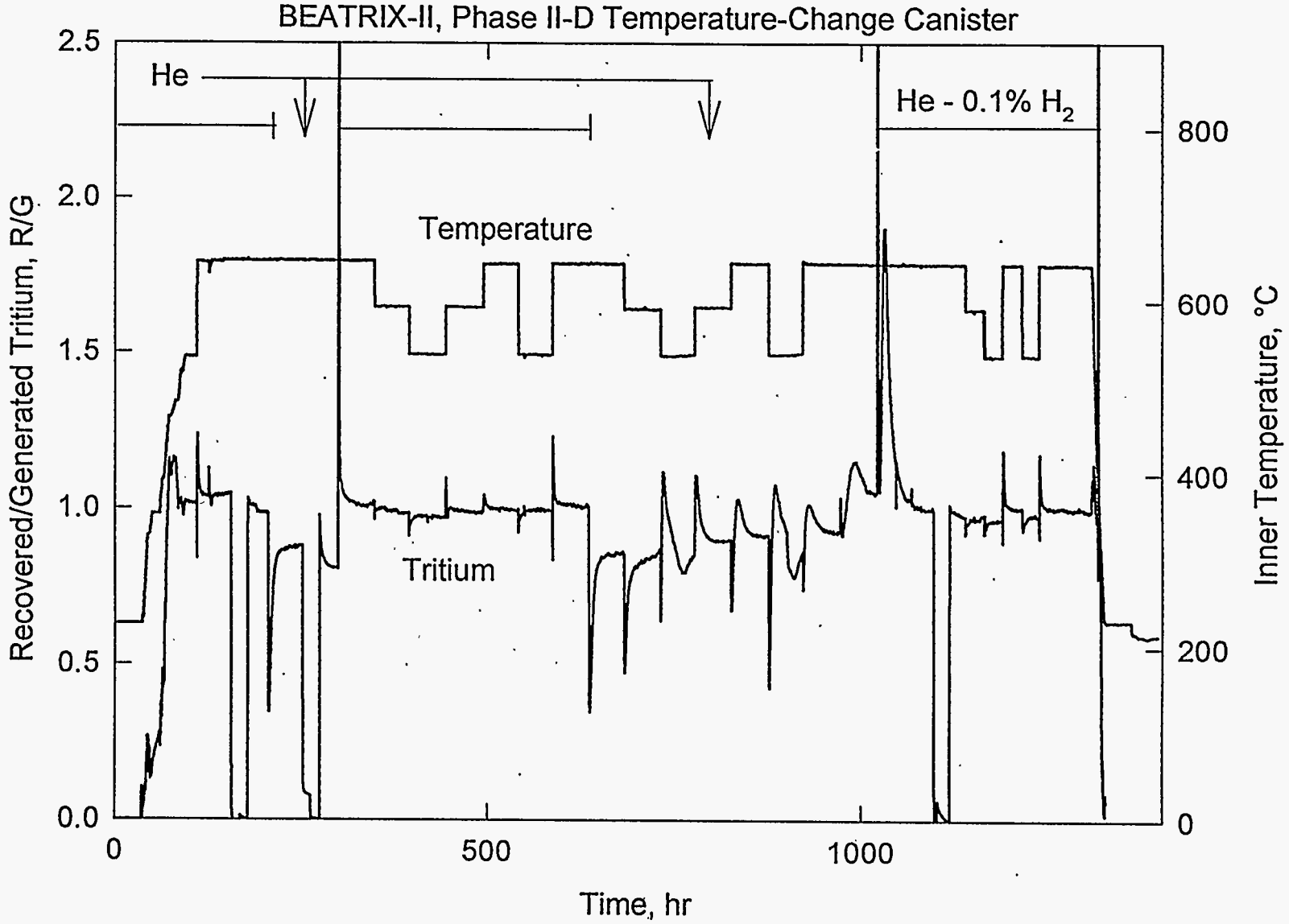

Figure B.8 Ratio of Recovered/Generated Tritium and the Average Inner Temperature for the Temperature-Change Canister in Phase II-D

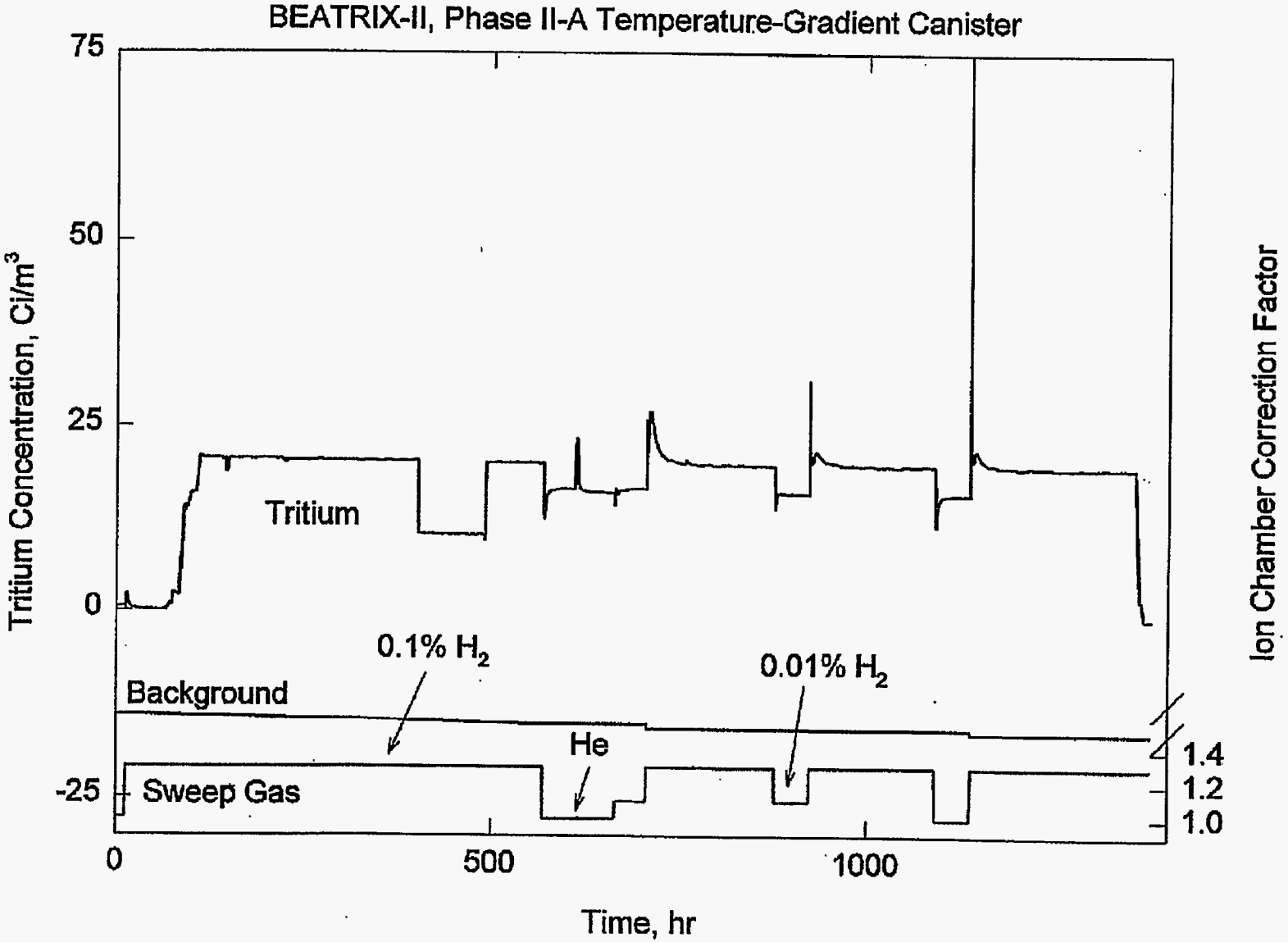

Figure B.9. Corrected Tritium Concentration and the Ion-Chamber Correction Factors Applied to the As-Measured Data for the Temperature-Gradient Canister in Phase II-A

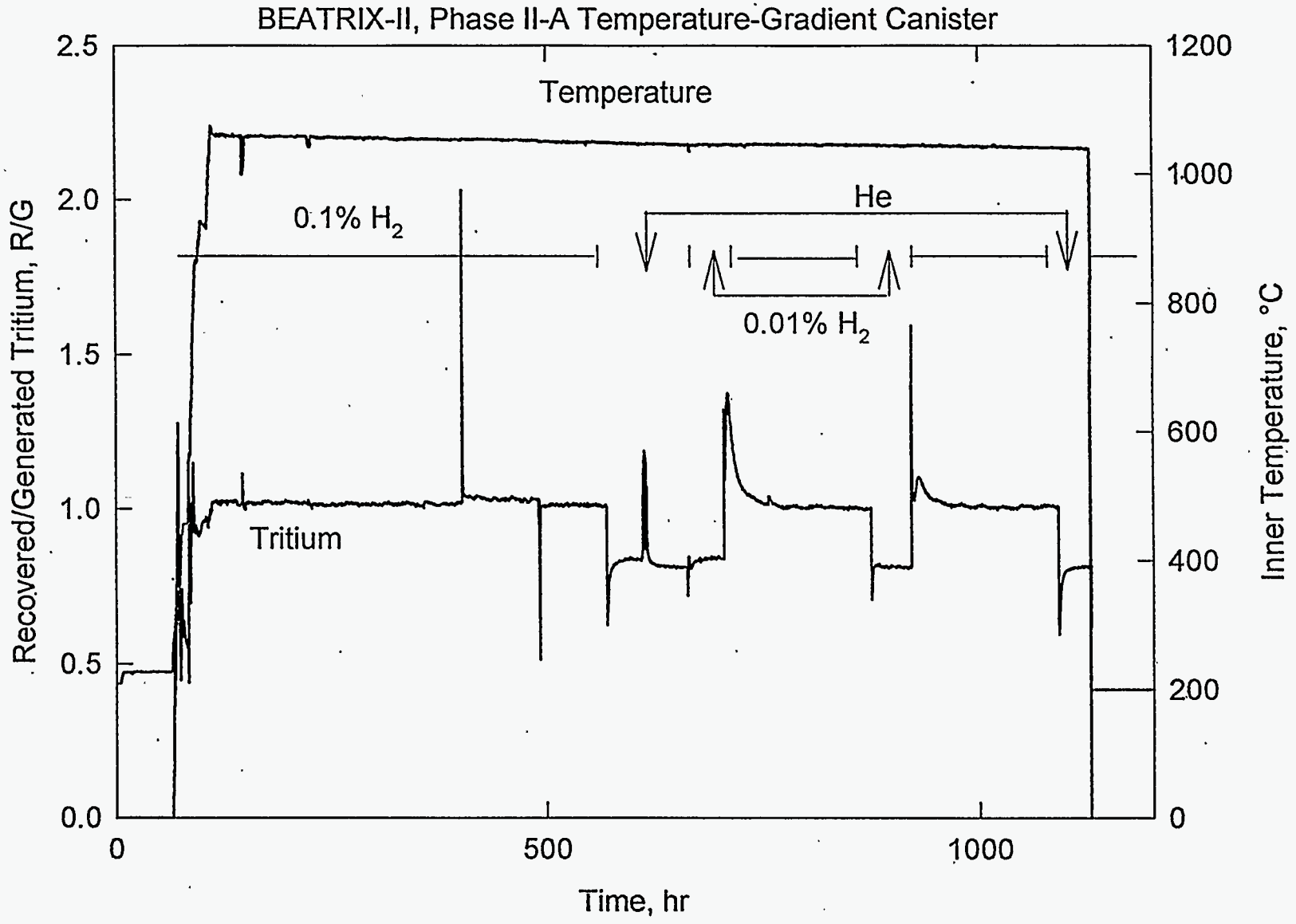

Figure B.10 Ratio of Recovered/Generated Tritium and the Average Inner Temperature for the Temperature-Gradient Canister in Phase II-A

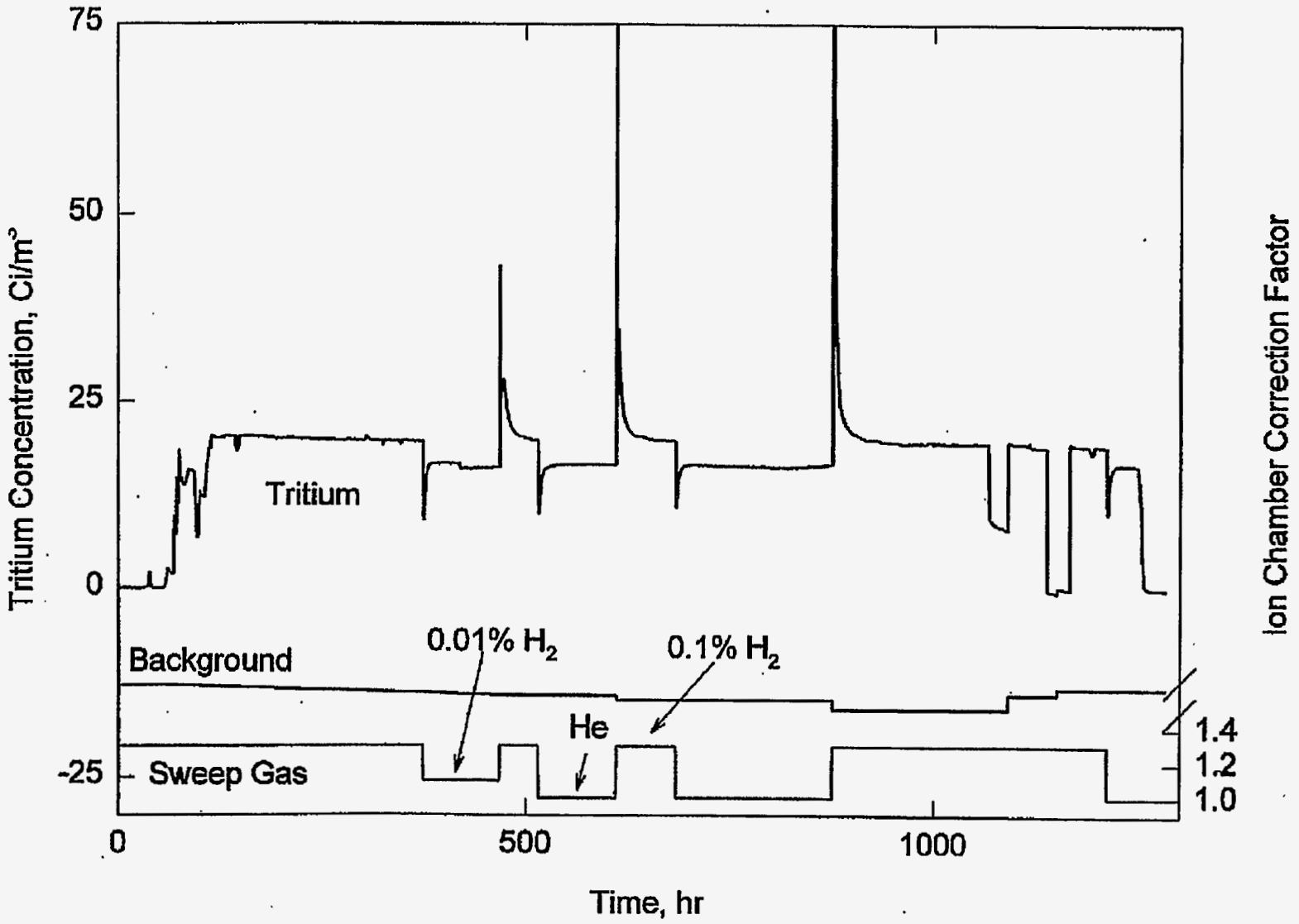

Figure B.11.

Corrected Tritium Concentration and the Ion-Chamber Correction Factors Applied to the As-Measured Data for the Temperature-Gradient Canister in Phase II-B

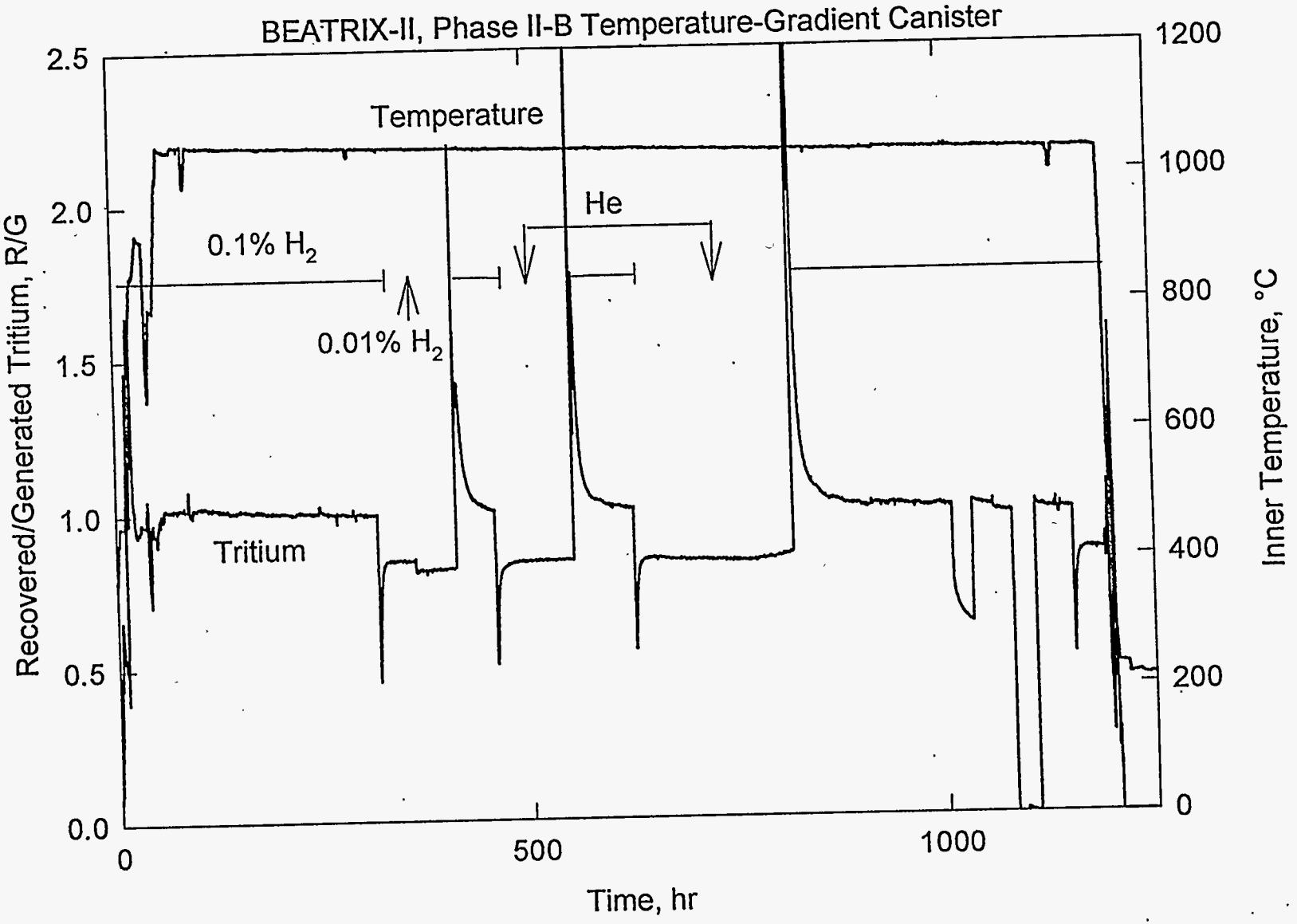

Figure B.12 Ratio of Recovered/Generated Tritium and the Average Inner Temperature for the Temperature-Gradient Canister in Phase II-B

Figure B.13. Corrected Tritium Concentration and the Ion-Chamber Correction Factors Applied to the As-Measured Data for the Temperature-Gradient Canister in Phase II-C

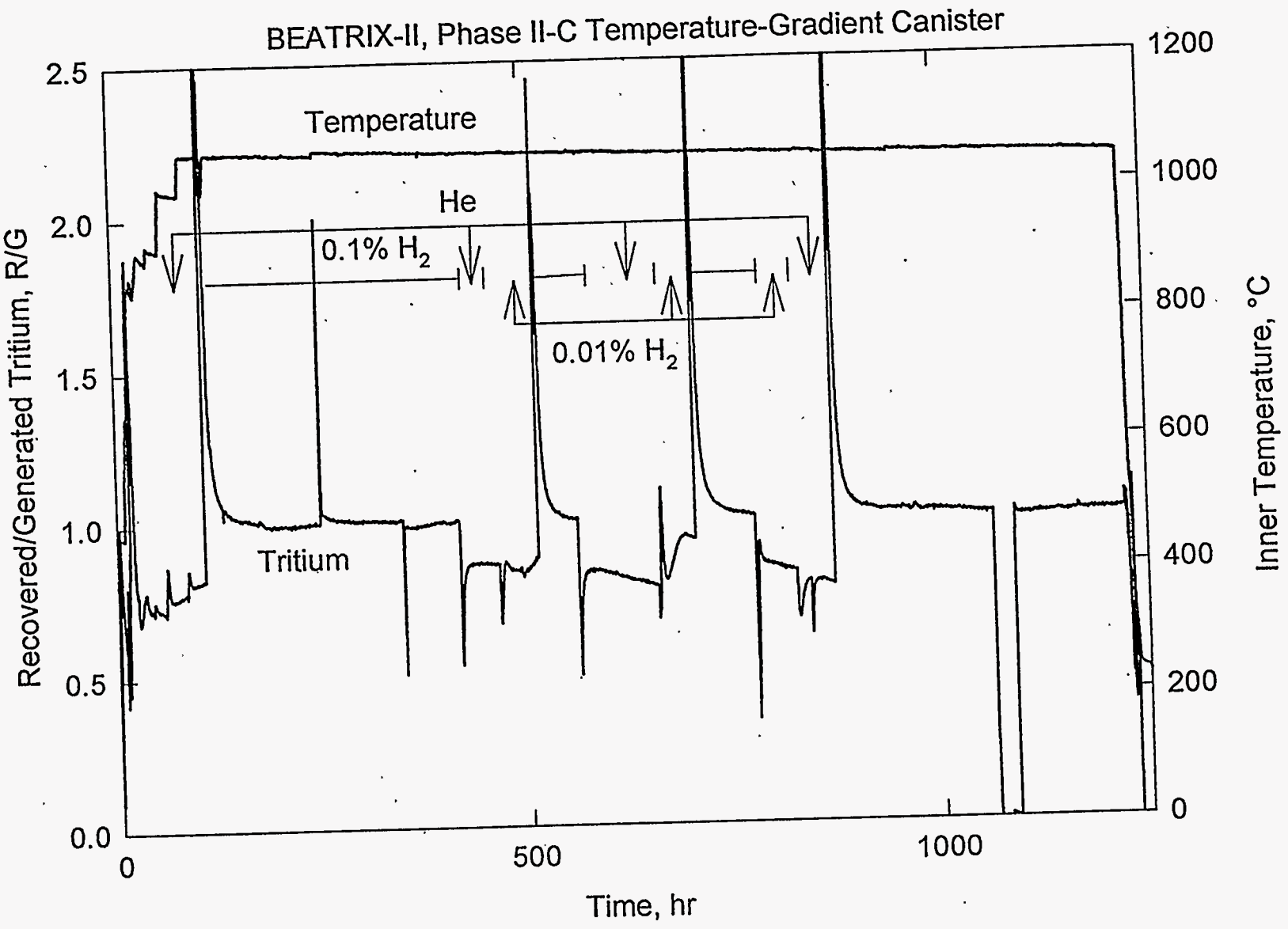

Figure B.14 Ratio of Recovered/Generated Tritium and the Average Inner Temperature for the Temperature-Gradient Canister in Phase II-C

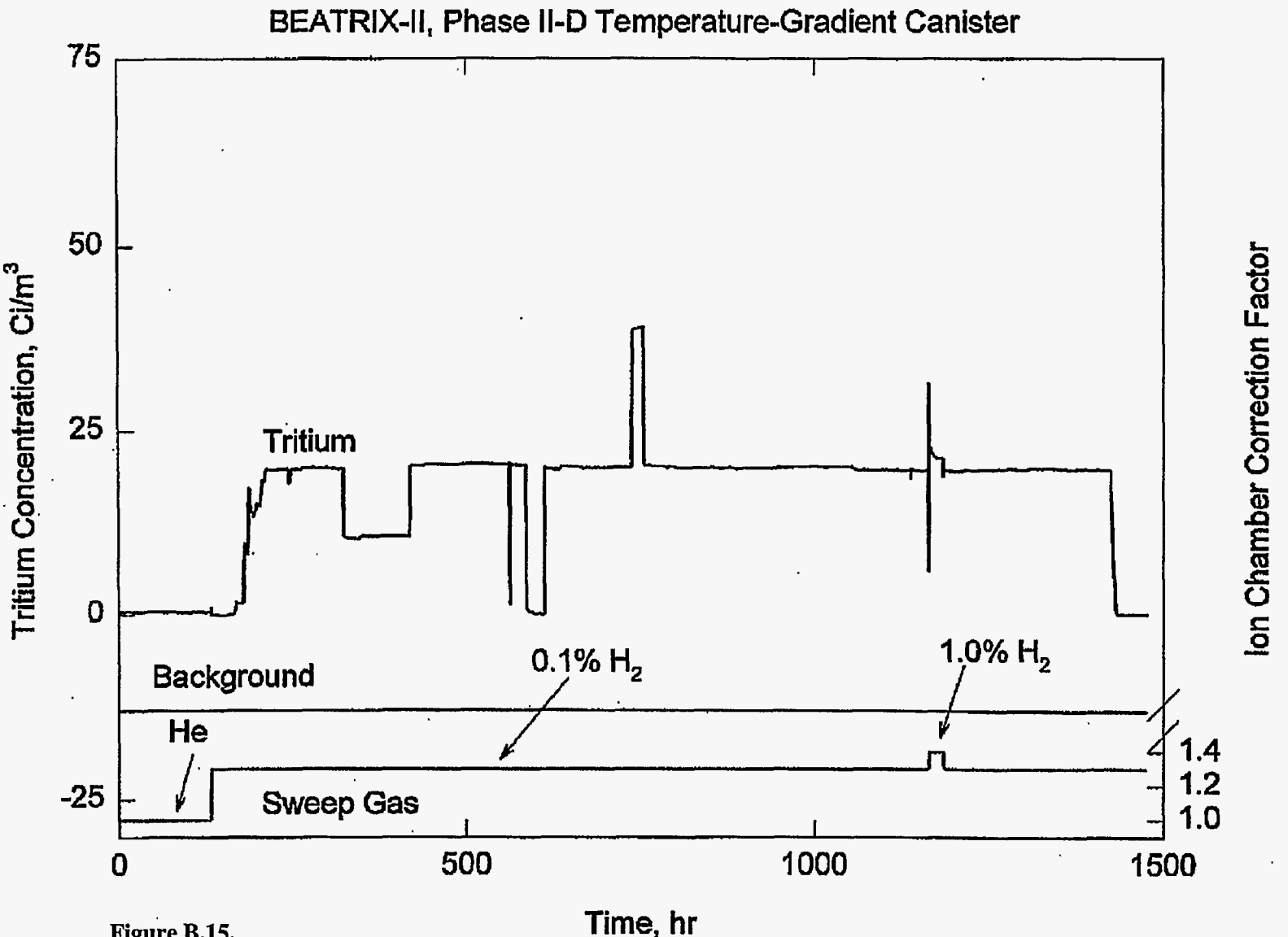

Figure B.15. Corrected Tritium Concentration and the Ion-Chamber Correction Factors Applied to the As-Measured Data for the Temperature-Gradient Canister in Phase II-D

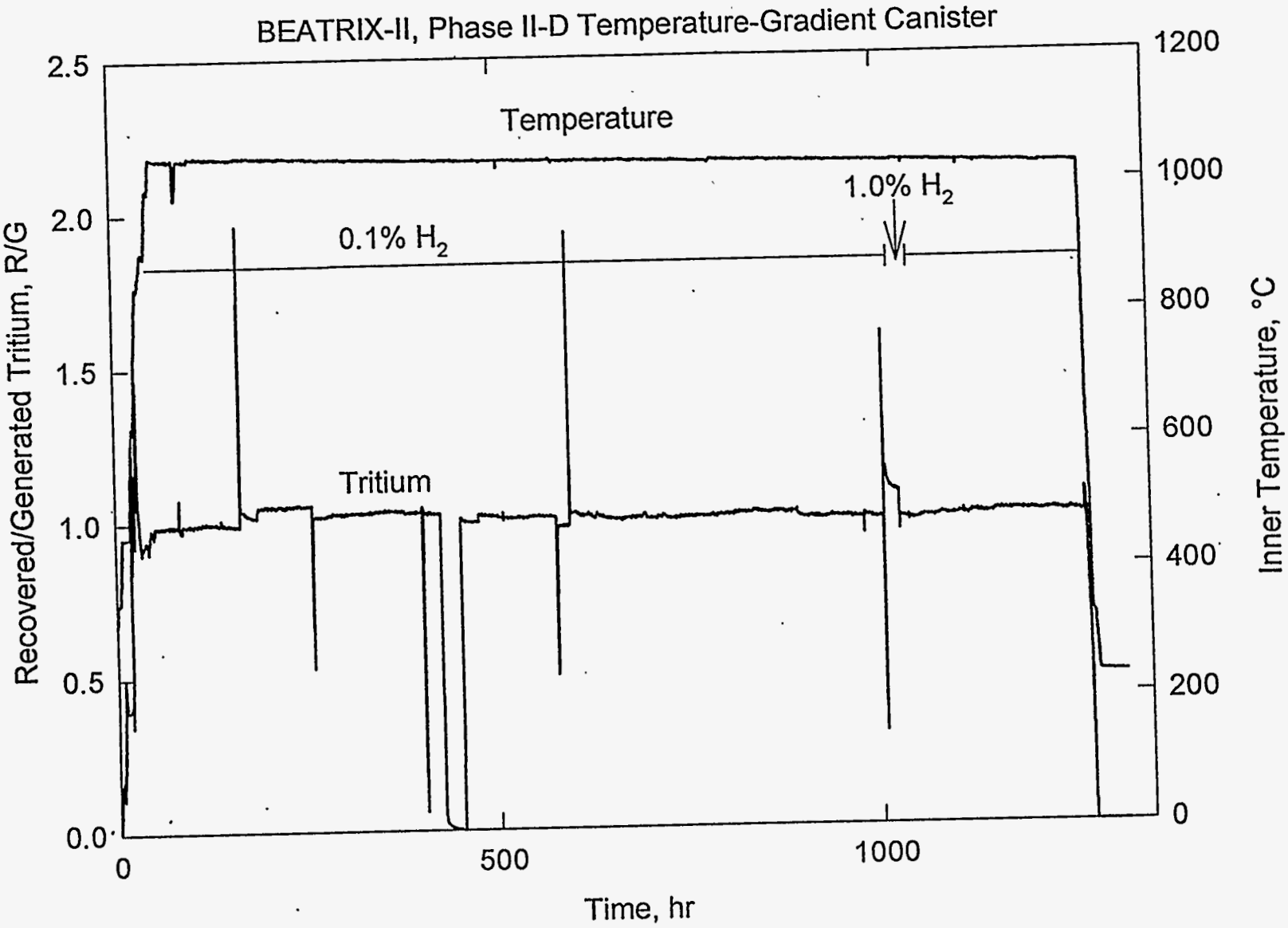

Figure B.16 Ratio of Recovered/Generated Tritium and the Average Inner Temperature for the Temperature-Gradient Canister in Phase II-D

Distribution

No. of Copies

OFFSITE

2 DOE/Office of Scientific and Technical Information

S. E. Berk
ER-533, GTN
U.S. Department of Energy
Office of Fusion Energy
Washington, D.C. 20545

R. E. Price
ER-533, GTN
U.S. Department of Energy
Office of Fusion Energy
Washington, D.C. 20545

F. W. Wiffen
ER-533, GTN
U.S. Department of Energy
Office of Fusion Energy
Washington, D.C. 20545

C. C. Baker
US ITER Program Office
University of California
San Diego
9500 Gilman Drive, Bldg 302
La Jolla, CA 92093

J. L. Anderson
Los Alamos National Laboratory
P.O. Box 1663
Los Alamos, NM 87545

C. G. Bathke
Los Alamos National Laboratory
P.O. Box 1663
Los Alamos, NM 87545

M. C. Billone
Argonne National Laboratory
9700 South Cass Avenue
Argonne, IL 60439

No. of Copies

OFFSITE

S. W. Tam
Argonne National Laboratory
9700 South Cass Avenue
Argonne, IL 60439

D. K. Sze
Argonne National Laboratory
9700 South Cass Avenue
Argonne, IL 60439

C. E. Johnson
Argonne National Laboratory
9700 South Cass Avenue
Argonne, IL 60439

J. P. Kopasz
Argonne National Laboratory
9700 South Cass Avenue
Argonne, IL 60439

R.F. Mattas
Argonne National Laboratory
9700 South Cass Avenue
Argonne, IL 60439

C. Wong
General Atomic
P.O. Box 85608
San Diego, CA 92121-1194

M. Abdou
School of Engineering and Applied Science
UCLA
Boelter Hall
405 Hilgard Avenue
Los Angeles, CA 90024

No. of Copies

FOREIGN

R. E. Green
Atomic Energy of Canada Ltd.
Research Company
Chalk River Nuclear Laboratory
Chalk River, Ontario
Canada KOJ 1JO

J. M. Miller
Atomic Energy of Canada Ltd.
Research Company
Chalk River Nuclear Laboratory
Chalk River, Ontario
Canada KOJ 1JO

R. A. Verrall
Atomic Energy of Canada Ltd.
Research Company
Chalk River Nuclear Laboratory
Chalk River, Ontario
Canada KOJ 1JO

E. O. Moeck
Atomic Energy of Canada Ltd.
Research Company
Chalk River Nuclear Laboratory
Chalk River, Ontario
Canada KOJ 1JO

H. K. Rae
Atomic Energy of Canada Ltd.
Research Company
Chalk River Nuclear Laboratory
Chalk River, Ontario
Canada KOJ 1JO

3 I. J. Hastings
Atomic Energy of Canada Ltd.
344 Slater Street
Ottawa, Ontario
Canada KJA 0J4

No. of Copies

FOREIGN

G. J. Phillips
Atomic Energy of Canada Ltd.
Research Company
Chalk River Nuclear Laboratory
Chalk River, Ontario
Canada KOJ 1JO

D. P. Dautovich
Canadian Fusion Fuels
Technology Project
2700 Lakeshore Road West
Mississauga
Ontario L5J 1K3
Canada

P. Gierszewski
Canadian Fusion Fuels
Technology Project
2700 Lakeshore Road West
Mississauga
Ontario L5J 1K3
Canada

K. Wong
Canadian Fusion Fuels
Technology Project
2700 Lakeshore Road West
Mississauga
Ontario L5J 1K3
Canada

T. Kondo
Tohoku University
Dept. of Machine Intelligence
and Systems Engineering
Aramaki, Aoba-ku, Sendai
980 Japan

No. of Copies

FOREIGN

T. Kurasawa
Dept. of Fusion Engineering Research
NAKA Fusion Research Establishment
Japan Atomic Energy Research Institute
NAKA-Machi Naka-gun
Ibaraki-ken 311-0
Japan

Y. Okuno
Dept. of Fusion Engineering Research
Japan Atomic Energy Research Institute
Tokai-mura Naka-gun
Ibaraki-ken 319-11
Japan

20 K. Noda
Department of Materials Science and Engineering
Japan Atomic Energy Research Institute
Tokai-mura Naka-gun
Ibaraki-ken 319-11
Japan

T. Takahashi
Department of Materials Science and Engineering
Japan Atomic Energy Research Institute
Tokai-mura Naka-gun
Ibaraki-ken 319-11
Japan

H. Yoshida
Department of ITER Project
801-1, Mukouyama, Naka-machi,
Naka-gun, Ibaraki-ken, 311-01
Japan

No. of Copies

FOREIGN

H. Moriyama
Department of Nuclear Engineering
Kyoto University
Yoshida, Sayko-ku
Kyoto 606-01
Japan

T. Terai
Department of Nuclear Engineering
University of Tokyo
Hongo, Bunkyo-ku
Tokyo 7-3-1
Japan

M. Yamawaki
Department of Nuclear Engineering
Faculty of Engineering
University of Tokyo
7-3-1 Hongo, Bunkyo-ku, Tokyo
Japan

S. Tanaka
Department of Nuclear Engineering
Faculty of Engineering
University of Tokyo
7-3-1 Hongo, Bunkyo-ku, Tokyo
Japan

Y. Gohar
ITER Joint Work Site
Max-Planck-Intit. f. Plasmaphysik
Boltzmannstr. 2.
D-85748 Garching bei Munche
Germany

No. of Copies

No. of Copies

FOREIGN

R. Raffray
ITER Joint Work Site
Max-Planck-Intit. f. Plasmaphysik
Boltzmannstr. 2.
D-85748 Garching bei Munche
Germany

F. Tehranian
ITER Joint Work Site
Max-Planck-Intit. f. Plasmaphysik
Boltzmannstr. 2.
D-85748 Garching bei Munche
Germany

ONSITE

1 DOE Richland Operations Office

D. D. Green, K8-50

2 Westinghouse Hanford Company

R. E. Bauer, L6-37
R. J. Puigh, H0-31

26 Pacific NW National Laboratory

D. L. Baldwin, P7-22
M. D. Freshley, K9-85
G. W. Hollenberg, P7-20 (20)
R. H. Jones, P8-15
B. F. Saffell, K5-22
D. J. Senor, P8-10
B. D. Shipp, K1-73
O. D. Slagle, P8-10

Technical report Files (5)